Engineering T cells with lipid nanoparticles for cancer immunotherapy

Xin, Li

Publication date:
2022

Document Version
Publisher's PDF, also known as Version of record

DTU Health Tech
Department of Health Technology

Engineering T cells with lipid nanoparticles for cancer immunotherapy

PhD Thesis

March 2022

Xin Li

Supervisors:

Thomas Lars Andresen
(Professor, Technical University of Denmark)
Gael Clergeaud Veiga
(Researcher, Technical University of Denmark)

Preface

The thesis is written and submitted in fulfillment of the requirements for acquiring the Ph.D. degree from the Technical University of Denmark (DTU). The work described in this thesis was the result of independent research work performed in the Colloids and Biological Interfaces Group (CBIO) headed by Professor Thomas Lars Andresen, which is part of the Department of Health Technology at DTU.

The work presented was carried out from April 2019 to March 2022, under the supervision of Professor Thomas Lars Andresen (main supervisor) and Researcher Gael Clergeaud Veiga (co-supervisor). This thesis does not contain any work that has been published or authored by other individuals or collectives, except for those that are cited. Individuals and collectives who have made significant contributions to Ph.D. research are identified in the thesis.

Copenhagen

March 31, 2022

Xin Li

Acknowledgment

First and foremost, I am very grateful to my supervisor Thomas Lars Andresen for giving me the opportunity to pursue my Ph.D. in the CBIO group and for guiding me through the three years. Next, I would like to express my deep gratitude to my co-supervisor Gael for his countless valuable guidance, encouragement, and academic inputs throughout my studies on a day-to-day basis, from whom I also learned to be passionate and see the positive in every situation.

Next, I would like to thank my close collaborators Sven, Hófí, Anna, and Paul for their unique contributions to our collaborative projects, the inspiring scientific discussions, and the joyful work together. My gratitude also goes to the whole CBIO group for creating a cheerful work environment and always being happy to help. A special thanks go to Arjen and Albert for being great office mates and for all the great discussions and fun times in the office. I would also like to thank all the people in building 423 for their help, inspiration, and creation of a pleasant working environment. I am especially grateful to our lunch group including Ann-Kathrin, Albert, Arjen, Carmen, Gael, and Sven who make the lunch breaks truly enjoyable. It was a good time to spend together.

Furthermore, I would like to express my sincere gratitude to my family and friends for their constant support, love, and understanding for me. Covid-19 had made it difficult to get together with all the people whom I miss a lot. I am especially grateful for having them during all this time, and my families are always the source of endless power for me. A big thanks also go to my friend Huimin for the great friendship, support, and for taking care of me when I am writing the thesis. Last but not least, I would like to thank my husband Yong who started this journey with me and went through all the ups and downs by my side, giving me tremendous patience and unconditional support.

Abstract

Cancer immunotherapy has become the fourth pillar of cancer treatment apart from surgery, radiation, and chemotherapy, most notably with checkpoint blockade antibodies and chimeric antigen receptor T cell therapy. Adoptive T cell therapy of either expanded tumor-infiltrating lymphocytes or genetically modified T cells has demonstrated a big breakthrough in the treatment of some established malignancies, especially leukemia and lymphoma. Despite the success in hematological malignancies, the response is severely limited in treating solid tumors due to immune dysfunction related to poor cell engraftment, tumor infiltration and engagement, and lack of target. Thus, co-administration of adjuvant drugs or genetic modification of T cells are often required. However, the methods for T cell engineering have so far met with challenges of unprecise modification, being complex and expensive. In addition, limited efficacy and significant toxicity have been major issues for the broader success of T cell therapy. To address these issues and enhance the anticancer efficacy of T cell therapy, in this Ph.D. thesis we developed a novel approach to engineer T cells by equipping the cells with lipid nanoparticles containing therapeutic agents. Using this strategy, we have loaded supportive small-molecule immunomodulators and mRNA in T cells via two different conjugation techniques.

In the first part, we developed and characterized a remote-loading method for loading small molecule immunomodulatory drugs into liposome carriers. A TLR-7 agonist Gardiquimod and SHP2 inhibitor SHP099 were tested as the candidate drugs, respectively. Both drugs were efficiently loaded into liposomes of various lipid compositions using the remote-loading method via an ammonium sulfate gradient. Complete drug loading was achieved at a drug-to-lipid ratio of 0.25/1 (mol/mol), and the drugs were entrapped inside the liposomes and sustainedly released out for more than 1 week in the cell culture medium. We further assessed the biological effects of the drugs *in vitro*. The liposomes exhibited prolonged effect and alleviated toxicity, and the capacity for co-loading drugs as combination therapy. The approach to efficiently load high concentrations of Gardiquimod and SHP099 allowed the use of lipid-based drug carriers for loading T cells with immunomodulators.

The second part of the Ph.D. thesis describes the strategy to load T cells with liposomal SHP099 nanocrystals, with the aim to improve the efficacy of adoptive T cell therapy. A novel formulation containing tri-arginine motifs (SR3) was designed to enable T cells attachment and loading through electrostatic interaction and membrane penetration. Using the remote-loading

method developed previously, SHP099 was loaded into lipid vesicles and formed nanocrystals in the core. By incubating T cells with SR3-SHP099, a high loading efficiency into T cells was achieved without affecting the T cell viability, and the nanocrystals formed a depot to sustainedly release SHP099 over more than 5 days. We found that SHP099 enabled prolonged inhibition of the PD-1/PD-L1 signaling compared to the anti-PD1 antibody. The SHP2 inhibition resulted in superior cytotoxicity of loaded OT.1 T cells against the target tumor cells in a co-culture cells lysis assay. In addition, loading the T cells did not affect the biodistribution of infused T cells *in vivo*, and the tumor-homing T cells were able to carry the lipid vesicles into the tumor tissue, enhancing the tumor accumulation of the cargos. On an established solid tumor model, adoptively transferred T cells loaded with SR3-SHP099 induced complete tumor eradication and a durable immune memory against re-challenging tumor formation on all treated mice. The efficacy was equivalent to that resulting from the repeated administered anti-PD-L1 antibody. These findings demonstrate that the combination of adoptive T cell therapy with SHP2 inhibition is a promising therapeutic strategy. Moreover, our T cells loading technique provides a precise and efficient drug delivery platform for targeting T cells.

In the third part, we explored another T cell loading technique by conjugating lipid nanoparticles (LNPs) to the surface of bioorthogonal glycoengineered T cells through SPAAC click chemistry. Conjugating drug-loaded nanoparticles to living cells represent a promising strategy for targeted drug delivery, because of the tissue homing properties in the specific cell types to overcome in vivo barriers. And covalent conjugation has advantages in cellular loading regarding stability and specificity. In this study, T cells were decorated with azide groups on their surface through metabolic glycoengineering, followed by reacting with dibenzylcyclooctyne (DBCO) modified LNPs. We first demonstrated highly specific and robust conjugation of liposomes to T cells, and the conjugation efficiency can be well-tuned by changing the azide and DBCO liposome presence. Based on the optimized procedure, we further developed DBCO functionalized mRNA-LNPs that can be conjugated to T cells. Preliminary results showed the conjugated LNPs delivered mRNA into T cells and subsequently transfected the T cells with the encoded gene.

Taken together, the work in this Ph.D. thesis integrated the topics of nanomedicine and T cell-based cancer immunotherapy, presenting a novel and versatile strategy for engineering therapeutic T cells by loading the cells with lipid-based nanoparticles encapsulating immunomodulatory drugs.

Resumé

Kræftimmunterapi er blevet den fjerde søjle i kræftbehandling, udover kirurgi, stråling og kemoterapi, hvor især checkpoint-blokadeantistoffer og kimærisk antigenreceptor T-celleterapi har været særligt interessante. Adoptiv T-celleterapi med enten dyrkede tumorinfiltrerende lymfocytter eller genetisk modificerede T-celler har fået et stort gennembrud til behandling af visse etablerede kræftsygdomme, især leukæmi og lymfom. På trods af successen med hæmatologiske kræftsygdomme, er terapien meget begrænset til behandling af solide tumorer grundet immundysfunktion relateret til dårlig celletransplantation, tumorinfiltration og -engagement samt mangel på terapeutiske mål. Co-administration med adjudantlægemidler eller genetisk modifikation af T-celler er således ofte påkrævet. Metoderne, der anvendes til T-celle engineering, har hidtil mødt udfordringer med præcis levering eller at de har været for komplekse og dyre at foretage. Derudover har begrænset effektivitet og betydelig toksicitet været store problemer for den bredere succes af T-celleterapi. For at løse disse udfordringer og forbedre anticancer-effektiviteten af T-celleterapi, udviklede vi i denne Ph.D.-afhandling en ny tilgang til at modificere T-celler ved at udstyre cellerne med lipid-baserede nanopartikler, der indeholder terapeutiske lægemidler. Ved at bruge denne strategi har vi co-formuleret adjudant småmolekylære immunmodulatorer og mRNA i T-celler via to forskellige konjugationsteknikker.

I den første del af denne afhandling præsenteres udviklingen og karakterisering af en remote-loading-metode til loading af småmolekylære immun-modulerende lægemidler, såsom Gardiquimod og SHP099, i liposomer. Disse lægemidler fungerer som henholdsvis TLR-7-agonist og SHP2-inhibitor, og begge kan forbedre anti-cancer-T-cellernes effektivitet. Lægemidlerne blev effektivt loadet i liposomer af forskellige lipidsammensætninger ved anvendelse af remote-loading-metoden via en ammoniumsulfatgradient. Fuldstændig lægemiddelskapacitet blev opnået ved et lægemiddel-til-lipid-forhold på 0,25/1 (mol/mol), og lægemidlerne blev indkapslet i liposomerne og udviste varig frigivelse i mere end 1 uge, målt i cellekulturmedium. Vi undersøgte også den biologiske effekt af stofferne in vitro. Liposomerne udviste forlænget virkning, sænket toksicitet og kunne co-formuleres med andre lægemidler til kombinationsterapi. Tilgangen til effektivt at loade høje koncentrationer af Gardiquimod og SHP099 muliggjorde anvendelsen af liposomerne, til udstyring af T-celler med immunmodulatorerne.

Anden del af ph.d.-afhandlingen beskriver en strategi for at udstyre T-celler med liposomale nanokrystaller af SHP099 med det formål at forbedre effektiviteten af adoptiv T-celleterapi. En ny formulering indeholdende tri-arginin-motiver (SR3) blev designet til at muliggøre vedhæftning på- og udstyring af T-celler gennem elektrostatisk interaktion og membranpenetrering. Ved at bruge den tidligere udviklede remote-loading-metode blev SHP099 loadet i lipidvesikler og dannede nanokrystaller deri. Ved at inkubere T-celler med SR3-SHP099 blev en høj loading-effektivitet opnået i T-celler, uden at påvirke deres levedygtighed, og nanokrystallerne dannede et depot for varig frigivelse af SHP099 over mere end 5 dage. Vi viste, at SHP099 muliggjorde langvarig inhibering af PD-1/PD-L1-signalering sammenlignet med anti-PD1-antistof, hvilket resulterede i bedre cytotoksicitet af ladede OT.1 T-celler mod targeterede tumorcellerne i et co-kulturcellelysisassay. Derudover påvirkede loading af T-cellerne ikke biodistribueringen in vivo, og de tumor-targeterende T-celler var i stand til at bære lipidvesiklerne ind i tumorvævet, hvilket forøgede tumorakkumuleringen af de loadede lægemidler. I en etableret solid tumormodel inducerede adoptivt overførte T-celler, loadet med SR3-SHP099, fuldstændig tumorudryddelse og varig immunhukommelse mod tumor-genudfordring på alle behandlede mus. Effektiviteten af behandlingen var ækvivalent med effektiviteten ved gentagne indgivelser med anti-PD-L1-antistof. Vores resultater viser, at kombinationen af adoptiv T-celleterapi med SHP2-hæmning er en lovende terapeutisk strategi. Derudover giver vores T-celle-loading-teknik en præcis og effektiv lægemiddelsleveringsplatform til T-celler.

I den tredje del af afhandlingen udforskes en anden T-celle-loading-teknik, der fungerer ved at konjugere lipidnanopartikler (LNP'er) til overfladen af bioortogonale T-celler gennem SPAAC-klikkemi. Kovalent konjugation har fordele ved cellulær loading med hensyn til stabilitet og specificitet. Konjugering af lægemiddels-loadede nanopartikler til levende celler repræsenterer en lovende strategi for målrettet lægemiddellevering, på grund af vævsmålsøgningsegenskaberne i specifikke celletyper for at komme igennem in vivo-barrierer. I dette studie blev T-celler dekoreret med azid-grupper på deres overflade gennem metabolisk glycoengineering, efterfulgt af reaktion med dibenzylcyclooctyne (DBCO)-modificerede LNP'er. Vi demonstrerede først meget specifik og robust konjugation af liposomer til T-celler, og konjugationseffektiviteten kan finjusteres ved at ændre tilstedeværelsen af azid- og DBCO-liposomer. Baseret på den optimerede procedure videreudviklede vi DBCO-funktionaliserede mRNA-LNP'er, der kan konjugeres til T-celler. Foreløbige resultater viser, at de konjugerede LNP'er leverer mRNA og efterfølgende transfekterer T-celler med det kodede gen.

Samlet set integrerede arbejdet i denne Ph.D.-afhandling emnerne nanomedicin og T-celle-baseret cancerimmunterapi, og præsenterede en ny og alsidig strategi til engineering af terapeutiske T-celler, ved at loade cellerne med lipid-baserede nanopartikler, der indkapsler immunmodulerende lægemidler.

List of contributions

List of discussed publications in this thesis

I. **Xin Li,** Hólmfridur R. Halldórsdóttir, Sven Weller, Anna Colliander, Martin Bak, Paul Kempen, Gael Clergeaud & Thomas L. Andresen.
Enhancing adoptive cell therapy by T cell loading of SHP2 inhibitor nanocrystals before infusion. *Submitted to ACS Nano*

II. **Xin Li,** Sven Weller, Gael Clergeaud & Thomas L. Andresen.
Click conjugation of lipid-based nanoparticles on metabolic glycoengineered T cells. *In preparation for submission to Journal of Controlled Release*

List of publications not included in this thesis

I. Weiguang Jin[ı], **Xin Li[ı]**, Gael Clergeaud Veiga, Thomas Lars Andresen, Kira Astakhova, Katrine Qvortrup**. [ı] Equal contribution to this work.**
Surface Engineering of PCN-224 Nanoparticles for enhanced miRNA stability, cell uptake, and synergistic anticancer. *In preparation for submission to Biomaterials*

II. Weiguang Jin, **Xin Li,** Gael Clergeaud Veiga, Thomas Lars Andresen, Charlotte Held Gotfredsen, Martin Nielsen, Kira Astakhova, Katrine Qvortrup.
FeII8L6 Metalloporphyrin Cage Binds Small RNAs through pi-Stacking and Electrostatic Interactions. *Submitted to Angewandte Chemie*

III. Sven Weller, **Xin Li**, Lars R. Petersen, Paul Kempen, Gael Clergeaud and Thomas L. Andresen .
Impact of antibody orientation, valency and density on polymeric nanoparticles for polyclonal expansion of human CD8+ T cells. *In Preparation for submission to RSC Nanoscale*

IV. Sven Weller, **Xin Li,** Hólmfridur Rósa Halldórsdóttir, Arjen Weller, Paul Kempen, Gael Clergeaud Veiga, Thomas L. Andresen.
Antibody-targeted PD-L1 and IL-2 encapsulating nanoparticles for localized tumor therapy. *In preparation.*

V. Sven Weller, Serhii Kostrikov, Sören Becker, Jan Niehaus, **Xin Li,** Kasper Bendix , Gael Clergeaud Veiga, Thomas L. Andresen.
Antibody conjugated giant shell quantum dots to label primary T cells for tracking applications. *In preparation*

Conference contribution

I. **Xin Li,** Hólmfridur Halldórsdóttir, Sven Weller, Anna Colliander, Ditte Jæhger, Martin Bak, Gael Clergeaud, Thomas Andresen.
Exploiting T cells as vehicles of liposomal SHP2i to enhance adoptive cell therapy. Abstract at the 36th Annual meeting of Society for Immunotherapy of Cancer's (SITC), Washington DC, 2021.

Content

List of Figures

List of Tables

Thesis objectives and outline

Objectives

The overall aim of this thesis is to provide beneficial approaches for modifying T cell functions, improving drug delivery efficiency, as well as investigating the novel combination strategies of T cells with other therapies to facilitate the development of cellular cancer immunotherapies. To achieve this, multidisciplinary studies integrating the knowledge in nanotechnology, cancer immunology, and pharmaceutical science were carried out. Herein, T cells were loaded with lipid nanoparticles encapsulating immunomodulatory drugs. The drug-loaded nanoparticles equipped the T cells with depots of large quantities of supporting adjuvant or immune modifiers, which represent an easy and versatile platform to engineer T cells. The results presented within this work provide knowledge about utilizing nanomedicine to enhance cancer immunotherapy, particularly adoptive T cell therapy, and bring insights into novel combinations of immunomodulatory drugs with T cell therapy for synergistic anti-cancer efficacy.

The main objectives of the Ph.D. thesis are:

I. The development of a remote-loading method for formulating immunomodulatory drugs into lipid nanoparticles with high loading efficiency and stability.
II. The development and assessment of different approaches to loading T cells with lipid-based nanoparticles for T cell engineering.
III. The exploration of novel drug delivery strategy by using immune cells as the drug delivery vehicle.
IV. The investigation of novel combination strategies of T cell therapy with other therapies for cancer treatment.

Thesis outline

This Ph.D. thesis is outlined in five chapters as follows:

Chapter 1 provides a general introduction of the principle, current state-of-art, and challenges of cancer immunotherapy. Special focus was put on T cell therapies, checkpoint inhibitors, and small molecule immunomodulators that were covered in the research scope of this thesis. Additionally, this chapter gives insight into enhancing cancer immunotherapy with nanomedicine. Further, this chapter introduced a novel drug delivery strategy by using immune cells as the drug delivery vehicle. The basic properties of different immune cell types, the advantages, and disadvantages as well as the techniques for loading cells with nanoparticulated drugs were discussed.

Chapter 2 consists of the development and characterization of the remote-loading method for efficient liposomal loading of two small-molecule immunomodulators. The successful formulation of the drugs as nanomedicine and the validation of biological activity set up the basis for the cellular loading in the following chapter.

Chapter 3 consists of a manuscript titled `Enhancing adoptive cell therapy by T cell loading of SHP2 inhibitor nanocrystals before infusion´, which presented the main research of this thesis. Using the loading method described in chapter 2, we developed a functional lipid nanoparticle platform for loading the small-molecule checkpoint inhibitor, SHP099, to T cells to improve their persistence and function, thus improving the antitumor efficacy.

Chapter 4 describes the development of another T cell loading strategy via covalent conjugation. Lipid nanoparticles were conjugated to the surface of T cells by the combination of metabolic labeling and click chemistry. mRNA was exploited as the therapeutic reagent carried by the LNPs into T cells, to provide prolonged transfection of T cells.

Chapter 5 summarizes the work of this thesis with concluding remarks.

Chapter 1

General Introduction

Cancer immunotherapy has become a key part of the clinical management of cancer. New immunotherapy treatments are being approved and developed, and new insights into the mechanisms and regulators that control the immune system are being discovered at a fast pace. However, a key challenge in improving the response rate of cancer immunotherapy exists in the precise and controlled modulation of the immune system. The therapeutics can lead to severe side effects such as autoimmunity and still fail to take optimal effects on the disease target. Advanced drug delivery systems including nanomedicines and the live cell-mediated delivery of nanoparticles can potentially improve the therapeutic index of cancer immunotherapies. The integration of nano-drug delivery into cancer immunotherapy to enhance the anticancer therapeutic efficacy underlies the research in this thesis.

1.1 Cancer Immunotherapy

Cancer immunotherapy, also known as immuno-oncology, is a form of cancer treatment that harnesses the power of the immune system to prevent, control, and eliminate cancer. It has shown remarkable response to a variety of cancers, potentially with fewer off-target toxicity than previous treatments (including chemotherapy, radiotherapy, and surgery) that directly kill cancer cells. The development of immuno-oncology is grounded on the demonstration of the theory of immune surveillance[1], by which the immune system eliminates tumor cells. The process was further depicted with a novel "three E's theory" of immunoediting to describe the interactions of cancer cells and the host immune system [2,3]. The process composes of three steps: 1) elimination of tumors at an early stage, 2) equilibrium when the immune system controls the tumor, and 3) escape when tumor cells are fully immunoedited and grow without immune control.

Immunotherapy can be applied in various ways by stimulating or boosting the immune system to initiate or enhance an anticancer immune response[4,5], which includes a series of stepwise events with the central aim to activate tumor-specific CD8+ cytotoxic T lymphocyte (CTL) responses against cancer cells. The steps are depicted as the Cancer-Immunity Cycle in a review by Chen[5]. As shown in **Figure 1.1**, the cancer-immunity cycle is completed with 7 steps: 1) neoantigens created by oncogenesis are released and captured by antigen-presenting cells (APCs) for processing. 2) APCs present the captured antigens on major histocompatibility complexes (MHC-I and MHC-II) to T cells. 3) The binding of T cell receptor (TCR) to antigens presented in MHC and the interaction of co-stimulatory molecules result in the priming and activation of T cell responses against the cancer-specific antigens. 4) The activated effector T cells traffic to tumors, 5) and infiltrate the tumor bed, 6) recognize and bind to cancer cells through the interaction between TCR and its cognate antigen bound to MHC-I, 7) finally kill their target cancer cells. Following the last step, killed cancer cells release additional tumor-associated antigens, leading to the recycling of the process. Each step is regulated by numerous stimulatory and inhibitory factors, and cancer cells can interfere with the cycle by multiple mechanisms including producing suppressive signals or loss of the MHC-I antigen presentation[6], thus evading the elimination by the immune system. Cancer immunotherapy aims to restore the process while avoiding generating autoimmune inflammatory responses.

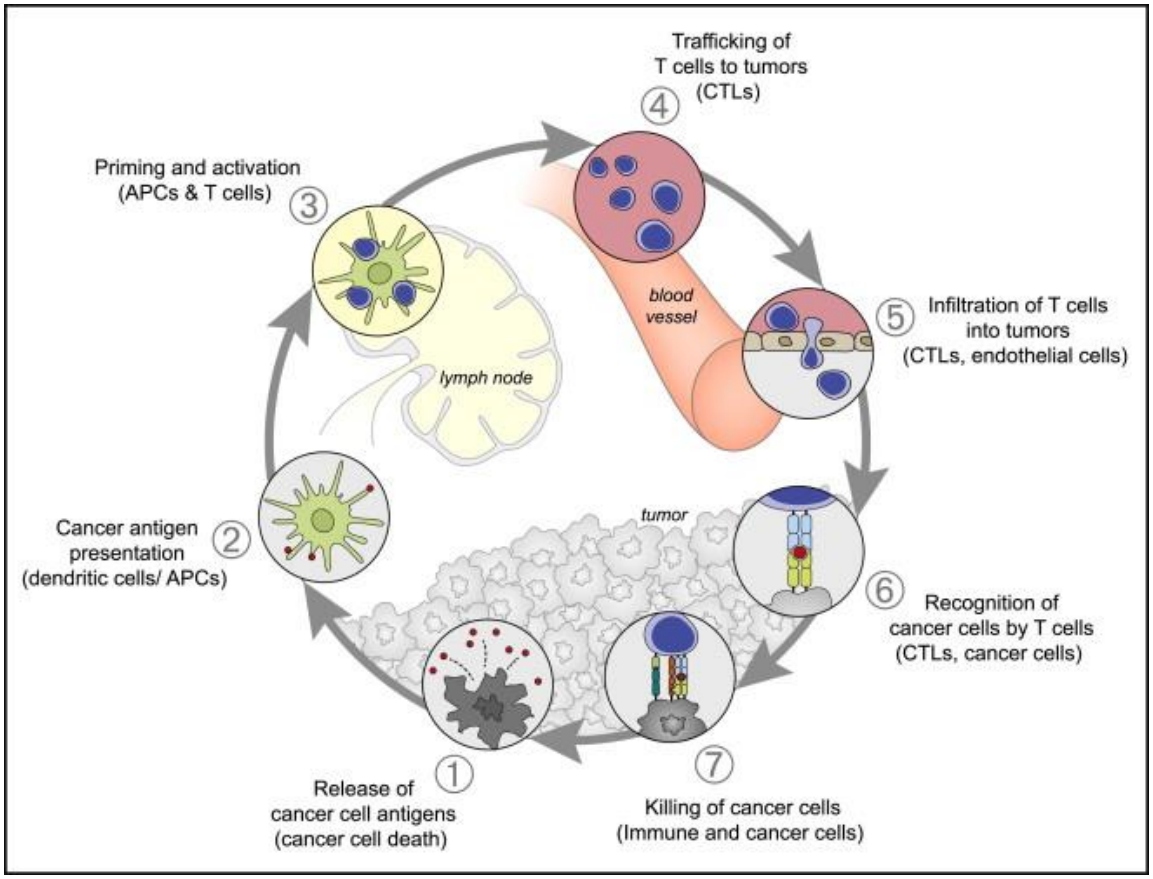

Figure 1.1 The Cancer-Immunity Cycle. This cycle can be divided into seven major steps, starting with the release of antigens from the cancer cell and ending with the killing of cancer cells. Each step is described above, with the primary cell types involved and the anatomic location of the activity listed. The figure is adapted from Chen et al[5].

The exploration of cancer immunotherapy started with the investigation of the cytokine family including interleukins, interferons, and chemokines[7]. The U.S. Food and Drug Administration (FDA) approved the cytokine interferon-α (IFNα) in 1986[8] for hairy leukemia and recombinant interleukin-2 (IL-2) for metastatic renal cancer in 1992 and metastatic melanoma in 1998[4,9]. Those only led to modest successes, which were counterbalanced with serious adverse events due to the high doses required. Long after that, the advent of T cell immune checkpoint inhibitors, including monoclonal antibody (mAb) that targets cytotoxic T lymphocyte antigen 4 (CTLA4), programmed cell death 1 (PD-1) or its ligand, PD-1 ligand 1 (PD- L1), together with the first chimeric antigen receptor (CAR) T cell therapies, brought cancer immunotherapy into the new era[10]. Until March 2022, FDA had approved over 60 immunotherapies that together cover almost every major cancer type, with more new immunotherapies being developed and immunotherapy clinical trials underway in nearly all forms of cancer. These cancer immunotherapies can be broken down into several major types including checkpoint inhibitors, adoptive cell therapy, oncolytic virus therapy, cancer vaccines, and

immunomodulators. A brief introduction of the main classes that are relevant for the work in this thesis is given below.

1.1.1 *Checkpoint inhibitors*

Immune checkpoints are natural parts of the immune system to balance immune responses and prevent T cells from attacking healthy tissues[11]. They represent the negative regulation of the immune system via regulatory T cells (Treg) and co-inhibitory molecules. T cell activation requires both the first signal when TCR binds to MHCI or MHCII expressed on APCs and the second signal from the co-stimulatory molecule interaction between CD28 on a T cell with CD80/CD86 on an APC. In addition to the first and second signals, the activation is regulated by other co-stimulatory and co-inhibitory molecules (**Figure 1.2**)[12]. Immune checkpoint inhibitors (CPIs) activate anti-tumor response through the disruption of inhibitory interactions at the checkpoints (anti-PD-1/PD-L1, anti-CTLA-4, anti-TIM-3, anti-LAG-3).

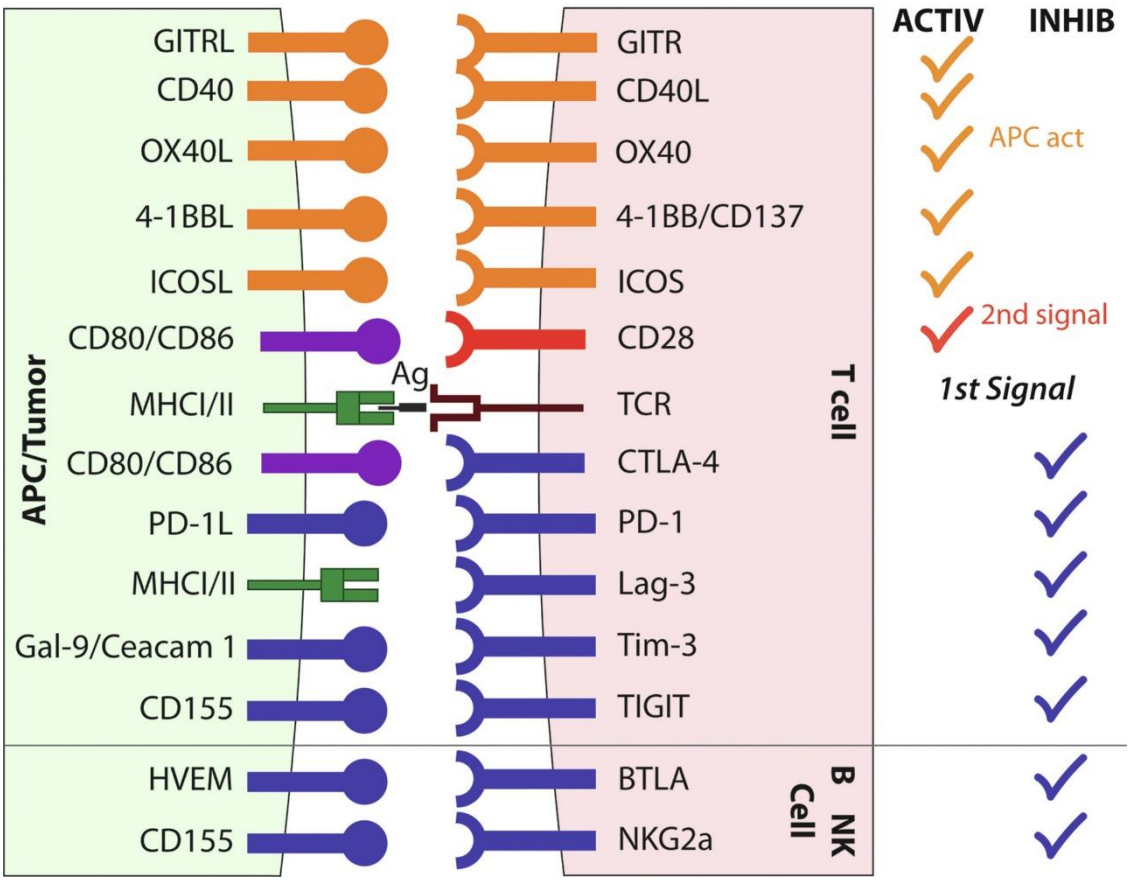

Figure 1.2 Co-stimulatory and co-inhibitory molecules. A selection of the best-studied molecules expressed by T cells and other cells, which either stimulate (orange) or inhibit (blue) the response. The figure is adapted from Jacob et al[12].

The two most studied checkpoint inhibition strategies are CTLA-4 inhibition and PD-1/PD-L1 blockade. CTLA-4 and PD-1 are expressed upon T cell activation, and both are expressed by Treg cells. CTLA-4 binds to CD80/CD86 with a higher affinity than CD28, thus it out-competes CD28 and blocks the co-stimulatory signal for T cell activation, keeping them from killing tumor cells and leading to tumor evasion[13]. The first CPI drug, Ipilimumab, is a mAb against CTLA-4. By blocking the interaction between CTLA4 and its ligands, T cells remain active to recognize and kill tumor cells. In contrast, the binding of PD-1 to PD-L1 leads to the blockade of signaling downstream of the TCR through the phosphatase SHP2[14]. The ligand of PD-1 is commonly upregulated on tumor cells to evade recognition and elimination by T cells[15], and PD-1 is more broadly expressed than CTLA-4. Apart from T cells, PD-1 is also induced on B cells and natural killer (NK) cells and limits their anti-tumor ability[13]. Therefore, PD-1 blockade can not only enhance the activity of T cells by also enhance the lytic function of NK cells in tissue and tumor microenvironment. As of March 2022, six PD-1 or PD-L1 inhibitors and one CTLA-4 inhibitor have been approved for treating various types of cancer. The therapy significantly prolonged the survival of patients, but it induced side effects in 86-90% of patients by activating autoimmune reactions and many of them were severe or life threatening[11]. Another big challenge is that the response rate remains very low, especially for the tumors lacking T cell infiltration. In addition, tumors have diverse mechanisms of immunosuppression that require new approaches for more precise treatments. To improve the response rate and minimize the side effects, several strategies might be beneficial including developing new CPIs, combination therapies of CPIs and other immunotherapies, or using advanced drug delivery systems, as will be underlined in the following parts of this thesis.

1.1.2 ***Adoptive T cell therapy***

Adoptive T cell therapy takes T cells from the cancer patient and transfers them back to the patient after *in vitro* expansion or functional modification, which produces the required number and specificity so that the T cells can directly recognize and kill tumor cells. There are three main types of adoptive T cell therapy: 1) Tumor-infiltrating lymphocytes (TILs), 2) T cells with engineered T cell receptors (TCRs), or 3) T cells engineered to express chimeric antigen receptors (CARs).

TILs are naturally enriched in tumors to recognize and kill cancer cells, and they showed stronger cytotoxicity activity after stimulation with IL-2 *in vitro*[16]. Although adoptive therapy with TILs exhibited a response rate of more than 50% in melanoma treatment[9], in some cases,

transferred T cells lacked sufficient specificity or numbers to eliminate a tumor[17]. Instead of relying on the innate T cell infiltration, autologous lymphocytes from the blood can be genetically engineered to express TCR or CAR with the desired specificity[18]. TCR T cells are engineered with a high affinity to tumor-associated antigens (TAAs) presented by MHCs, and they have been tested for both hematological and solid cancers[19]. But T cells have not been as successful as TILs in melanoma, with only 2/18 of patients showing partial response in a clinical trial[20]. One of the key mechanisms of tumor escape is that tumors can lose or downregulate MHC molecules, thus hiding from being recognized by TCR T cells[21]. Furthermore, the high-affinity TCR caused on-target off-tumor side effects by attacking healthy cells that express low-level TAAs[22].

Unlike TCR T cells, CAR T cells are MHC-independent and can directly recognize the targeted antigen on tumor cells. Having advanced to the third generation, CARs are hybrid receptors composed of an extracellular antigen-specific scFv domain, a TCR complex CD3-derived immunoreceptor tyrosine-based activation motif (ITAM) signaling chain, and a co-stimulatory domain[6]. The antigens on the membrane surface of tumor cells bind to the extracellular domain, activate both the first signal and second signal chain for T cell response. With various target antigens being studied, CAR-Ts targeting CD19 in B cell leukemias and lymphomas have seen the most success and two products have been approved for clinical use by FDA. Recently, A follow-up study examining two of the first leukemia patients receiving CAR-T immunotherapy 10 years ago has shown they remain free of cancer cells, leading researchers to declare that they have been cured by the therapy.

The stunning results have encouraged intense research to develop more effective T cell therapies. However, there remain some major challenges to overcome. The production procedure of T cell therapy is complex, expensive, and time-consuming because a ‘new drug’ is required for every patient; T cells can cause severe side effects of cytokine release syndrome and neurotoxicity[23]; moreover, the efficacy of these T cells is limited by the suppressive TME and tumor antigen heterogeneity in solid tumors[24].

1.1.3 *Small molecule immunomodulators*

While biological drugs are currently dominating in cancer immunotherapy, small molecule drugs (SMIs) are gaining greater attention with the increasing understanding of intracellular signaling pathways and kinase targets. SMIs have some unique advantages over large

molecules. They generally have a shorter half-life which favors acute and reversible action and reduce the risk of lasting systemic side-effects[25]; in addition, SMIs have better penetration into the tumor and hold the ability to cross the cell membrane to access intracellular targets that cannot be targeted by large molecules such as mAbs[25], and they engage classic targets of large molecules in different mechanisms. These features make them beneficial both as monotherapy and in combination with other cancer immunotherapies such as CPIs[26], cancer vaccine[27], and T cell therapy[28]. Zanden et al[29]. has made a comprehensive review of the SMIs that target molecules correspond to diverse receptors or enzymes involved in the intracellular immunomodulation signal transduction, which can modulate the immune response in every step in the cancer-immunity cycle.

To begin with, SMIs include chemotherapeutics that induce immunogenic cell death, release antigens to facilitate T cell recognition. Then pathogen-associated molecular patterns (PAMPs) or danger-associated molecular patterns (DAMPs) activate DCs through pattern recognition receptor (PRR). Thereby agonists of PRR are being pursued as potential immunotherapies or adjuvants to prime responses following tumor cell vaccination to enhance DC activation and maturation. The most studied PRR agonists are for the 13 toll-like receptors (TLRs), which are expressed on a variety of immune cells including DCs, B cells, macrophages, NK cells, and T cells either on the surface or in endosomes (TLR3, 7, 8, and 9)[30]. A TLR7 agonist Imiquimod has been approved by FDA for treating basal cell carcinoma, with other compounds based on the same structure (imidazoquinoline derivatives) under investigation for treating solid cancer, based on their role as vaccination adjuvants.

Another PRR that SMIs target is the stimulator of IFN genes (STING). It locates on the endoplasmic reticulum membrane, binds to, and is activated by cyclic dinucleotides (CDNs) produced by cyclic-GMP-AMP synthase (cGAS) when DCs take up the DNA released by necrotic tumor cells[31]. Activation of STING leads to the expression of IFNs and cytokines that promote DC activation and T cell priming. The pathway can be activated by synthetic CDNs and their phosphorothioate derivatives. Severa STING agonists are undergoing clinical trials as vaccine adjuvants or in combination with CPI therapies (e.g., ADU-S100, MK-1454)[32].

Small molecules can also target PD-1/PD-L1 as a new strategy for CPI therapies other than using mAB. A series of compounds from BMS (BMS-103, -202, -1001, etc.) was reported to induce PD-L1 dimerization on the cell surface, which leads to PD-L1 internalization[33]. Receptor internalization is dose-dependent and correlates with $CD8^+$ T cell infiltration and anti-

tumor efficacy in a syngeneic mouse model. Another small molecule CPI (CA-170) is currently being evaluated in a Phase I clinical trial for patients with advanced solid tumors and lymphomas. In addition to inhibiting the surface ligand, some SMIs work by interfering with the PD-1/PD-L1 signal transduction like SHP2 inhibitors[34] or the transcription of PD-1 genes[35]. Small molecule CPIs are supplementary to antibody-based CPIs as they inhibit the pathways in different mechanisms and are more controllable regarding bioavailability.

Furthermore, SMIs are used to target immunosuppressive factors in the TME like MDSCs, Tregs, and tumor-associated macrophages (TAM), which aggravate T cell dysfunction and impair the effects of immunotherapy. One example is the inhibition of IDO1, an enzyme involved in the signaling pathway of Treg cell expansion and MDSCs recruitment[36]. Epacadostat, a specific and potent IDO1 inhibitor, was tested in a clinical trial in combination with pembrolizumab (anti-PD-1 mAb) and showed promising results for patients with multiple advanced solid tumors but increased anti-PD-1 efficacy was not seen in melanoma patients. Tregs in the TME can also be targeted by A2A, which binds to adenosine and results in the expansion of Tregs; and retinoic acid receptor-related orphan receptor gamma (RORγt), which is a transcription factor involved in the proinflammatory IL-17 pathway in T cells. Small molecule A2A antagonists (e.g. CPI-444, AZD4635, Vipadenant, Preladenant, and PBF-509)[32] and RORγt antagonists (e.g. LYC-53772, SR1078)[37,38] are developed to relieve the Treg-mediated immune suppression in the TME. They have shown the effects of inducing the production of cytokines and chemokines, decreasing the proliferation of Tregs, and revoking immunosuppression by tumor cells in vitro and on mice models, and some moved further to phase I/II clinical trials[36].

Another major class of SMIs for cancer immunotherapy are the broad spectrums of kinase inhibitors including but not limited to PI3K, TGFb Kinase, BTK and ITK, VEGF, FAK, and MAPK pathway inhibitors[39]. These kinases play multiple roles in the cellular activities of both tumor cells and immune cells, and a comprehensive understanding of the functions is required for designing drugs targeting them to improve the benefits of cancer treatment.

Similar to biological drugs, SMIs also face systemic cytotoxicity due to uncontrolled immune activation. In addition, as they are used in combination with other therapies such as anti-PD-1 antibodies and cancer vaccines, the timing of administration and accumulation locations of the SMIs will significantly affect the outcome. Advantages lie in that small molecules are easier for modification and formulation. A study showed phospholipid-conjugated TLR7 agonist

widens the therapeutic window and reduces off-target receptor binding compared to the original compound, leading to tumor-specific $CD8^+$ cell-dependent adaptive immune responses that suppressed late-stage metastatic tumor growth in the lungs[39]. Nano-drug delivery technologies are also promising for addressing these limitations by improving the pharmacokinetic profiles and intracellular delivery[40].

1.2 Nanomedicines for cancer immunotherapy

The immunotherapies described above (checkpoint inhibitors and small molecule immunomodulators), and undescribed here (e.g., cytokines, cancer vaccines), each face delivery challenges in common or unique ways. The success of most cancer immunotherapies relies on the engagement with their targets at the right time and site, otherwise, they may cause significant autoimmunity-related side effects upon systemic administration. In this perspective, nanomedicines utilizing nanoparticle-based drug delivery systems (DDS) may provide great potential to enable targeted and controlled delivery to desired tissues or cell types[41], and increase the safety and therapeutic efficacy of cancer immunotherapies.

Nanoparticles (NPs) are structures with sizes typically ranging from 1-100 nm in at least one dimension. In practice, the concept is broadened to particles that are up to several hundred nanometers in size. There is a variety of NPs composed of different materials, structures, and physiochemical properties, among which liposomes, solid lipids nanoparticles, dendrimers, polymers, silicon or carbon materials, and magnetic nanoparticles are the most common examples of nanocarriers that have been tested as drug delivery systems (**Figure 1.3**). Nanomaterials used for drug delivery must be biocompatible. They can be loaded with active drugs such as nucleic acids, peptides, proteins, or small molecules by adsorbing or covalently attaching the drugs to the surface of the nanocarrier or encapsulating the drugs inside[42]. The nanocarrier can improve the drug solubility and protect them from degradation. Once the nanomedicine reaches the desired tissues, the therapeutic agents are released. A controlled release of drugs from the nanocarriers can be achieved through changes in the physiological environment such as temperature, pH, osmolality, or via enzymatic activity. Furthermore, the surface of NPs can be modified to incorporate long-chain polymers such as poly (ethylene glycol) (PEG) through a process called PEGylation[43]. The PEGylated NPs prolonged the circulatory half-life of drugs because the PEG molecules form a tight hydration layer around the NPs, hindering the protein adsorption and subsequent uptake by the mononuclear phagocyte system.

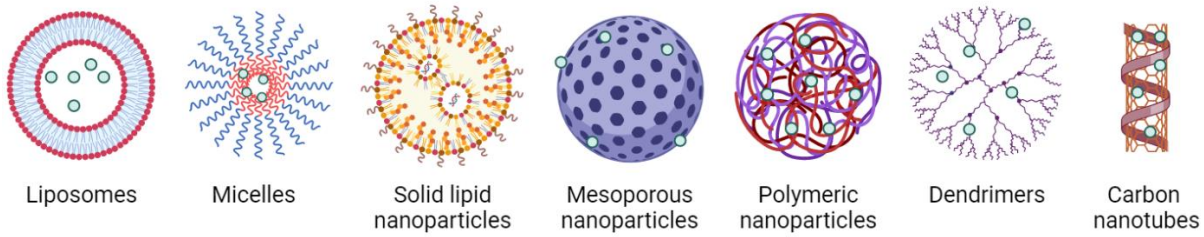

Figure 1.3 Nanoparticles as drug delivery systems.

1.2.1 *Passive and active targeting of nanomedicines*

Nanomedicines were first used in cancer therapy to modify the drug pharmacokinetics of chemotherapies and improve tumor accumulation through enhanced permeation and retention (EPR) effect[44]. The EPR effect is based on the physiological abnormalities in tumor vasculatures and size properties of NPs. Compared to normal vasculatures, tumor vessels have highly irregular structures and are dysfunctional with greater permeability for macromolecules. NPs with a size of 10-100 nm are too large to enter healthy tissue through the vasculature but can permeate through the dysfunctional tumor vasculatures into tumors. Once inside the tumor, the impaired lymphatics prevent the NPs from being cleared, thus the NPs accumulate there. For decades, the EPR effect has been exploited extensively as a way of passively targeted delivery of nanomedicines to tumors[45].

Nanomedicines can further be functionalized by targeting antibodies and small molecules ligands such as folic acids, peptides, etc. to actively target tumor-associated receptors. Tumor cells often upregulate certain markers as released protein or cell surface receptors that can be recognized by the targeting molecules on NPs, leading to the binding or internalization of NPs to tumor cells[46].

Although the passive and active delivery of nanomedicines sounds promising by concept, the reality is that only 0.7% (median) of administered NPs could reach tumors through the EPR effect and the ratio is still less than 1.0% even with active targeting, according to a comprehensive review that analyzed 117 studies of nanomedicine delivery in the last 30 years[47]. The low delivery efficiency of NPs seriously hindered the clinical translation of nanomedicines. There are a lot of important factors such as the sizes, administration routes that significantly affect the biodistribution of NPs[48].

Unlike traditional cytotoxic drugs that rely on accumulation as much as possible to kill tumor cells, cancer immunotherapies may not need to distribute through the entire tumor to achieve the therapeutic effect. Instead, immunotherapies act by a series of complex interactions between the innate and adaptive immune cells in tumors and lymphoid organs, which can lead to up-scale immune reactions. Immune cells have the innate ability to penetrate through physiological barriers such as the BBB and the blood-testis barrier[49], and immune cell-mediated cytotoxicity is often highly targeted because of antigen-specific responses. Utilizing a nanomedicine strategy for cancer immunotherapy may reveal a different story than traditional chemotherapies.

1.2.2 *Nanomedicine delivery for immunotherapy*

Promoting immunogenic tumor cell death.

Traditional anti-tumor treatments like chemotherapy and radiotherapy that aim to directly kill tumor cells can also enhance antitumor immunity. The mechanism lies in that these treatments may induce immunogenic cell death (ICD), which is associated with the release of tumor antigens and danger signals (e.g., cytosolic DNA) capable of activating DCs via PRRs, such as TLRs and cGAS/STING[50]. The ICD generates vaccine-like functions to activate the immune response to tumors. Nanomedicine can promote the ICD by increasing the tumor accumulation of the cytotoxic agents and provides the modality for combination immunotherapies. For example, using doxorubicin (DOX) loaded, highly integrated mesoporous silica nanoparticles (DOX@HIMSNs) for systemic treatment of highly metastatic triple-negative breast cancer (TNBC), it was found that the therapeutic effect of DOX@HIMSN was only partially attributed to its anticancer cytotoxicity, but mainly due to that DOX@HIMSN could induce anticancer immune responses including dendritic cell (DC) maturation and antitumor cytokine release[51]. The clinically approved liposomal formulation of DOX, Doxil, was evaluated for its ability to boost the antitumor response of different cancer immunotherapies including CPIs (anti–PD-L1, PD-1, and CTLA-4 mAbs) and TNF receptor agonists (OX40 and GITR ligand fusion proteins) in syngeneic mouse models[52]. In a preventative CT26 mouse tumor model, both doxorubicin and Doxil synergized with anti–PD-1 and CTLA-4 mAbs. In vivo pharmacodynamic studies showed that Doxil treatment decreased the percentage of tumor-infiltrating regulatory T cells, and in combination with anti–PD-L1, increased the percentage of tumor-infiltrating CD8 + T cells. In the tumor, Doxil administration increased CD80 expression on mature dendritic cells. Nanomaterials can be designed to directly interact with external energy sources, allowing

amplification of ICD induced by treatments such as radiotherapy, photodynamic therapy, photothermal or magnetic hyperthermia[53].

Targeting antigen-presenting cells and T cells.

Nanoparticles can also be designed to target immunotherapy agents directly to antigen-presenting cells and T cells[54,55]. Immune cells such as T cells have the innate ability to actively migrate to tumors, and instead of delivering the therapeutic agents to tumors, immunotherapeutic drugs can trigger and boost immune responses by stimulating APCs or T cells in the blood, lymphoid tissues. In one study, an aliphatic-polyester (poly (lactic-co-glycolic acid) (PLGA) NP-based vaccine was developed to target APCs and improve T cell priming[54]. The NPs carrying ovalbumin (OVA) antigen and TLR agonist CpG interacted with DCs and were internalized by 50-60% in vitro and 30-40% in vivo, respectively. The formulation of NPs had a significant impact on the activation of APCs as indicated by the level of CD86, MHC-I, and MHC-II. The NPs with the optimal APC activation efficacy induced profound antigen-specific response of $CD4^+$ and $CD8^+$ T cells *in vivo*[54]. In another example, T cells were targeted by PLGA-NPs encapsulating either TGF-β inhibitor to restore T cells function or TLR-7/8 agonists to the TME to recruit tumor-infiltrating $CD8^+$ T cells[55]. The NPs were modified with anti-PD-1 antibody fragments on the surface to target PD-1^+ T cells in the circulation and tumor. The targeted delivery of TGFβ inhibitor delayed tumor growth and extended the survival of colorectal tumor-bearing mice, whereas free drugs showed no effect at the same doses. Delivering TLR7/8 agonist to the TME promoted the tumor-infiltration of CD8+T cells and sensitized tumors to subsequent anti-PD-1 therapy[55]. Targeted delivery of immunotherapeutic nanomedicine to tumor-infiltrating immune cell subsets, rather than targeting tumor cells is an attractive strategy to improve the anti-tumor response.

Intracellular delivery of hydrophilic SMIs and nucleic acids.

Another major application of NPs for drug delivery is to promote intracellular delivery. It is especially interesting for mRNA vaccines as they have shown great effect for covid-19, and cancer therapeutic mRNA using the lipid nanoparticle technology is currently being intensively explored[56]. In cancer immunotherapy, nanomaterials are used for the delivery of nucleic acids that encode immunomodulatory proteins, and SMIs such as the agonists of endosomal TLR and STING signaling, to the cytosol. The hydrophilic nature and negative charge prevent these molecules from being taken up by cells and escaping from the endosome into cytosol[57].

Furthermore, for in vivo delivery, they must diffuse through the compact extracellular matrix to reach the target cells and mRNA drugs must avoid degradation by endonuclease[9]. Nanomaterials can improve cell uptake and enable the escape from the endosome. An example is delivering mRNA to T cells. Researchers have screened libraries of ionizable lipid nanoparticle (LNP) formulations with varied excipient compositions for improved mRNA delivery to T cells with low cytotoxicity[58]. When compared to electroporation, the top formulation induced comparable CAR expression in primary human T cells with reduced cytotoxicity while demonstrating potent cancer cell killing. The results showed the impact of excipient optimization on LNP performance in mRNA delivery for T cell engineering. A recent study demonstrated direct in vivo generation of transient antifibrotic CAR T cells by delivering modified mRNA in T cell-targeted LNPs[59]. Approaches using polymer NPs and liposomes have also been reported for encapsulating the cyclic dinucleotide STING agonist and TLR agonists for cytosol delivery to the targeted cells[60,61]. Another appealing approach is the use of synthetic polymers that directly engage the signaling pathways. A polyvalent STING agonist, which is a pH-sensitive polymer that activated innate immunity pathways through the polymer-induced formation of STING–PC7A condensates has been described[62]. Compared to the natural STING ligand, the polymer stimulated a prolonged pro-inflammatory production and induced an anti-tumor response of $CD8^+$ T cells.

1.3 Immune cell-mediated drug delivery

The new advanced drug delivery systems have been under development to increase delivery efficiency and safety. One of the most interesting approaches is living cells-based drug delivery. Circulatory cells including red blood cells (RBCs), monocytes, platelets, and lymphocytes have natural advantages for drug delivery such as good biocompatibility, long-circulating in the bloodstream, inherent targeting properties, and the ability to migrate through biological barriers[63]. In the context of cancer, immune cells are continuously recruited to the TME that can be either anti- or pro-tumorigenic. Tumor eradication requires the anti-tumor response from infiltrated lymphocytes e.g., T cells, NK cells, and tumor escape also relies on the recruitment of immunosuppressive immune cells. Unlike free drug molecules or nanoparticles, immune cells do not rely on passive diffusion to reach the target tumor site but traffick into TME through a migration cascade consisting of some sequential steps of leukocyte-endothelium or leukocyte-leukocyte interactions in postcapillary venules (small veins with a diameter of about 50μm which are located directly after the sites of increased vascular permeability during

inflammation) (**Figure 1.4**)[64,65]. Furthermore, they can find metastatic cancers and migrate deep into the core of solid tumors, which are hardly reachable for NPs. Researchers have delivered drug-loaded NPs, as well as magnetic and photodynamic NPs with immune cells by either encapsulating the NPs inside cells or attaching them to the cellular surface. However, living cell-mediated drug delivery is a relatively complex system that requires consideration of multiple parameters including and not limited to cell type, payload, cell loading approach, release rate from nanoparticles for achieving the optimal outcome.

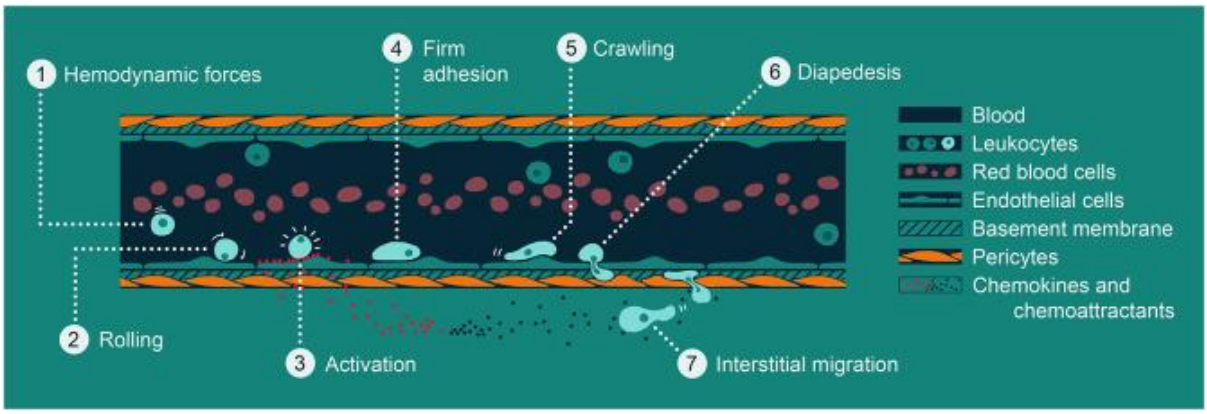

Figure 1.4 The migration cascade of leukocytes in normal postcapillary venules. The figure is adapted from Combes et al.[65]

1.3.1 *Choice of immune cells for drug delivery*

Red blood cells

Red blood cells (RBCs) are ideal drug carriers thanks to their long-circulation time, simple and flexible structure as well as large quantity in the body. RBCs are biconcave disk-shaped cells (7μm diameter and 2μm thick), lacking organelles and nucleus while rich in hemoglobin in the cytoplasm. They compose more than 99% of blood, transport oxygen to all parts of the body, and can circulate for up to 120 days[66]. The high deformable and flexible structure enables RBCs to reach almost all vascularized tissues. However, RBCs do not normally have migration machinery to extravasate from the circulation to tissues. They are cleared by the MPS in the spleen and liver[66]. Avoiding membrane alterations due to the drug loading protocols, incorporating the CD47 marker on the surface as a "do not eat me" signal can potentially prevent RBC elimination [63]. As drug carriers, RBCs have been explored to load drugs inside the cuvette or attach nanoparticles on the surface for prolonged circulation[67]. It has also been tried to target RBCs to specific organs by incorporating magnetic materials into RBCs and then

using an external magnetic field to lead them to the targeted organ or functionalizing the surface RBCs with targeting moieties[65]. In an example of using RBCs for delivering doxorubicin for cancer therapy, RBCs obtained similar therapeutic effects as the liposomal drug formulation; however, it showed differences in biodistribution as they accumulated more in the liver, spleen, and lungs instead of in the heart and skin, resulting in fewer adverse side effects[68]. RBCs as drug delivery carriers offer the opportunity to alter the biodistribution and pharmacokinetics of free or nanoparticulate drugs, but RBCs are not likely to deliver drugs to extravascular targets due to their non-extravasate property.

Monocytes and macrophages

Monocytes constitute about 10% of the circulating leukocytes in humans that ensure rapid recruitment during infection and inflammation[69]. Monocytes are precursors to macrophages and are typically stored in the spleen and remain in circulation before differentiating into macrophages to enable constant macrophages replenishment. In the context of tumors, monocytes are recruited by the chemoattractant gradient containing inflammatory cytokines, CSF1, CCL2, CXCL12, and VEGFA to the tumor[49]. Upon crossing the endothelial basement membrane, monocytes differentiate into macrophages, which are referred to as tumor-associated macrophages (TAMs). Monocytes have many advantages for drug delivery over nanoparticles such as the ability to migrate to the inflammation signals including tumors, cross the blood-brain barrier to reach the disease sites, and reach the hypoxic areas of tumors[70]. In addition, monocytes/macrophages are phagocytes that are prone to uptake NPs. These unique features have inspired the use of monocytes and macrophages as drug delivery carriers of nanoparticle-encapsulated therapeutic reagents for improving the distribution and efficacy. In one example, delivery of liposomal DOX by macrophages was demonstrated in both subcutaneous and metastasis xenograft tumor models[71]. By MR imaging, researchers confirmed that macrophages containing iron oxide could migrate and infiltrate deeply into tumors. The DOX encapsulated liposomes were loaded into macrophages and successfully delivered to tumors while preserving the activity of the cell carrier and cytotoxicity of DOX, achieving an improved antitumor effect. Interestingly, macrophages also have the direct tumor-killing ability in an antigen-independent and immediate manner, giving them the potential to be used as cell therapy. However, in the case of cancer, TAMs tend to polarize to a tumor-promoting M2 phenotype due to the immunosuppressive TME, which is associated with tumor growth, angiogenesis, chemotherapy resistance, and metastasis[72]. To address this issue in

adoptive macrophages therapy, backpack particles were prepared to load macrophages with IFN-γ to regulate the cellular phenotype *in vivo*[73]. The backpack particles were prepared with biocompatible polymers (PLGA, PVA), and each contain a cell-adhesive layer comprised of hyaluronic acid modified with an aldehyde (HA-Ald) and poly(allylamine) hydrochloride (PAH) to enable macrophage adhesion. The results demonstrated backpacks evade phagocytosis for several days and release cytokines to stimulate durable polarization of macrophages toward antitumor phenotypes. Adoptive transferring of backpack-loaded macrophages reduced metastatic burdens and slowed tumor growths compared with the treatment of an equal dose of macrophages with free cytokines. It represents a potential new solution to control and maintain phenotypes of adoptive cellular immunotherapies.

T cells and B cells

Lymphocytes including T cells, B cells, and NK cells make up the adaptive immune system. B cells originate from the bone marrow and are responsible for humoral immunity. Upon antigen exposure, B cells traffic to the secondary lymphoid organs, such as the lymph nodes, and differentiate into plasma cells to synthesize antibodies[74]. The plasma cells can go back to systemic circulation to reach the remote infection/inflammation sites. T cells instead, originate from the thymus and play a central role in cell-mediated immunity. T cells can be divided into two major subsets: (i) cytotoxic T cells that are responsible for destroying infected cells ($CD8^+$ T cells) and (ii) helper T cells that facilitate the maturation of B cells and activation of cytotoxic T cells ($CD4^+$ T cells)[75]. After leaving the thymus, naïve T cells that have not been activated by APCs circulate throughout the body, migrating and localizing in secondary lymphoid organs. Naïve T cells can enter the lymph nodes within high endothelial venules (HEV) or through the afferent lymphatic vessel via L-selectin and CCR7-mediated interactions with the corresponding ligands[76]. Once activated in the lymphoid tissues, T cells change the surface expression of functional molecules such as downregulating CCR7, and upregulating adhesion receptors to acquire the capacity to migrate into non-lymphoid tissues. The location where activated T cells migrate to is modulated by the acquired adhesion receptors/ligands on T cells as well as the corresponding adhesion ligands/receptors in the tissues where the priming occurs. Moreover, T cells can proliferate into large quantities upon activation and produce long immune memory. As described in 1.1.2, adoptive T cell therapies have been developed based on the functions of T cells to detect and destroy cancer cells. However, the immunosuppressive TME exerts big obstacles in T cell therapies by preventing T cell proliferation, persistence, and

cytotoxic ability. T cells have been used in several cases for delivering therapeutic nanoparticles containing killing drugs such as photothermal therapy (PTT)[77], chemotherapies[78,79] or immunomodulators80, and adjuvant cytokines[81] that support T cell therapy. For example, lipid nanoparticles containing cytokines (IL-15 and IL-21) were tethered to the surface of melanoma-specific Pmel-1 effector T- cells using a thiol-reactive maleimide group to treat melanoma lung/bone marrow tumors as illustrated in **Figure 1.5** [82]. Intravenous infusion of Pmel-1 effector T cells loaded with IL-15 and IL-21 NPs promoted T cell expansion *in vivo* and was able to eradicate B16F10 melanoma tumors in mice.

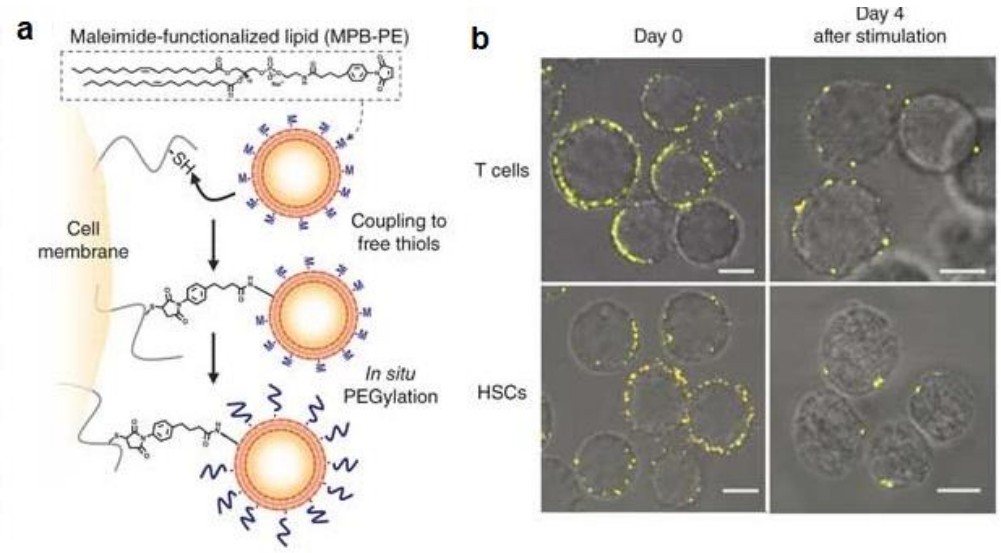

Figure 1.5 Conjugation of nanoparticles to the cell surface via maleimide-thiol reaction. **(a)** Maleimide-thiol cell surface conjugation of lipid nanoparticles. MPB-PE: 1,2-dioleoyl-sn-glycero-3-phosphoethanolamine-N-[4-(p-maleimidophenyl) butyramide]. **(b)** Confocal microscopy images of $CD8^+$ effector T cells and hematopoietic stem cells (HSCs) immediately after conjugation with fluorescent DiD-labeled multilamellar lipid nanoparticles (left) and after 4 days of in vitro expansion (right). Scale bars, 2 μm. The figure is adapted from Stephan et al[82].

Other circulatory cells

A variety of other cell types also have the potential as platforms for the cellular delivery of nanoparticles. Dendritic cells have been used in cell therapies as therapeutic cancer vaccines[83]. Natural killer cells attack and kill tumor cells independent of tumor-specific antigens, thus are explored to be an alternative to T cells. Conjugating nanoscale TRAIL liposomes to human natural killer cells was demonstrated to enhance their endogenous therapeutic potential in killing cancer cells cultured in engineered lymph node microenvironments[84]. These cells carry

out essential functions in normal biological processes and anti-cancer immune responses. The use of cell-mediated drug delivery has created new possibilities for these cells. For this purpose, the first step is to incorporate nanoparticles either inside or on the surface of the carrier cells.

1.3.2 *Incorporation of nanoparticles to cells*

Cells are composed of biomolecules including phospholipids, cholesterol, glycolipids, glycoproteins, and proteins. The structure of cells and biological components enable the selection of a range of techniques to incorporate nanoparticles either to their surface or inside cells. As illustrated in **Figure 1.6**, the strategies that have been used for loading live cells with NPs can be divided into four main classes, (i) surface adsorption, (ii) ligand-receptor mediated non-covalent conjugation, (iii) covalent conjugation, and (iv) internalization. Each method offers unique advantages and disadvantages that should be considered based on the cell types and aim of drug delivery.

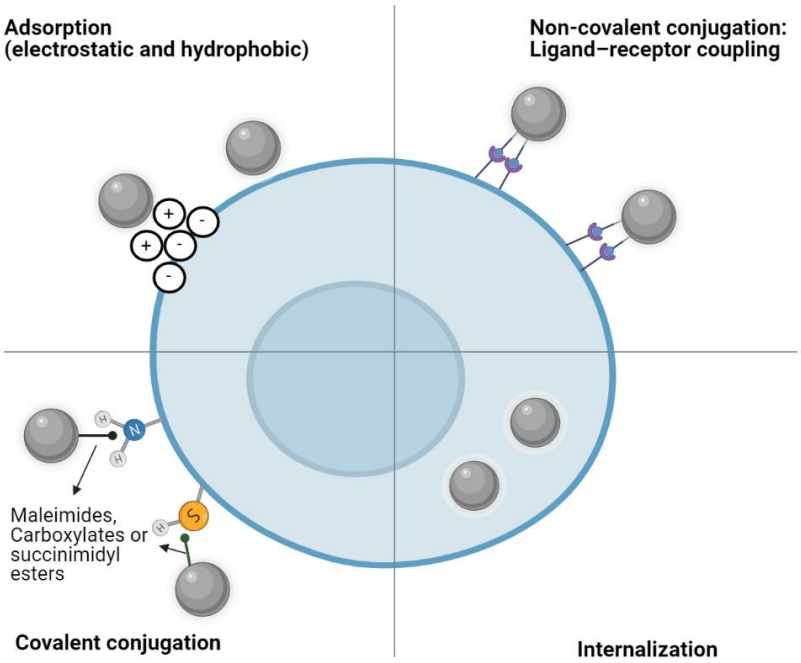

Figure 1.6 Methods for nanoparticle incorporation to cells.

Surface adsorption of nanoparticles is the simplest method. It can happen through electrostatic interactions or hydrophobic interactions. The plasma membrane of cells is negatively charged contributed by the phosphate, carboxylate, and sialic acid groups. Thereby cationic nanoparticles can be adsorbed to the surface[67]. However, positively charged materials tend to be toxic to cells, especially at high doses[85]. The adsorption of nanoparticles by hydrophobic interactions (van Der Waals forces and hydrogen bonding) has also been studied on RBCs[63].

Passive adsorption of nanoparticles on cells is simple since it requires the least modification of the cells and NPs. But the binding force between NPs and cells is weak, which may lead to the premature detachment of the cargo before arriving at the target tissue.

Ligand-receptor mediated non-covalent conjugation is an alternative approach to non-specific passive adsorption. Cells present multiple receptors on the surface to mediate certain functions, which allows the conjugation of synthetic NPs decorated with the cognate ligands in a specific and more stable way. The approach was first explored by Rubner *et al*. who used CD44-hyaluronic acid (HA) and Fc Receptor-Fc interactions to conjugate polyelectrolyte multilayer (PEM) patches to cells[86,87]. A superparamagnetic PEM patch was attached to the membrane of T and B lymphocytes using CD44-HA interactions. After patch attachment, B cells responded to an applied magnetic field, and T cells continued to migrate on ICAM-coated surfaces mediated by chemokines[86]. The ability of antigen-specific lymphocytes to home to and accumulate in antigen-bearing tissues potentiated the applications of this technique in immunoengineering, such as bioimaging or lymphocyte-directed drug delivery vehicles. Besides the HA-CD44 binding, they have also used mouse IgG antibodies to bind to the Fc receptors of immune cells to decorate cell surfaces with backpacks. The antibodies were introduced onto a final PEM film through biotinylation[87]. In theory, utilizing ligand-receptor interactions can be a platform technology to attach NPs to various cell types by simply changing the attachment ligand on the particle surface according to the targeted receptor. However, different receptors may lead to very different surface half-life by varying the binding affinity or initiating cell endocytosis[81]. In a study where Li *et al.* used monoclonal antibody-functionalized liposomes to screen for slowly internalizing T cell surface proteins that could be used as specific anchors for the cytokine nanogel backpack[81]. Surface receptors including CD2, CD8, CD11α, CD90, and CD45 were tested as the anchor, and targeting most of the receptors led to substantial internalization of liposomes within a few days, with the only exception that liposomes targeting CD45 exhibited prolonged cell surface retention. The phenomenon can be used for selecting the targeting receptor depending on whether the drugs act after internalization or by staying on the surface. Whereas this approach has shown success in attaching multiple particles to cells, there remain some particular challenges such as the control of site-specific conjugation and orientation of antibody or antibody fragment ligands; the insufficient binding affinity between ligand and receptor; in addition, most receptors are expressed on more than one cell types and involved in crucial biological processes, which can

cause non-specific binding to undesired cell types or the triggering of undesired biological responses upon ligand-receptor interaction[63].

Covalent conjugation utilizes reaction groups on the cellular surface to form a covalent bond with a complementary partner group on the surface of NPs. Cell surfaces are rich in proteins and glycocalyx, providing reaction groups mostly in the form of amines and thiols that can be targeted using activated esters and maleimides[88]. The abundant thiol groups on T cells have been used by various studies to covalent conjugate lipid or polymer-based NPs to their surface via maleimide groups[80,89,90]. Using this approach, cytokines[82], NPs containing SMIs[80], or nucleic acid [91] were loaded to T cells without causing cytotoxicity or affecting key T cells' functions by the carrier. The amount of thiol groups is related to the status of T cells activation and the conjugation is reversible in reducing conditions. The thiol-mediated covalent bonding showed prolonged surface retention and avoided particle internalization by T-cells, in contrast with nanoparticle attachment to some receptors on T-cell surfaces. In addition, the stronger binding force provided by covalent bonds prevents the detachment of NPs when migrating through the endothelium, which is required for cell carriers like T cells, monocytes, and macrophages. Apart from the naturally expressed groups, exogenous groups such as azide can be incorporated into the cell surface through metabolic glycoengineering. The incorporated groups allow the conjugation of complimentary groups on the NPs or small molecules[92]. When choosing a reaction for covalent conjugation, the conjugation site on the proteins must not negatively affect the cell activity of the protein. The reaction conditions should also be considered since reaction kinetics are affected by the concentration of cells and NPs as well as pH and temperature.

Internalization of NPs is another technique that normally relies on the natural phagocytosis ability to take up nanomaterials. Thereby this approach is typically utilized to load macrophages or monocytes, by incubating NPs with cells ex vivo for a sufficient time to allow cellular internalization[93]. It has been used to incorporate gold nanoparticles[93], nanozymes[94], or echogenic polymer/C5F12 bubbles and doxorubicin-loaded polymer vesicles[95] into macrophages and monocytes. Notably, even cells that do not have a phagocytosis nature can internalize NPs due to the small size[96,97] or with the help of cell penetration peptides or internalization antibodies[98]. It is particularly required in the cases when drugs act on intracellular targets, e.g. mRNA, intracellular kinases, or danger signals (TLR, STING), thus the NPs need to be designed such to allow cellular internalization and delivery of the active

compound to the appropriate organelle. This method typically does not require modification of cells or NPs and leaves the cell membrane unaltered. It can potentially protect the nanoparticles from interacting with non-target tissue *in vivo*. However, biodegradable nanoparticles can be degraded within the cell, resulting in premature drug release.

1.3.3 ***Challenges and future perspective***

Immune cell-mediated drug delivery has been a very exciting and rapidly evolving research topic. The variety of cell types and cell loading techniques, especially the immerging of more efficient and biocompatible cell surface conjugation chemistries facilitate the generation of nanoparticle decorated cells for the specific indication. Conceptually, cell-mediated drug delivery can enhance drug targeting and reduce off-target delivery. However, it is still in the early stage and most studies have been performed in small animals, which may end up very differently in humans. Technically, there are challenges regarding the cell loading methods that whether the cell functions remain uncompromised after loading, and whether the NPs can be stably loaded in cells in the circulation upon exposure to the multiple barriers and interactions with other cells or proteins[63]. Furthermore, the release of the drug and/or drug-loaded NPs from the cells after arriving at the target site needs to be well-tuned to prevent premature drug release or insufficient drug release for the optimal effect. The principles for stimuli-responsive drug release from nanoparticles can in theory also be applied in this context. There is a wide range of endogenous and exogenous stimuli that have been well illustrated for triggering targeted drug release in the tumor microenvironment[99]. For example, in thermo-responsive systems, magnetically responsive systems, ultrasound- or light-triggered drug delivery, as well as systems responsive to the lowered interstitial pH, the difference in redox status or enzymes have been developed. When using immune cells for drug delivery, the cells are not only used to mediate the delivery of NPs or active compounds but also play an important therapeutic role. This is particularly exemplified in T cells in the context of adoptive T cell therapy, which combines their direct cytotoxicity against tumor cells and the ability to enhance drug delivery. Taken together the advantages and challenges of immune cell-mediated drug delivery, provide a new perspective as a novel strategy to address the current limitations of nano-drug delivery. Further studies can be devoted to exploring the application of the systems and bringing it forward with more advanced cell, nanoparticle modification techniques, and drug targets.

1.4 References

1. Shankaran, V., H. Ikeda, A. T. Bruce, J. M. White, P. E. Swanson, L. J. Old, and R. D. Schreiber. IFNg and lymphocytes prevent primary tumour development and shape tumour immunogenicity. *Nature* **410**, 1107–1111 (2001).
2. Dunn, G. P., Old, L. J. & Schreiber, R. D. The three Es of cancer immunoediting. *Annual Review of Immunology* vol. 22 329–360 (2004).
3. Fridman, W. H. From Cancer Immune Surveillance to Cancer Immunoediting: Birth of Modern Immuno-Oncology. *The Journal of Immunology* **201**, 825–826 (2018).
4. Rosenberg, S. A. Human Cancer IL-2: The First Effective Immunotherapy for human cancer. *J Immunol References* **192**, 5451–5458 (2014).
5. Chen, D. S. & Mellman, I. Oncology meets immunology: The cancer-immunity cycle. *Immunity* **39**, 1–10 (2013).
6. Sharma, P., Hu-Lieskovan, S., Wargo, J. A. & Ribas, A. Primary, Adaptive, and Acquired Resistance to Cancer Immunotherapy. *Cell* (2017) doi:10.1016/j.cell.2017.01.017.
7. Dinarello, C. A. Historical insights into cytokines. *Eur. J. Immunol* S34-35 (2007) doi:10.1002/eji.200737772.
8. Smalley, R. v. Interferon in the treatment of cancer. *The Medical clinics of North America* **Suppl**, 31–36 (1986).
9. Riley, R. S., June, C. H., Langer, R. & Mitchell, M. J. Delivery technologies for cancer immunotherapy. *Nature Reviews Drug Discovery* **18**, 175–196 (2019).
10. Esfahani Md Msc, K. *et al.* A review of cancer immunotherapy: from the past, to the present, to the future. *Current Oncology* **27**, (2020).
11. Heinzerling, L., de Toni, E., Schett, G., Hundorfean, G. & Zimmer, L. Checkpoint-Inhibitoren. *Deutsches Arzteblatt International* **116**, 119–126 (2019).
12. Jacob, J. B., Jacob, M. K. & Parajuli, P. *Review of immune checkpoint inhibitors in immuno-oncology*. *Advances in Pharmacology* vol. 91 (Elsevier Inc., 2021).
13. Pardoll, D. M. The blockade of immune checkpoints in cancer immunotherapy. *Nat Rev Cancer* **12**, 252–264 (2016).
14. Yokosuka, T. *et al.* Programmed cell death 1 forms negative costimulatory microclusters that directly inhibit T cell receptor signaling by recruiting phosphatase SHP2. *Journal of Experimental Medicine* (2012) doi:10.1084/jem.20112741.
15. Zou, W. & Chen, L. Inhibitory B7-family molecules in the tumour microenvironment. *Nature Reviews Immunology* **8**, 467–477 (2008).
16. Muul, L. M., Spiess, P. J. & Rosenberg, S. A. Identification of specific cytolytic immune responses against autologous tumor in humans bearing malignant melanoma . Information about subscribing to The Journal of Immunology is online at :

IDENTIFICATION OF SPECIFIC CYTOLYTIC IMMUNE RESPONSES AGAINST A. *The Journal of Immunology* **138**, 989–995 (1987).

17. Yee, C. *et al.* Adoptive T cell therapy using antigen-specific CD8+ T cell clones for the treatment of patients with metastatic melanoma: In vivo persistence, migration, and antitumor effect of transferred T cells. *Proceedings of the National Academy of Sciences* **99**, 16168–16173 (2002).

18. Fesnak, A. D., June, C. H. & Levine, B. L. Engineered T cells: The promise and challenges of cancer immunotherapy. *Nature Reviews Cancer* **16**, 566–581 (2016).

19. Wright, S. E. *et al.* Cytotoxic T-lymphocyte immunotherapy for ovarian cancer: A pilot study. *Journal of Immunotherapy* **35**, 196–204 (2012).

20. Morgan, R. A. *et al.* Cancer regression in patients after transfer of genetically engineered lymphocytes. *Science* **314**, 126–129 (2006).

21. Algarra, I., Cabrera, T. & Garrido, F. The HLA crossroad in tumor immunology. *Human Immunology* **61**, 65–73 (2000).

22. Linette, G. P. *et al.* Cardiovascular toxicity and titin cross-reactivity of affinity-enhanced T cells in myeloma and melanoma. *Blood* **122**, 863–871 (2013).

23. Fitzgerald, J. C. *et al.* Cytokine Release Syndrome After Chimeric Antigen Receptor T Cell Therapy for Acute Lymphoblastic Leukemia. *Critical care medicine* **45**, 124–131 (2017).

24. Lai, J. *et al.* Adoptive cellular therapy with T cells expressing the dendritic cell growth factor Flt3L drives epitope spreading and antitumor immunity. *Nature Immunology* 1–13 (2020) doi:10.1038/s41590-020-0676-7.

25. Liston, D. R. & Davis, M. Clinically Relevant Concentrations of Anticancer Drugs: A Guide for Nonclinical Studies. *Clin Cancer Res* **23**, (2017).

26. Li, J. *et al.* PD-1/SHP-2 inhibits Tc1/Th1 phenotypic responses and the activation of t cells in the tumor microenvironment. *Cancer Research* (2015) doi:10.1158/0008-5472.CAN-14-1215.

27. Ma, F., Zhang, J., Zhang, J. & Zhang, C. The TLR7 agonists imiquimod and gardiquimod improve DC-based immunotherapy for melanoma in mice. *Cellular and Molecular Immunology* **7**, 381–388 (2010).

28. Rudd, C. E., Chanthong, K. & Taylor, A. Small Molecule Inhibition of GSK-3 Specifically Inhibits the Transcription of Inhibitory Co-receptor LAG-3 for Enhanced Anti-tumor Immunity. *Cell Reports* **30**, 2075-2082.e4 (2020).

29. Kerr, W. G. & Chisholm, J. D. The Next Generation of Immunotherapy for Cancer: Small Molecules Could Make Big Waves. *The Journal of Immunology* **202**, 11–19 (2019).

30. Mancini, R. J., Stutts, L., Ryu, K. A., Tom, J. K. & Esser-Kahn, A. P. Directing the Immune System with Chemical Compounds. *ACS Chem. Biol* **9**, (2014).

31. Woo, S. R. *et al.* STING-dependent cytosolic DNA sensing mediates innate immune recognition of immunogenic tumors. *Immunity* **41**, 830–842 (2014).

32. Huck, B., Kçtzner, L. & Urbahns, K. Small Molecules DriveBig Improvements in Immuno- Oncology Therapies. *Angew.Chem.Int. Ed.* **57**, 412–4428 (2018).

33. Zak, K. M. *et al.* Structural basis for small molecule targeting of the programmed death ligand 1 (PD-L1). *Oncotarget* **7**, 30323–30335 (2016).

34. Marasco, M. *et al.* Molecular mechanism of SHP2 activation by PD-1 stimulation. *Science Advances* **6**, (2020).

35. Augello, G. *et al.* The Role of GSK-3 in Cancer Immunotherapy: GSK-3 Inhibitors as a New Frontier in Cancer Treatment. *Cells* **9**, (2020).

36. van der Zanden, S. Y., Luimstra, J. J., Neefjes, J., Borst, J. & Ovaa, H. Opportunities for Small Molecules in Cancer Immunotherapy. *Trends in Immunology* **41**, 493–511 (2020).

37. Chang, M. R. *et al.* Synthetic RORγt Agonists Enhance Protective Immunity. (2016) doi:10.1021/acschembio.5b00899.

38. Hu, X. *et al.* Synthetic RORγ agonists regulate multiple pathways to enhance antitumor immunity. (2016) doi:10.1080/2162402X.2016.1254854.

39. Hosoya, T. *et al.* Induction of oligoclonal CD8 T cell responses against pulmonary metastatic cancer by a phospholipid- conjugated TLR7 agonist. *PNAS* **115**, E6836–E6844 (2018).

40. Zhang, Y., Li, N., Suh, H. & Irvine, D. J. Nanoparticle anchoring targets immune agonists to tumors enabling anti-cancer immunity without systemic toxicity. *Nature Communications* **9**, (2018).

41. Irvine, D. J. & Dane, E. L. Enhancing cancer immunotherapy with nanomedicine. *Nature Reviews Immunology* **20**, 321–334 (2020).

42. Wilczewska, A. Z., Niemirowicz, K. & Markiewicz, K. H. Nanoparticles as drug delivery systems. *Pharmacological Reports* **64**, 1020–2037 (2012).

43. J Milton Harris, R. B. C. Effect of pegylation on pharmaceuticals. *Nat. Rev. Drug Discov.* **2**, 214–221 (2003).

44. Shi, J., Kantoff, P. W., Wooster, R. & Farokhzad, O. C. Cancer nanomedicine: progress, challenges and opportunities. *Nature Reviews Cancer* **17**, 20–37 (2016).

45. Guimarães, D., Cavaco-Paulo, A. & Nogueira, E. Design of liposomes as drug delivery system for therapeutic applications. *International Journal of Pharmaceutics* **601**, (2021).

46. Gao, X., Cui, Y., Levenson, R. M., Chung, L. W. K. & Nie, S. In vivo cancer targeting and imaging with semiconductor quantum dots. *Nature Nanotechnology* **22**, 969–976 (2004).

47. Stefan Willhelm *et al.* Analysis of nanoparticle delivery to tumours. *Nature Reviews Materials* **1**, 16014 (2016).

48. Bertrand, N., Wu, J., Xu, X., Kamaly, N. & Farokhzad, O. C. Cancer nanotechnology: The impact of passive and active targeting in the era of modern cancer biology. *Advanced Drug Delivery Reviews* **66**, 2–25 (2014).

49. Tiet, P. & Berlin, J. M. Exploiting homing abilities of cell carriers: Targeted delivery of nanoparticles for cancer therapy. *Biochemical Pharmacology* **145**, 18–26 (2017).

50. Krombach, J. *et al.* Priming anti-tumor immunity by radiotherapy: Dying tumor cell-derived DAMPs trigger endothelial cell activation and recruitment of myeloid cells. *OncoImmunology* **8**, (2019).

51. Zheng, D.-W. *et al.* Highly Integrated Nano-Platform for Breaking the Barrier between Chemotherapy and Immunotherapy. (2016) doi:10.1021/acs.nanolett.6b01432.

52. Rios-Doria, J. *et al.* Doxil Synergizes with Cancer Immunotherapies to Enhance Antitumor Responses in Syngeneic Mouse Models. *Neoplasia (United States)* **17**, 661–670 (2015).

53. Duan, X., hristina Chan, C. & Wenbin Lin, A. Nanoparticle-Mediated Immunogenic Cell Death Enables and Potentiates Cancer Immunotherapy. *Angew.Chem.Int. Ed.* **58**, 670–680 (2019).

54. Zupančič, E. *et al.* Rational design of nanoparticles towards targeting antigen-presenting cells and improved T cell priming. *Journal of Controlled Release* **258**, 182–195 (2017).

55. Schmid, D. *et al.* T cell-targeting nanoparticles focus delivery of immunotherapy to improve antitumor immunity. *Nature Communications* **8**, 1–11 (2017).

56. Oberli, M. A. *et al.* Lipid Nanoparticle Assisted mRNA Delivery for Potent Cancer Immunotherapy. *Nano Lett* **17**, 1326–1335 (2017).

57. Lorenz, C. *et al.* Protein expression from exogenous mRNA: Uptake by receptor-mediated endocytosis and trafficking via the lysosomal pathway. *RNA Biology* **8**, (2011).

58. Billingsley, M. M. *et al.* Orthogonal Design of Experiments for Optimization of Lipid Nanoparticles for mRNA Engineering of CAR T Cells. *Nano Letters* (2021) doi:10.1021/acs.nanolett.1c02503.

59. Rurik, J. G. *et al.* CAR T cells produced in vivo to treat cardiac injury. *Science (New York, N.Y.)* **375**, 91–96 (2022).

60. Lu, X. *et al.* Engineered PLGA microparticles for long-term, pulsatile release of STING agonist for cancer immunotherapy. *Science Translational Medicine* **12**, 1–16 (2020).

61. Paßlick, D. *et al.* Delivering all in one: Antigen-nanocapsule loaded with dual adjuvant yields superadditive effects by DC-directed T cell stimulation. *Journal of Controlled Release* **289**, 23–34 (2018).

62. Li, S. *et al.* Prolonged activation of innate immune pathways by a polyvalent STING agonist. *Nature Biomedical Engineering* **5**, 455–466 (2021).

63. Anselmo, A. C. & Mitragotri, S. Cell-mediated delivery of nanoparticles: Taking advantage of circulatory cells to target nanoparticles. *Journal of Controlled Release* **190**, 531–541 (2014).

64. Luster, A. D., Alon, R. & von Andrian, U. H. Immune cell migration in inflammation: Present and future therapeutic targets. *Nature Immunology* vol. 6 1182–1190 (2005).

65. Combes, F., Meyer, E. & Sanders, N. N. Immune cells as tumor drug delivery vehicles. *Journal of Controlled Release* **327**, 70–87 (2020).

66. Muzykantov, V. R. Drug delivery by red blood cells: Vascular carriers designed by mother nature. *Expert Opinion on Drug Delivery* vol. 7 403–427 (2010).

67. Chambers, E. & Mitragotri, S. Prolonged circulation of large polymeric nanoparticles by non-covalent adsorption on erythrocytes. *Journal of Controlled Release* **100**, 111–119 (2004).

68. Lucas, A., Lam, D. & Cabrales, P. Doxorubicin-loaded red blood cells reduced cardiac toxicity and preserved anticancer activity. *Drug Delivery* **26**, 433–442 (2019).

69. Shi, C. & Pamer, E. G. Monocyte recruitment during infection and inflammation. *Nature Reviews Immunology* vol. 11 762–774 (2011).

70. Yaman, S., Chintapula, U., Rodriguez, E., Ramachandramoorthy, H. & Nguyen, K. T. Cell-mediated and cell membrane-coated nanoparticles for drug delivery and cancer therapy. *Cancer Drug Resistance* 879–911 (2020) doi:10.20517/cdr.2020.55.

71. Choi, J. *et al.* Use of macrophages to deliver therapeutic and imaging contrast agents to tumors. *Biomaterials* **33**, 4195–4203 (2012).

72. Williams, C. B., Yeh, E. S. & Soloff, A. C. Tumor-associated macrophages: Unwitting accomplices in breast cancer malignancy. *npj Breast Cancer* vol. 2 (2016).

73. Wyatt Shields, C. *et al.* Cellular backpacks for macrophage immunotherapy. *Science Advances* **6**, 1–12 (2020).

74. Lebien, T. W. & Tedder, T. F. B lymphocytes: How they develop and function. *Blood* **112**, 1570–1580 (2008).

75. Lrich, U., von A Ndrian, H., Harles, C. & Ackay, R. M. T-cell function and migration. *Advances in immunology* 1020–1034 (2000).

76. Girard, J. P., Moussion, C. & Förster, R. HEVs, lymphatics and homeostatic immune cell trafficking in lymph nodes. *Nature Reviews Immunology* vol. 12 762–773 (2012).

77. Kennedy, L. C. *et al.* T cells enhance gold nanoparticle delivery to tumors in vivo. *Nanoscale Research Letters* **6**, 283 (2011).

78. Huang, B. *et al.* Active targeting of chemotherapy to disseminated tumors using nanoparticle-carrying T cells. *Science Translational Medicine* **7**, (2015).

79. Steinfeld, U., Pauli, C., Kaltz, N., Bergemann, C. & Lee, H. H. T lymphocytes as potential therapeutic drug carrier for cancer treatment. *International Journal of Pharmaceutics* **311**, 229–236 (2006).

80. Liu, S. *et al.* Adoptive CD8 + T-cell grafted with liposomal immunotherapy drugs to counteract the immune suppressive tumor microenvironment and enhance therapy for melanoma . *Nanoscale* **13**, 15789–15803 (2021).

81. Tang, L. *et al.* Enhancing T cell therapy through TCR-signaling-responsive nanoparticle drug delivery. *Nature Biotechnology* **36**, (2018).

82. Stephan, M. T., Moon, J. J., Um, S. H., Bersthteyn, A. & Irvine, D. J. Therapeutic cell engineering with surface-conjugated synthetic nanoparticles. *Nature Medicine* **16**, 1035–1041 (2010).

83. Wculek, S. K. *et al.* Dendritic cells in cancer immunology and immunotherapy. *Nature Reviews Immunology* (2020) doi:10.1038/s41577-019-0210-z.

84. Mitchell, M. J., Wayne, E., Rana, K., Schaffer, C. B. & King, M. R. Trail-coated leukocytes that kill cancer cells in the circulation. *Proceedings of the National Academy of Sciences of the United States of America* **111**, 930–935 (2014).

85. Xia, T. *et al.* Comparison of the abilities of ambient and manufactured nanoparticles to induce cellular toxicity according to an oxidative stress paradigm. *Nano Letters* vol. 6 1794–1807 (2006).

86. Swiston, A. J. *et al.* Surface functionalization of living cells with multilayer patches. *Nano Letters* **8**, 4446–4453 (2008).

87. Polak, R. *et al.* Liposome-Loaded Cell Backpacks. *Advanced Healthcare Materials* **4**, 2832–2841 (2015).

88. Li, P. Y., Fan, Z. & Cheng, H. Cell Membrane Bioconjugation and Membrane-Derived Nanomaterials for Immunotherapy. *Bioconjugate Chemistry* **29**, 624–634 (2018).

89. Wayteck, L. *et al.* Hitchhiking nanoparticles: Reversible coupling of lipid-based nanoparticles to cytotoxic T lymphocytes. *Biomaterials* **77**, 243–254 (2016).

90. Stephan, M. T., Stephan, S. B., Bak, P., Chen, J. & Irvine, D. J. Synapse-directed delivery of immunomodulators using T-cell-conjugated nanoparticles. *Biomaterials* **33**, 5776–5787 (2012).

91. Zhou, H. *et al.* In situ poly I:C released from living cell drug nanocarriers for macrophage-mediated antitumor immunotherapy. *Biomaterials* **269**, 120670 (2021).

92. Kim, W. *et al.* In vivo tracking of bioorthogonally labeled T-cells for predicting therapeutic efficacy of adoptive T-cell therapy. *Journal of Controlled Release* **329**, 223–236 (2021).

93. Choi, M. R. *et al.* A cellular trojan horse for delivery of therapeutic nanoparticles into tumors. *Nano Letters* **7**, 3759–3765 (2007).

94. Batrakova, E. v *et al.* A Macrophage - Nanozyme Delivery System for Parkinson ' s Disease. 1498–1506 (2007).

95. Huang, W. C. *et al.* Tumortropic monocyte-mediated delivery of echogenic polymer bubbles and therapeutic vesicles for chemotherapy of tumor hypoxia. *Biomaterials* **71**, 71–83 (2015).

96. Betzer, O. *et al.* In-vitro Optimization of Nanoparticle-Cell Labeling Protocols for In-vivo Cell Tracking Applications. *Scientific Reports* **5**, 1–11 (2015).

97. Sanz-Ortega, L. *et al.* T cells loaded with magnetic nanoparticles are retained in peripheral lymph nodes by the application of a magnetic field. *Journal of Nanobiotechnology* **17**, 1–20 (2019).

98. Rurik, J. G. *et al.* CAR T cells produced in vivo to treat cardiac injury. *Science (New York, N.Y.)* **375**, 91–96 (2022).

99. Mura, S., Nicolas, J. & Couvreur, P. Stimuli-responsive nanocarriers for drug delivery. *Nature Materials* vol. 12 991–1003 (2013).

Chapter 2

Development and characterization of the remote-loading method for liposomal loading of small-molecule immunomodulatory drugs.

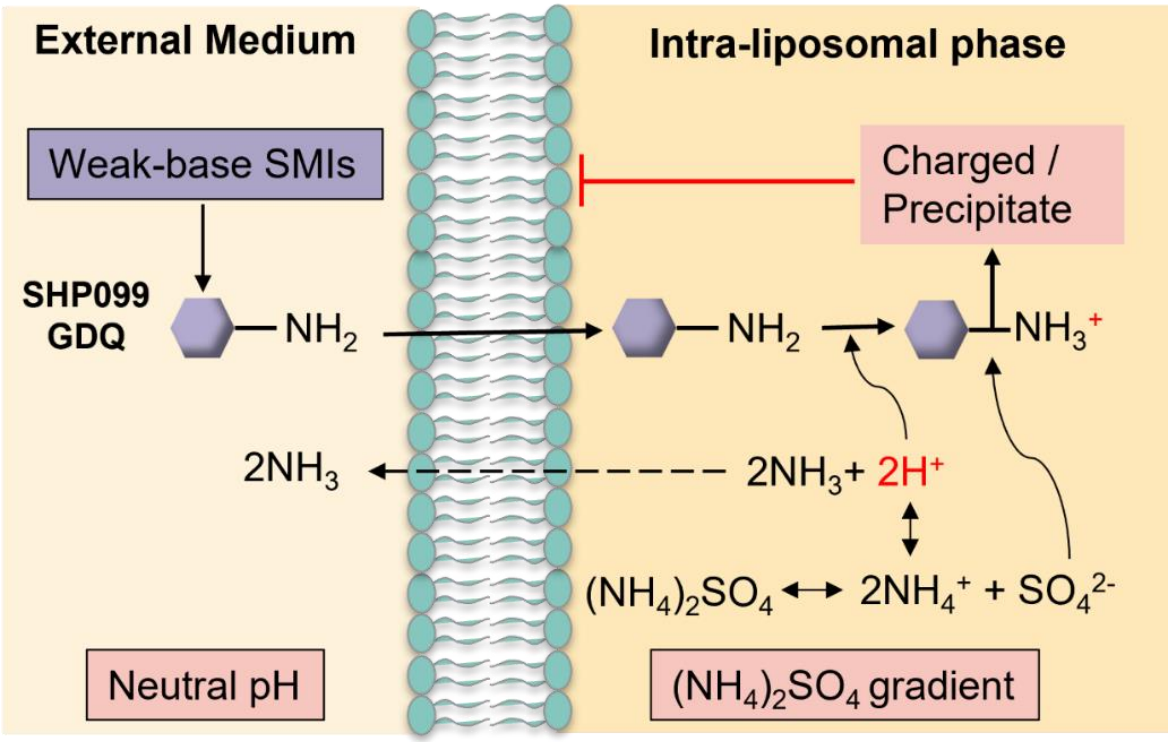

2.1 Abstract

This chapter describes the development and characterization of a remote-loading method for loading into liposomes two small-molecule immunomodulatory drugs – Gardiquimod (GDQ) and SHP099. Gardiquimod is a selective toll-like receptor 7/8 (TLR-7/8) agonist for both mouse and human forms of TLR-7/8. In cancer therapy, it functions as a cancer vaccine adjuvant to facilitate the maturation of antigen-presenting cells. On the other hand, SHP099 is an allosteric inhibitor of SHP2, which is a critical regulator of the RAS-MAPK pathway and plays an important role in cancer cell growth, as well as in immune cell functions in T cells and macrophages. They have both shown great potential for cancer immunotherapy. However, there exist delivery challenges regarding the low solubility of the compounds and the suboptimal biodistribution upon systemin administration, which limit the bioavailability and efficacy of these drugs. We hypothesized that these critical issues with GDQ and SHP099, as well as other small-molecule immunomodulators can be resolved with liposome delivery.

The remote-loading technique was optimized and applied for achieving a high drug loading efficiency. The drugs were encapsulated in the aqueous core of liposomes via an ammonium sulfate gradient to form stable drug crystals and allow prolonged liposomal retention (>7 days in 10% serum). With this loading method, the loading efficacy for both drugs reached more than 90% at the drug-to-lipid (D/L) ratio of 1/4 (mol/mol), which is over 10-fold higher than what is normally achieved by passive loading methods. We further investigated the biological activity (TLR-7/8 stimulation by GDQ and PD-1/PD-L1 signaling blockade by SHP099), the cytotoxicity, and the combination feasibility with other therapies in the same formulation.

2.2 Introduction

Small molecule immunomodulators (SMIs) have shown multiple utilities in cancer immunotherapy. These compounds are generally hydrophobic since their targets are normally buried deep in hydrophobic or intracellular domains[1]. Most of the small-molecule pharmaceutical compounds fall into the low solubility classes of the Biopharmaceutical Classification System (BCS) [2], which limits their bioavailability resulting in the suboptimal delivery[3]. Moreover, the non-targeted distribution upon systemic administration may lead to toxicity and hyper-inflammation reactions. Several technologies have been used to improve drug solubility, including pH adjustment, co-solvency, surfactant solubilization, amorphous solid dispersion and co-crystal methods, and nano- or micro-technology[3]. Among these

methods, using nanocarriers as vehicles has drawn extensive attention. Nanoparticles (NPs) are generally formulated with biocompatible and biodegradable materials, and insoluble drugs can be encapsulated in the hydrophobic compartment to improve solubility and dissolution. Apart from improving the solubility, NPs also can improve drug targeting through passive or active ways as described in chapter 1.2, thus potentially improving the therapeutic index and preventing systemic toxicity related to the undesired distribution of SMIs.

Lipid-based nanocarriers represent particles composed of lipid excipients, including solid lipid nanoparticles (LNPs), micro- or nano-emulsions, polymer-lipid hybrid nanoparticles, and liposomes. Among them, liposomes are the first used and so far, the most established nanocarrier for improving drug delivey[4]. They are artificial sphere-shaped colloidal vesicles consisting of unilamellar or multilamellar lipid membranes surrounding an aqueous core. This unique structure allows them to encapsulate hydrophilic drugs in the core and hydrophobic drugs in the lipid bilayer. Liposome properties differ considerably regarding the size, surface charge, lamellarity, drug encapsulation, and retention with respect to lipid composition and producing method[5]. The lipid components in the bilayer determine the 'rigidity' or 'fluidity' and the charge of the bilayer, which leads to different drug loading and stability, as well as *in vivo* ditribution[6]. For instance, unsaturated phosphatidylcholine species from natural sources give much more permeable and less stable bilayers, whereas saturated phospholipids with long acyl chains form rigid and less impermeable bilayers structures[4]. Since Doxil®, the first liposomal drug approved by the FDA in 1995[7], there have been more than 15 liposomal drugs on the market covering applications in cancer, infection, pain management, and eye diseases. Most of them are applied in cancer chemotherapy. Due to the similar small-molecular properties, there have been great interests in transferring the success in delivering chemotherapies to SMIs or combination therapies for improved therapeutic efficacy[8,9].

The selection of the method to encapsulate drugs into liposomes, either via passive or active loading, affects the amount and stability of the loaded drug. In the process of passive loading, drugs are added during liposome formation, with hydrophobic drugs dissolved with lipids in the organic phase and hydrophilic drugs dissolved in the aqueous phase for dispersing the lipid[10]. In general, hydrophilic drugs are retained in the aqueous phase, both inside and outside the liposomes, while hydrophobic drugs are encapsulated inside the lipid bilayer of liposomes. There are significant limitations of passive loading. First, the loading efficiency achieved by passive loading is quite low, with the typical drug-to-lipid ratio (D/L) less than 0.05 (w/w) [11].

In addition, the weak association between the drugs and the liposomes often results in poor drug retention and storage stability. Passive loading is often related to a "burst release" phenomenon that a large percentage of the entrapped drug is released fast in an early release phase. The method of active loading, also known as remote loading, was thus developed to reach a sufficiently high intra-liposomal drug concentration, with the example of Doxil produced with this technique[12,13]. During remote loading, the drug is loaded into preformed liposomes by a transmembrane gradient as a driving force (**Figure 2.1A**)[14]. An amphiphilic drug dissolved in the exterior aqueous phase can diffuse across the membrane as uncharged molecules, followed by interaction with the trapping agent in the core to form a charged state or precipitate, thus the drug is locked inside liposomes. This method requires the drug to be an amphipathic weak acid or base with a logD in the range of -2.5 to 2.0 at pH 7[15], and the driving force caused by the transmembrane gradient can "pump" the drug from the exterior into the liposome and retain the drug there[16]. For example, the ammonium gradient is used successfully for the remote loading of doxorubicin as well as other weak base drugs[17], while the acetate gradient is effective for loading weak acids. Remote loading allows complete drug encapsulation at a higher D/L (> 0.2, w/w). In addition, the ion gradient promotes the formation of stable drug complexes inside the aqueous core of liposomes, thus providing improved drug retention and formulation stability[13,18,19].

In this chapter, we exploited the remote loading method to load SMIs that meet the criteria for remote loading into liposomes, aiming to improve the pharmaceutical properties and potentiate the drug delivery for cancer immunotherapy. As proof-of-principle, a Toll-like receptor 7/8 (TLR-7/8) agonist, Gardiquimod (GDQ), and an Src Homology Region 2-Containing Protein Tyrosine Phosphatase-2 (SHP-2) inhibitor, SHP099 were tested. The structure and logD at different pH were shown in **Figure 2.1B**. Different salt gradients, as well as lipid compositions, were evaluated for optimizing the loading conditions. Ammonium sulfate gradient exhibited great loading ability for both compounds in various liposome formulations. The results demonstrate that remote loading is a robust and versatile tool for improving drug solubility, liposomal loading efficiency, retention, and stability, which underlies the application of these SMIs in cancer immunotherapy.

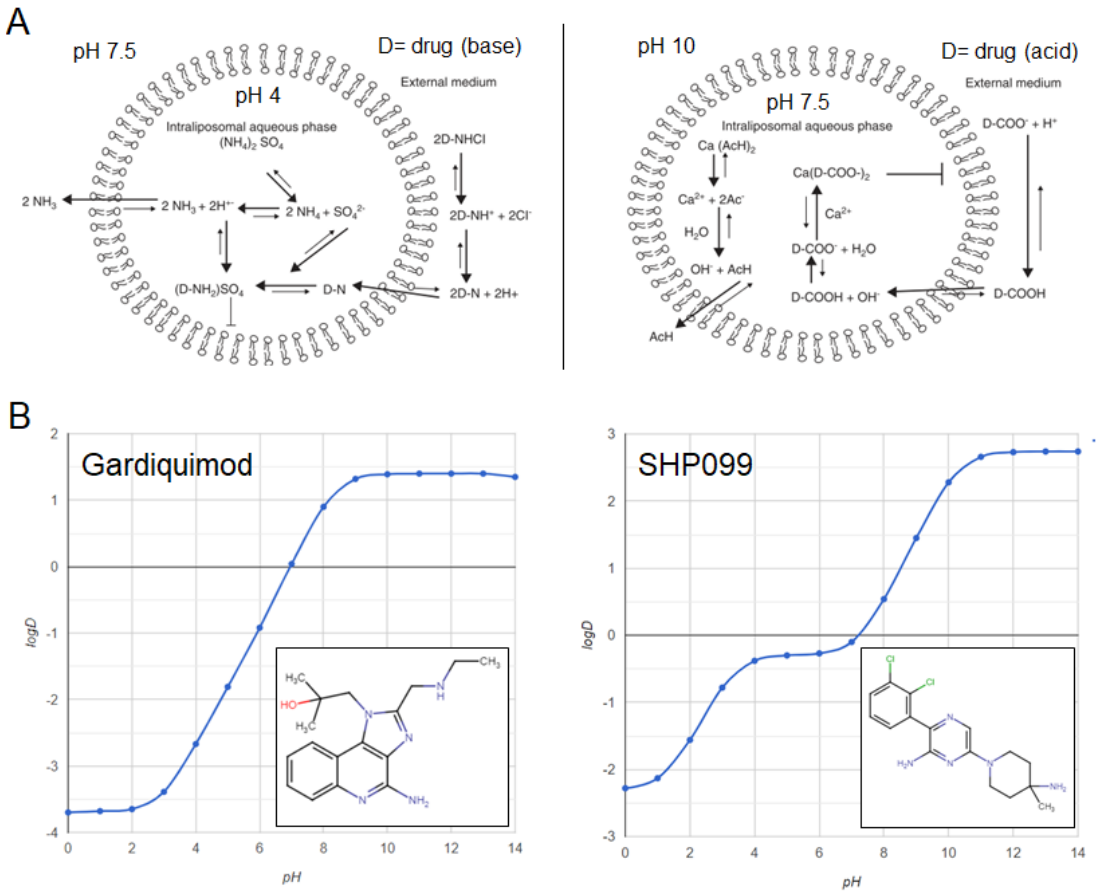

Figure 2.1 Principle of remote loading. **(A)** Schematic illustration of the process of remote-loading using ammonium sulfate or calcium acetate. **(B)** LogD-pH curves of Gardiquimod and SHP099, predicted by LogD Predictor (ChemAxon).

2.3 Remote-loading of TLR agonist – Gardiquimod

Toll-like receptors (TLR) are a family of highly conserved germline-encoded pattern-recognition receptors that are essential for host immune responses. TLR ligands represent a promising class of immunotherapeutic or vaccine adjuvants with the potential to boost innate and adaptive immune responses in tumor therapy[20]. GDQ is a potent TLA-7/8 agonist; the core structure is 1H-imidazoquinoline, as found in related drugs such as imiquimod and resiquimod. It functions as an immune response modifier that activates antigen-presenting cells and promotes activation of T and natural killer (NK) cells[21]. GDQ is a small molecule (MW = 313.4) with a logD of around 0 at pH 7, and the solubility is less than 1mg/mL in water. These properties make it a potentially good candidate for remote loading into liposomes[12].

2.3.1 *Efficient remote loading with ammonium gradient*

Since GDQ is a weak base, we selected ammonium as the gradient ion and tested the effect of different counterions. 250mM of $(NH_4)_2SO_4$ (Am. sulfate), $(NH_4)_2HPO_4$ (Am. phosphate) and $(NH_4)_2C_6H_6O_7$ (Am. citrate) solutions presented the pH of 5.1, 8.0, and 4.8, respectively. We prepared the classic stealth liposomes (HSPC:Cholesterol: DSPE-PEG_{2k} of mole ratio 57:38:5) with each of the gradient solutions inside and Hepes buffer (25mM HEPES, 150mM NaCl, pH 7.5) as the exterior phase after buffer exchange. GDQ was incubated with each of the preformed liposomes for 3 hours at 60 ℃, which is higher than the lipid transition temperature of HSPC (T_m, 55 ℃). As summarized in **Table 2.1,** The liposomes exhibited comparable homogeneous size distribution (diameter: ~125 nm, PDI: < 0.06) and surface charge (~ -8.5 mV). At a fixed drug-to-lipid (D/L) ratio of 0.25 (mol/mol), complete encapsulation was achieved with 250mM of Am. sulfate gradient (**Figure 2.2A**). While the encapsulation efficiency (EE) was lower when using Am. phosphate (61.3%) or Am.citrate (81.3%). The different encapsulation efficiency arose from the counteranion of the ammonium ion due to the different capacities of GDQ to aggregate with the different anions. Zucker et. al[12] has reviewed that for most amphipathic weak bases drugs, the ranking of the counterions of ammonium concerning the stabilizing ability is sulfate>phosphate>citrate>glucoronate. Thus, we chose sulfate as the optimal counterion for GDQ. When changing the gradient salt concentration, we observed the correlated decrease in EE, and only 55.1% of GDQ was loaded in liposomes with 100mM Am. sulfate (**Figure 2.2B**). A sufficient magnitude trans-membrane salt gradient is required to provide enough driving force and the ion exchange for efficient loading. Low salt concentration inside the liposomes only led to medium loading. However, a high concentration of gradient ions may disrupt the liposome structure due to an osmolality unbalance between the inner and outer phases of the lipid membrane. An ammonium sulfate solution of 250mM was used as the loading gradient in the following parts.

Table 2.1 Size, polydispersity index (PDI), and ζ-potential of Gardiquimod liposomes with different salt gradients measured in 10mM HEPES saline or HEPES glucose buffer. (Mean ± SD, n=3)

Salt gradient	Size (nm)	PDI	ζ- potential (mV)
Am. Sulfate	125.7±0.4	0.039	-9.3±1.1
Am. Phosphate	128.4±0.3	0.037	-8.4±0.4
Am. Citrate	127.7±0.5	0.059	-8.6±0.6

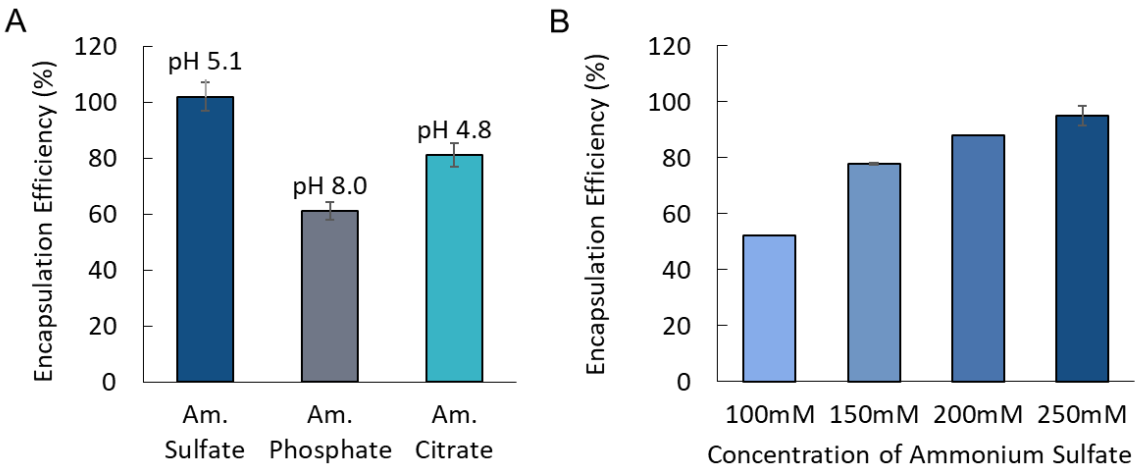

Figure 2.2 Encapsulation efficiency (EE%) of Gardiquimod (GDQ) in stealth liposomes (HSPC:Chol: DSPE-PEG=57:38:5 mole ratio) with **(A)** different ammonium salt gradients and **(B)** ammonium sulfate at various concentrations. Liposomes were incubated with GDQ for 3 h at 60 °C at a drug/lipid molar ratio of 1:4. Data are presented as means ± SD (n=3).

2.3.2 *Remote-loading of Gardiquimod in liposomes of different compositions*

We next examined whether the condition can be used to load GDQ in other liposome formulations. The degree of saturation, length of the acyl chain, and charge of lipid have a major impact on drug loading, as it affects the membrane fluidity, permeability, interaction with drug molecules, etc. As representative formulations, we prepared saturated stealth liposomes (DSPC:Cholesterol: DSPE-PEG2k of mole ratio 57:38:5), unsaturated stealth liposomes (DOPC:Cholesterol: DSPE-PEG2k of mole ratio 57:38:5), and saturated cationic liposomes (DSPC:Cholesterol: DSTAP of mole ratio 54.5:38:7.5). The size (~120 nm) and the polydispersity index (PDI < 0.05 for all samples) of all liposomes were comparable and remained unchanged after GDQ loading (**Figure 2.3A**). Cationic liposomes with DSTAP presented a highly positive charge (+ 35.8 mV) while the PEGylated liposomes were negatively charged with the zeta potential of around -12 mV (**Figure 2.3B**). We observed a significant impact from the charge on the encapsulation of GDQ. Under the same loading condition (inner: 250 mM ammonium sulfate; outer: 25 mM HEPES buffer, pH 7.5; D/L= 0.25 mol/mol, 60°C for 3h), both saturated and unsaturated stealth liposomes could completely load the drug with the EE% of 100% and 97.5%, respectively. In contrast, the EE dropped to 77.2% with the cationic formulation (**Figure 2.3C**). A possible explanation for the decreased EE might be the interaction of cationic lipid with other lipids and the polarized drug. It has been reported that incorporating cationic lipid affected the packing of phospholipids, thus altering the membrane

fluidity, vesicle size and the physical interaction might also hinder the permeation of drug molecules into the core of liposomes[22,23].

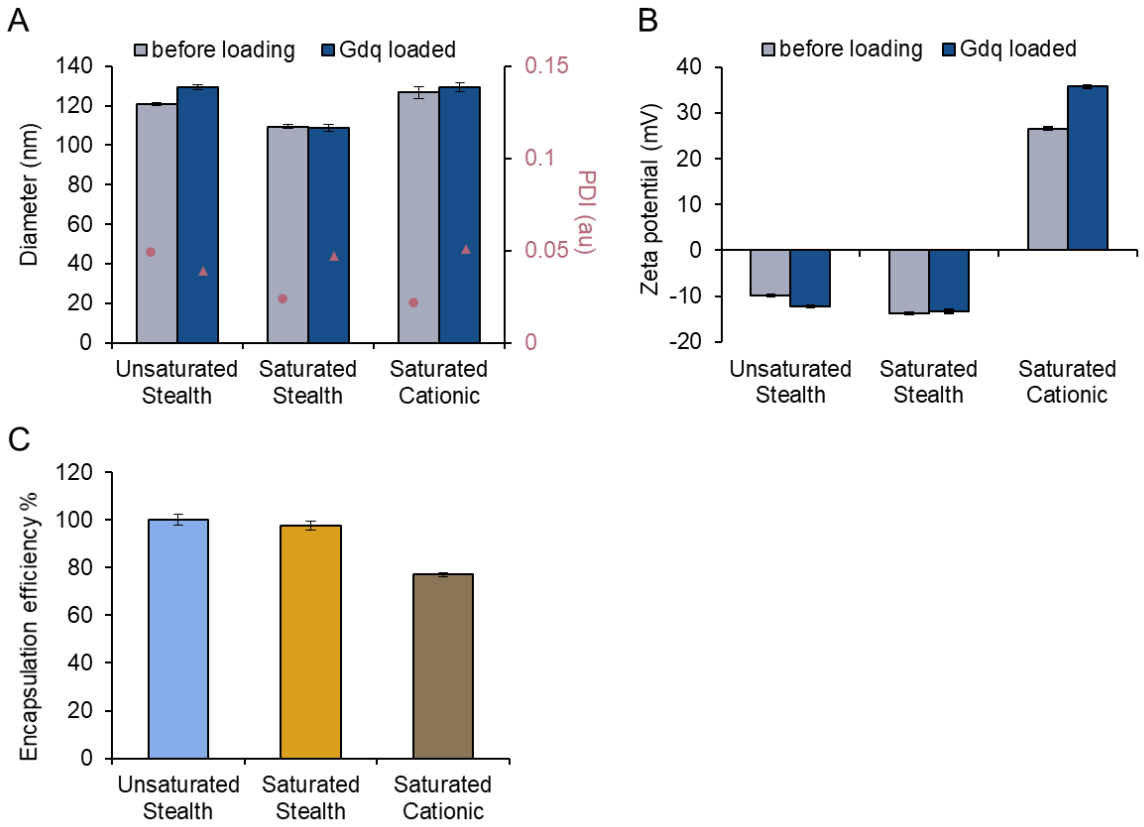

Figure 2.3 Remote loading of Gardiquimod (GDQ) into liposomes of different formulations via an ammonium sulfate gradient (interior: 250 mM $(NH_4)_2SO_4$, pH 5.1; exterior buffer: 25 mM HEPES,150 mM NaCl, pH 7.4). **(A)** Size and **(B)** surface charge of the liposomes before and after remote loading with GDQ. **(C)** Encapsulation efficiency of GDQ inside liposomes.

2.3.3 ***Release of remote-loaded Gardiquimod from liposomes***

GDQ release from saturated and unsaturated liposomes loaded using 250 mM ammonium sulfate gradient was investigated in PBS buffer and medium containing 10% FBS at 37 ℃. As shown in **Figure 2.4**, there is a significantly faster drug release of unsaturated liposomes compared to saturated ones both in PBS and serum medium. The saturated GDQ liposomes were very stable in PBS. No detectable drug was released from saturated liposomes in PBS in the first 24h, while an initial burst release of 31.4% was measured from unsaturated liposomes, and the two formulations released 9.4% and 75.4%, respectively after 1 week (168h). The different release profiles were anticipated because of the distinct T_m that the high T_m of

saturated liposomes makes the lipid bilayer more rigid and less permeable and vice versa for unsaturated liposomes. FBS-containing medium was used to mimic the *in vivo* condition, which significantly accelerated the drug release from saturated liposomes, leading to almost 50% drug release within 72h (**Figure 2.4**). Unsaturated liposomes reached complete release within 7 days in serum medium. This can be explained by the interaction of big molecules such as proteins with the liposomes, which might lead to the aggregation or break of liposomes and the release of the loaded drug.

The release results demonstrate that the ammonium sulfate gradient is a promising method for the encapsulation of GDQ into liposomes composed of saturated lipid. The slow drug release from these liposomes in PBS buffer is necessary for long storage and to avoid drug leaking before reaching their target. Furthermore, the drug was sustainably released with a similar amount released in each time interval, indicating that liposomes remote-loaded with GDQ using an ammonium sulfate gradient can provide controlled release of the drug.

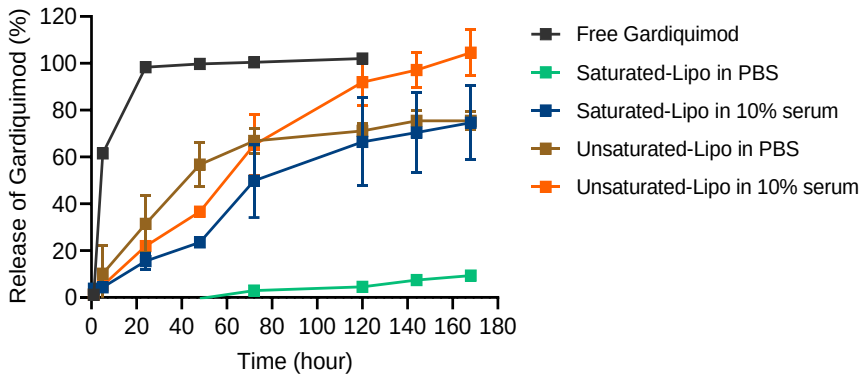

Figure 2.4 Release of Gardiquimod from saturated and unsaturated liposomes in buffer or 10% serum. Data are presented as means±SD (n=3)

2.3.4 *TLR-7 stimulation by Gardiquimod liposomes*

We next examined the TLR-7 stimulation by GDQ in free form or remote-loaded in liposomes of different lipid compositions. We used HEK-Blue™ hTLR7 cells that express the human TLR7 gene and an NF-κB/AP-1-inducible SEAP (secreted embryonic alkaline phosphatase) reporter gene. SEAP levels increase upon TLR7 stimulation, thus can be measured to monitor the TLR7 stimulation. As shown in Figure 2.5, free GDQ exhibited the most potent TLR7

stimulation even at low concentrations, however, it led to significant toxicity to cells and the signal dropped at high concentrations. In contrast, both GDQ liposomes showed dose-dependent TLR7 stimulation without compromising the viability. Even though the free GDQ allowed fast TLR7 stimulation at the early time, the signal did not increase over time, whereas the stimulation by liposomes kept increasing and exceeded the effect of the free drug after 24 hours. Furthermore, unsaturated liposomes showed stronger TLR7 stimulation than saturated ones at the same concentration, which was because the unsaturated liposomes had a faster drug release as described in 2.3.3. The effect of the drug depends on the release kinetics since free GDQ was directly accessible to cells, thus giving the prompt effect, which also disappeared fast. By loading the drug into liposomes, they formed a depot, and the drugs were gradually released, getting into cells and binding to the target. A sustained and prolonged effect was achieved by remote-loading GDQ into liposome vesicles.

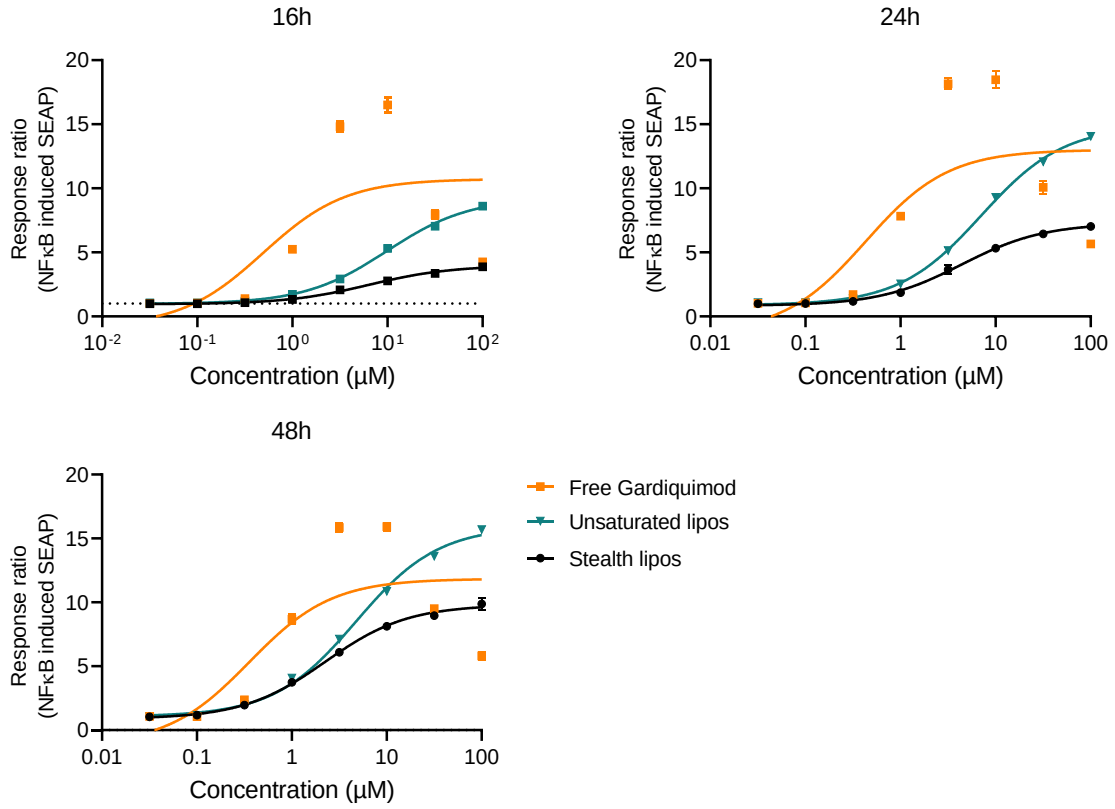

Figure 2.5 Dose-response of HEK-Blue™ hTLR7 cells to Gardiquimod in different formulations. HEK-Blue™ hTLR7 cells were cultured in a HEK-Blue™ Detection medium with increasing concentrations of Gardiquimod). After 16h, 24h, and 48h incubation, TLR7-induced NF-κB/AP1 responses were assessed by measuring SEAP levels in the supernatant by reading the OD at 630 nm. OD fold increase over non-induced cells is shown.

2.3.5 *Co-loading Gardiquimod and chemotherapeutics into liposomes*

Previous studies have shown that co-administration of chemotherapy and TLR-7 agonists provided synergistic antitumor efficacy. Chemotherapeutics such as doxorubicin (DOX) induce immunogenic cell death (ICD), meanwhile, TLR-7 agonists can promote DC maturation and T cell infiltration, together they provoke the antitumor immune response[24]. However, simultaneous and sustained codelivery of drugs can be challenging. Since remote-loading with ammonium sulfate gradient has demonstrated great success with DOX liposomes, we assessed the capacity of the method to co-encapsulate DOX and GDQ for combinational therapy. We first selected a cationic formulation to load the combination of DOX and GDQ at various relative ratios (DOX: GDQ = 1:1, 2:1, and 4:1 mol: mol) while keeping the total D/L ratio at 0.25 and tested the encapsulation efficiency (interior: 250 mM ammonium sulfate; exterior: 25 mM HEPES buffer, pH 7.5; 60°C for 3h). The size of liposomes was the same at all drug ratios (**Figure 2.6A**), so does the drug encapsulation efficiency. Adding DOX did not impact the loading of GDQ into liposomes at the same time. We observed no difference in the loading of the two compounds, that the encapsulation efficiency of around 80% was achieved for each (**Figure 2.6B**). The reason for the high loading efficiency might be that there was an excess ammonium gradient that provided enough driving force to load both drugs at the drug to lipid (D/L) ratio of 0.25. However, Cryo-TEM images revealed a different state of drugs inside the liposomes (**Figure 2.6C**). DOX crystals were formed in the core of co-loaded liposomes. In contrast, no obvious precipitation of GDQ was observed in the liposomes although the liposomes encapsulated GDQ at a similar concentration. The compounds had different interactions with the counterion sulfate.

We also investigated the application of the loading condition in stealth liposome formulations to co-load DOX and GDQ added at a 1:1 mole ratio. The size distribution and surface charge were not altered after adding DOX and were similar compared to GDQ liposomes of the same lipid compositions (**Table 2.2**). Both DOX and GDQ were successfully loaded into liposomes with a high encapsulation efficiency at ~90%, ~100%, and 76-85% in saturated stealth, unsaturated stealth, and cationic liposomes, respectively (**Table 2.2**).

We then tested the cytotoxicity of free or cationic liposomal DOX in the CT26 cancer cell line. As shown in **Figure 2.7**, GDQ did not induce cell cytotoxicity at all concentrations and

formulations, and the cytotoxicity of DOX was well preserved in liposomes. Free DOX exhibited stronger cytotoxic against CT26 cells than liposomal DOX. Similar to what was observed in the TLR-7 stimulation assay, the slow release of drugs from liposomes prevented immediate exposure to high concentrations.

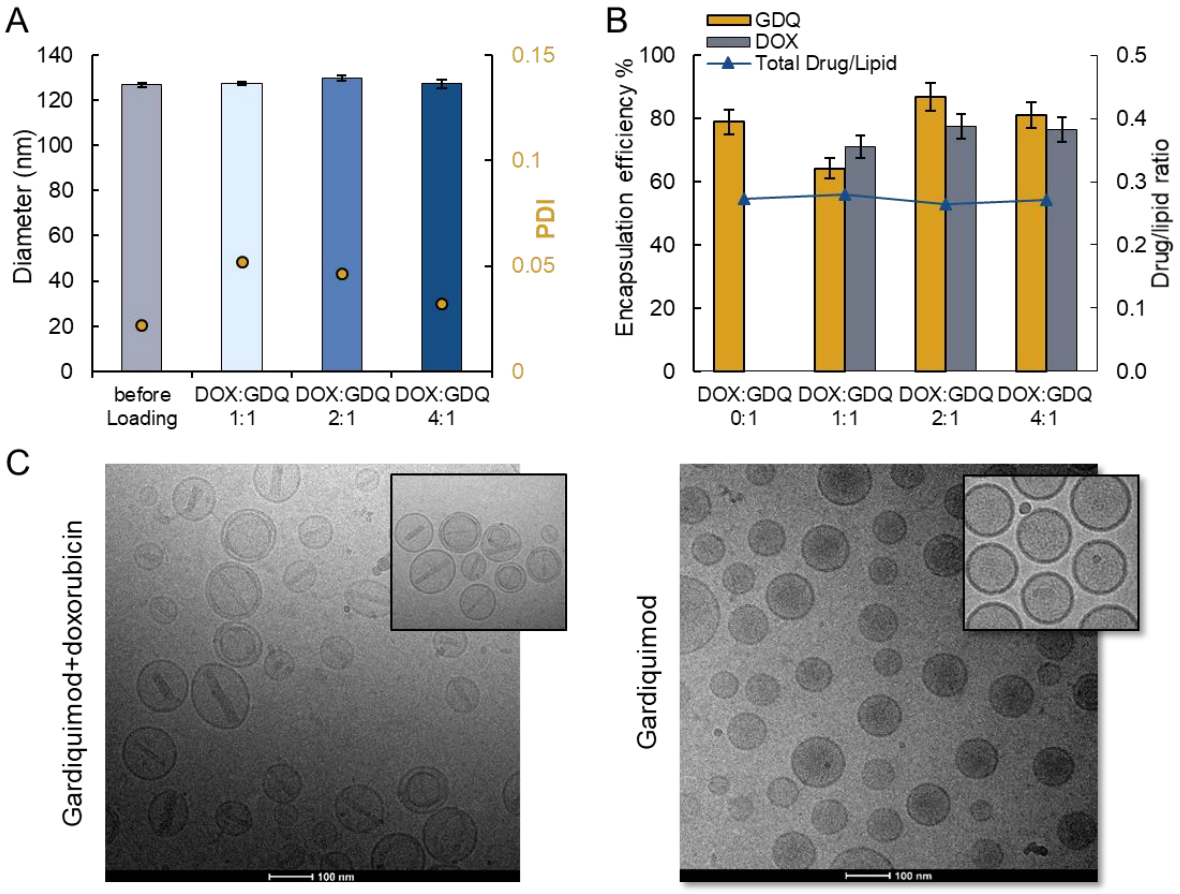

Figure 2.6 Characterization of liposomes co-loading Doxorubicin (DOX) and Gardiquimod (GDQ). **(A)** Size and PDI of cationic liposomes loaded with a combination of DOX and GDQ at different ratios. **(B)** Encapsulation efficiency of DOX and GDQ in cationic liposomes. (C) Cryo-TEM images of liposomal DOX+GDQ and liposomal GDQ.

Table 2.2 Physico-chemical properties and drug encapsulation efficiency of GDQ-DOX co-loaded liposomes. (Mean ± SD, n=3)

Liposome Formulations	Characteristics			Encapsulation efficiency (%)	
	Size (nm)	PDI	ζ-potential (mV)	GDQ	DOX
Saturated Stealth	119.8 ± 0.2	0.009	-11.1 ± 1.0	89.6	92.6
Unsaturated Stealth	125.9 ± 2.5	0.063	-12.3 ± 2.7	100	100
Saturated Cationic	131.8 ± 1.8	0.097	29.3 ± 1.3	76.2	85.3

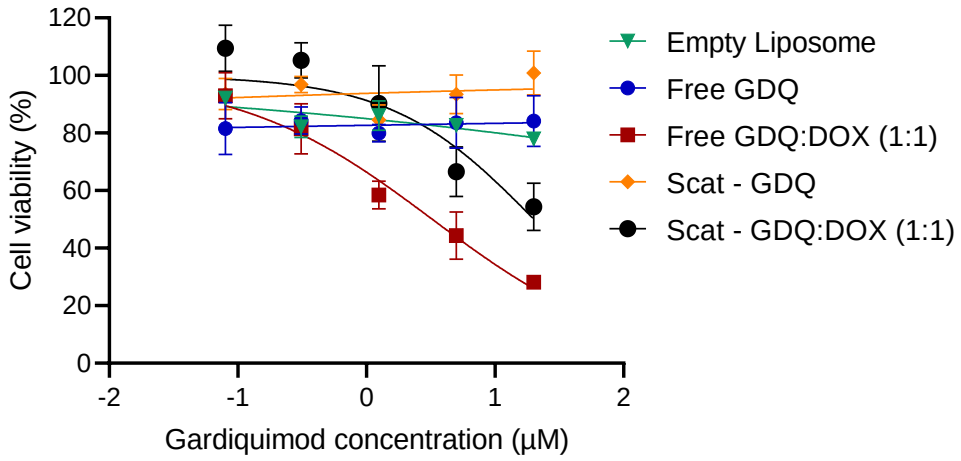

Figure 2.7 Cytotoxicity of different DOX and GDQ formulations against CT26 tumor cells after incubation for 24 hours. Data = mean (± SD), n=3.

2.4 Remote-loading of SHP2 inhibitor – SHP099

Src homology-2-containing protein tyrosine phosphatase 2 (SHP2) is a major phosphatase involved in several cellular processes that regulates cell survival and proliferation through activating the RAS-ERK pathway[25]. It also mediates programmed cell death 1 (PD-1) and T-lymphocyte attenuator (BTLA) immune checkpoint pathways[26]. SHP2 inhibition denotes a novel opportunity for cancer therapy, particularly for developing PD-1 inhibitors in cancer immunotherapy. Previous studies have demonstrated great anti-tumor efficacy of SHP2 inhibitors for KRAS-mutant cancer[27,28]. However, the preclinical efficacy of SHP2 inhibitors remains suboptimal, especially for cancer types that are not driven by RTKs; moreover, the doses required for obtaining tumor control are often very high through oral administration, e.g. the optimal dose of SHP099 is found to be 100mg/kg SHP099 every day by the oral route.

These point to the need for advanced drug delivery systems that can provide sustained and tumor-targeted delivery of SHP2 inhibitors.

In this Ph.D. thesis, we applied the remote-loading method for encapsulating an allosteric SHP2 inhibitor, SHP099 into liposomes. SHP099 is an amphipathic weak base (**Figure 2.1B,** MW = 352.26, clogP = 2.74), which is slightly soluble in water (~ 1mg/mL at pH 7). It provides a good match for remote-loading, but so far there haven´t been studies showing the validation and application of remote-loaded SHP099 liposomes. We applied the loading method for GDQ to load SHP099 into both stealth and cationic liposomes because the two compounds have similar physicochemical properties. As shown in **Table 2.3,** both formulations exhibited homogeneous size distributions of 110 -140 nm, and the encapsulation efficiency was 91.4 ± 2.1% and 85.3 ± 1.0%, respectively. Similar to GDQ, the cationic liposomes also showed slightly lower loading efficiency of SHP099 than the PEGylated stealth ones. Cryo-TEM images revealed that the encapsulated SHP099 formed disk-shaped crystals inside the lipid layer (**Figure 2.8A**). The shape of the crystals was distinct to DOX, and multiple nano-crystallizations exist in the same lipid vesicle. The precipitation provided good stability to the SHP099 liposomes. As shown in **Figure 2.8B**, when stored in PBS at 4 °C or 37 °C, minimal drug release from stealth liposomes was observed (less than 10% in three days). The extended release of SHP099 from stealth liposomes was determined in the cell culture medium containing 10% FBS at 37 °C. SHP099 was released at an even rate for more than 7 days (**Figure 2.8C**).

Table 2.3 Lipid composition, size distribution, ζ- potential, and drug encapsulation efficiency of SHP099 liposomes. (Mean ± SD, n=3)

Formulation	Lipid composition (mol %)				Liposome characteristics			SHP099 EE %
	HSPC	DSTAP	Chol	DSPE-PEG2k	Size (nm)	PDI	ζ- potential (mV)	
Stealth	57	0	38	5	119.4 ± 5.6	0.053	-12.4 ± 1.0	91.4 ± 2.1
Cationic	54.5	7.5	38	0	134.1 ± 8.9	0.043	29.3 ± 3.0	85.3 ± 1.0

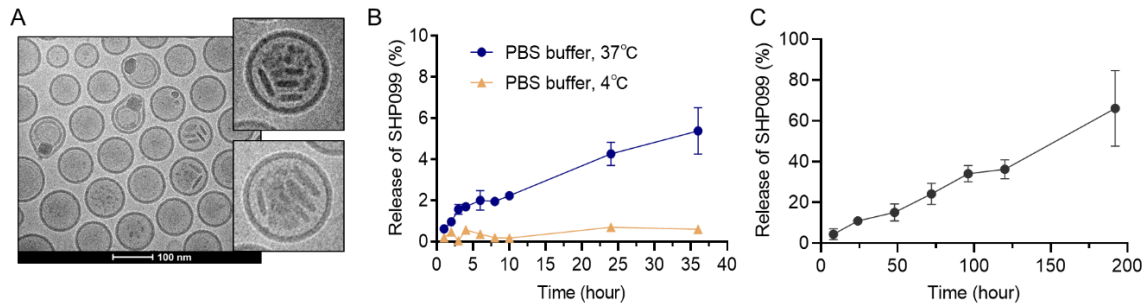

Figure 2.8 Crystallization of SHP099 inside liposomes. (**A)** Cryo-TEM images of SHP099 liposomes. **(B)** Release of SHP099 from saturated stealth liposomes in PBS buffer at 37 °C or 4 °C. **(C)** Extended SHP099 release from saturated stealth liposomes in 10% serum at 37 °C. Data are presented as means ± SD (n=3).

SHP2 is a downstream signal hub of the PD-1/PD-L1 pathway, thus we suppose the combination of SHP2 inhibition with T cell therapy would be a promising strategy for enhancing the efficacy of T cells. For this purpose, we explored the effect of SHP099 formulations on T cells, with a focus on PD-L1/PD-1 signal transduction. We first evaluated the effect of SHP099 on T cell survival and proliferation. Murine T cells were stained with Cell Trace Violet to track the proliferation before treatment with either free SHP099 or liposomal SHP099 for 72h. As shown in **Figure 2.9A**, free SHP099 had significant inhibition on T cell proliferation even at 1 μM, and completely halted T cell proliferation at 25 μM. Encapsulating the SHP099 into liposomes shielded the cytotoxicity toward T cells, showing a mild anti-proliferation effect at 25 μM. This was due to the sustained release of the compound from liposomes, which ensured a prolonged drug exposure to the targeted cells. We further assessed the blockade of PD-1/PD-L1 signaling of SHP099 using a commercially available bioluminescent reporter assay. As illustrated in **Figure 2.9B**, the Jurkat T cells are engineered to stably express human PD-1 and a luciferase reporter induced by NFAT. The T cells are co-cultured with cognate CHO cells (CHO-K1) that are engineered to express a cell surface protein to activate TCRs in an antigen-independent manner. The CHO-K1 cells also stably express human PD-L1, and therefore, when the two cell types are co-cultured, the PD-1/PD-L1 interaction inhibits TCR signaling and NFAT-mediated luciferase activity. Adding an inhibitor of the PD-1/PD-L1 pathway releases the inhibitory signal and results in NFAT-mediated luciferase activity, making it a suitable indicator for the effect of SHP099 on the PD-1/PD-L1 pathway in T-cells. SHP099 induced a concentration-dependent activation of the NFAT luciferase production (**Figure 2.9B**), which indicated the PD1/PD-L1 blockade. The effect

from free drugs and liposomes was comparable, which was not as strong as an anti-PD-1 antibody.

Whereas researchers have reported the success of loading SHP099 along or in combination with other drugs into liposomes as effective strategies for cancer immunotherapy, only poor efficiencies were achieved by passive loading, which encapsulated 67% of SHP099 at a molar D/L ratio of less than 0.05[29]. Herein we showed a major improvement in the liposomal formulation of SHP99, achieving very high loading efficiency by using the ammonium sulfate gradient-mediated remote-loading method. These results of preliminary characterization and biological evaluation inspired the work upcoming in the following Chapter 3, which resulted in a manuscript about using SHP099 to enhance T cell-based immunotherapy.

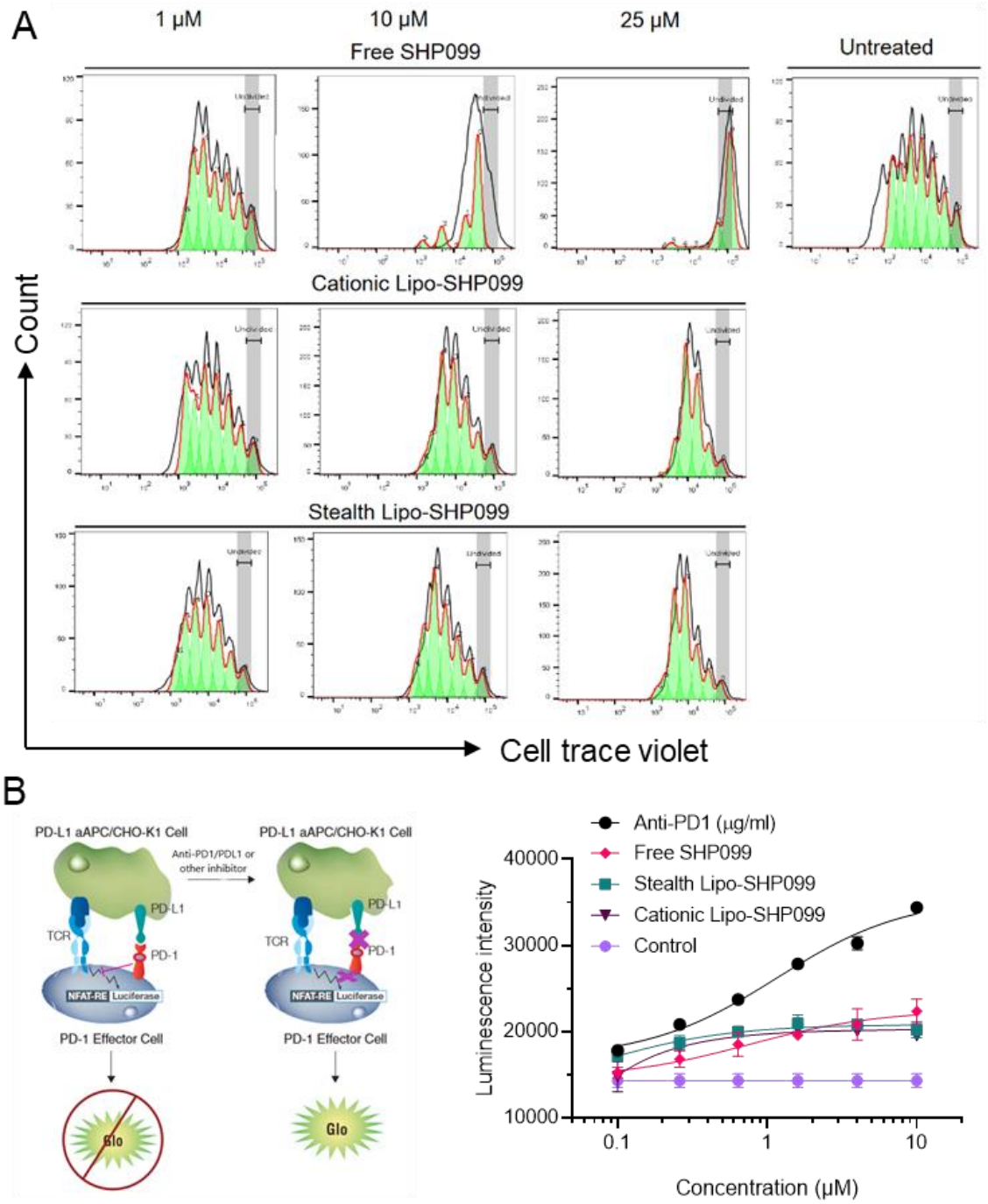

Figure 2.9 Effect of SHP099 on T cell proliferation and PD1/PD-L1 signal transduction. **(A)** In vitro effect of free SHP099 and liposomal SHP099 on T-cell proliferation. Murine T-cells were treated with different concentrations (1μM, 10μM, or 25μM) of SHP099 for 72h, and T-cell proliferation was assessed by Cell-trace Violet dilution. **(B)** Activities of SHP099 and PD-1 antibody in alleviating PD1/PD-L1 checkpoint inhibition on TCR-mediated T-cell activation. The graphs present relative luminescence normalized to the DMSO-treated controls. Each data point represents the mean ± SD (n=3).

2.5 Conclusions

In summary, we developed and characterized a remote loading method for two representative SMIs – Gardiquimod and SHP099 – into liposomes. Both of them were loaded into either stealth or cationic liposomes via the ammonium sulfate gradient. Complete drug loading was achieved at a high D/L of 0.25/1 (mol/mol), and the drugs were retained stably in liposomes and sustained release for more than 1 week in medium containing serum. SHP099 formed nanocrystal structures inside liposomes. The biological activities of the drugs were well preserved, while through liposomal loading, we reduced the undesired cytotoxicity towards immune cells. The liposomal GDQ showed prolonged TLR-7 stimulation compared to free drugs. Furthermore, we demonstrate that the method can be applied to prepare co-formulations of DOX and GDQ with high loading efficiency. Considering the proven synergistic effect of chemotherapy and TLR agonists, it provides a potential approach to further explore the synergistic cancer chemo-immunotherapy. This simple and efficient drug loading method paved the way for following exploration of the SMIs as effective cancer immunotherapeutic agents presented in Chapter 3.

2.6 Material and methods

2.6.1 *Materials*

Hydrogenated phosphatidylcholine (HSPC), 1,2-stearoyl-3-trimethylammonium-propane (DSTAP), Cholesterol, 1,2-distearoyl-sn-glycero-3-phosphoethanolamine-N-[amino(polyethylene glycol)-2000] (DSPE-PEG2000) were purchased from Avanti Polar lipids (Alabaster, AL, USA). Gardiquimod was purchased from InvivoGen (San Diego, USA), 6-(4-amino-4-methyl piperidine-1-yl)-3-(2,3-dichlorophenyl)pyrazin-2-amine (SHP099.HCl) was synthesized and purified by Anna Colliander from our lab. Unless specifically stated, all other chemicals were from Sigma Aldrich (Brøndby, Denmark) and of analytical grade.

2.6.2 *Liposome preparation*

Empty liposomes

Lipids were dissolved in tert-butanol: Milli-Q water (9:1), mixed to the desired lipid composition, snap-frozen in liquid nitrogen, and freeze-dried overnight. Three main liposome

formulations were investigated with the following lipid molar ratios: Saturated stealth (HSPC: Cholesterol: DSPE-PEG2000, 57:38:5), Unsaturated stealth (DOPC: Cholesterol:DSPE-PEG2000, 57:38:5), Saturated cationic (HSPC:Cholesterol: DSTAP, 54.5:38:7.5). Mixed lipid powder was hydrated with the gradient salt solutions to a lipid concentration of 20-50 mM and placed stirring at 70°C or 45°C for 1 hour. The resulting liposomes were homogenized by extruding 21 times through a 100 nm polycarbonate filter using a mini-extruder (Avanti Polar Lipids, Alabaster, 358 AL, USA). The temperature was maintained during the extrusion process.

Remote loading of drugs into liposomes

Liposomes were first prepared following the procedure described above. After extrusion, liposomes were dialyzed for 48 hours against HEPES buffered saline (25mM HEPES, 150mM NaCl, pH 7.4) in Slide-A-Lyzer dialysis cassettes (10K MWCO), with two times buffer exchanges. Subsequently, the liposomes suspension was added to Gardiquimod or SHP099 in powder form at a drug/lipid mol ratio of 1:4. The solution was incubated at 60°C for 3 hours under stirring conditions. After cooling down, the non-encapsulated drug was removed by dialysis (Slide-A-Lyzer, 10K MWCO). Before and after purification, the lipid and drug concentrations were measured by ICP-MS and HPLC, respectively as described below, to determine the final drug/lipid ratio. The encapsulation efficiency (EE) was calculated according to the following equation:

$$\text{Encapsulation efficiency (\%)} = \frac{(\text{C (loaded drug)} / \text{C (lipid)})}{(\text{C (total drug)} / \text{C (total lipid)})} \times 100\%$$

2.6.3 ***Physicochemical characterization of liposomes***

The size distribution and zeta potential of liposomes were measured by dynamic light scattering (DLS) using a ZetaSizer Nano ZS (Malvern, UK). The morphology was examined by cryogenic transmission electron microscopy (cryo-TEM) using a Tecnai T20 G2 (Thermo Fisher Scientific, Waltham, USA). Lipid concentration was determined using Inductively Coupled Plasma Mass Spectrometry (ICP-MS).

2.6.4 ***Drug release study***

The release of encapsulated drugs from liposomes was analyzed by analytical reversed-phase (RP)-HPLC in PBS or cell culture medium containing 10% fetal bovine serum (FBS). Briefly,

100 µL of liposome solutions were added in Slide-A-Lyzer MINI dialysis devices (Thermo Scientific) with molecular weight cut-offs of 10K. Then, the dialysis devices were put into conical tubes containing 1.6 mL of release medium at 37 °C. At specific time points, 100 µL of the release medium was drawn, and the same volume of fresh solution was added. The amount of the drug released at each time point was determined by HPLC.

2.6.5 *Determination of phospholipid concentration by ICP-MS*

The total lipid concentration of liposome stocks was determined by measuring the phosphorus concentration using Inductively Coupled Plasma Mass Spectrometry (ICP-MS). Samples were first diluted 5,000 times in an ICP-MS diluent (2% HCl, 10 ppb Ga) to fall within a standard range of 25-100 ppb phosphorus. The phosphorus content was then measured on an ICAP-Q from Thermo Fisher Scientific. The total lipid concentration was calculated based on the ratio of the lipids in formulations containing a phosphorus atom (HSPC, DSPE-PEG, and DOPC).

2.6.6 *Determination of drug concentration by HPLC*

The concentration of Gardiquimod and SHP099 was measured using analytical reversed-phase (RP)-HPLC on LC-20AD liquid chromatography (Shimadzu Corporation). The HPLC Eluent A consisted of a 5% CH_3CN aqueous solution with 0.1% trifluoroacetic acid (TFA); HPLC Eluent B consisted of 0.1% TFA in CH_3CN. Liposomes were diluted 20 times in MQ water and compared to serial standard solutions. An XBridge C8 (5 µm, 4.6x150 mm) column (Waters) was used and quantification of both compounds, using UV detection at 320 nm with an SPD-M20A Photodiode Array Detector fitted with a Deuterium Tungsten lamp (Shimadzu Corporation). A gradient from 0% to 100% B over 15 minutes was applied (flow rate 1 ml/min). Gardiquimod liposomes were diluted 4 times in dialysis buffer and compared to a Gardiquimod standard (25-100 µg/mL diluted in MQ).

2.6.7 *MTS viability assay*

CT26 cells were grown in DMEM medium supplemented with 10% (v/v) fetal bovine serum (FBS; Gibco-Invitrogen), 1% penicillin/streptomycin (Gibco-Invitrogen) at 37 °C in a humidified incubator containing 5% CO_2. Before the assay, cells were plated in a 96-well plate (1000~5000 cells/well). After 24 h of incubation, the cells were treated with different concentrations of free Gardiquimod and doxorubicin dissolved in DMSO (final DMSO <0.1%), or loaded in liposomes, respectively. After 24 h of treatment, the culture medium was removed,

and 100 µL of fresh medium was added to each well followed by incubation for another 24 h. Cell viability was analyzed by the CellTiter 96® AQueous MTS Reagent according to the manufacturer´s protocol. The background was subtracted (cell-free media + MTS solution) and readings were normalized according to the viability of untreated cells (regarded as exhibiting 100% viability).

2.6.8 *TLR-7 stimulation by HEK-Blue assay*

TLR-7 stimulation by Gardiquimod was evaluated using HEK-Blue™ hTLR7 Cells (InvivoGen, Catalog # hkb-htlr7), which are SEAP Reporter 293 cells expressing the human TLR7 gene. Cells were maintained in a complete growth medium supplemented with 10 µg/ml of blasticidin and 100 µg/ml of Zeocin. The cells were passaged for less than four generations and be 50-80% confluent before using them. Briefly, cells were gently collected and suspended in HEK-Blue Detection medium at ~220,000 cells per ml; 180 µL of cell suspension (~40,000 cells) was added to each well of a 96-well plate that contains 20 µL of free Gardiquimod or liposomal Gardiquimod stock solutions in triplicates, thus the final drug concentration was $1/10^{th}$ of the added concentration. After incubation for 16h, 24h, and 48h, respectively, the TLR7 stimulation responses were assessed by measuring SEAP levels in the supernatant by reading the OD at 630 nm with a microplate reader. The response rate was calculated by dividing the readout from treated cells by the untreated ones.

2.6.9 *PD-1/PD-L1 blockade assay*

A thaw-and-use PD-1/PD-L1 Blockade Bioassay kit (Promega) containing PD-1 effector cells, PD-L1 aAPC/CHO-K1 cells, culture medium, and Bio-Glo luciferase assay buffer and substrate was used. The tests were carried out according to the manufacturer´s protocols. PD-L1 aAPC/CHO-K1 cells were plated and incubated at 37°C for 16 hours before the addition of SHP099 or anti-PD1, together with PD-1 Effector Cells. The cells were co-incubated at 37°C for 6 hours. Mixed cell suspensions without any treatment were used as the control, and an assay medium without cells was used to read the background signal. Subsequently, Bio-Glo™ Reagent was added to each well, and luminescence was measured by reading on a microplate reader with glow luminescence reading. Fold induction = RLU (induced–background)/RLU (control–background).

2.7 References

1. Van der Zanden. *et al*. Opportunities for Small Molecules in Cancer Immunotherapy. *Trends in Immunology* **41**, 493–511 (2020).

2. Charalabidis, A. *et al.*. The Biopharmaceutics Classification System (BCS) and the Biopharmaceutics Drug Disposition Classification System (BDDCS): Beyond guidelines. *International Journal of Pharmaceutics* **566**, 264–281 (2019).

3. Kalepu, S. & Nekkanti, V. Insoluble drug delivery strategies: Review of recent advances and business prospects. *Acta Pharmaceutica Sinica B* **5**, 442–453 (2015).

4. Akbarzadeh, A. *et al. Liposome: Classification, preparation, and applications*. *Nanoscale Research Letters* vol. 8 http://www.nanoscalereslett.com/content/8/1/102 (2013).

5. Rahman, M., Alam, K., Beg, S., Anwar, F. & Kumar, V. Liposomes as topical drug delivery systems: State of the arts. *Biomedical Applications of Nanoparticles* 149–161 (2019) doi:10.1016/B978-0-12-816506-5.00004-8.

6. Nakhaei, P. *et al.* Liposomes: Structure, Biomedical Applications, and Stability Parameters With Emphasis on Cholesterol. doi:10.3389/fbioe.2021.705886.

7. Barenholz, Y. Doxil® - The first FDA-approved nano-drug: Lessons learned. *Journal of Controlled Release* **160**, 117–134 (2012).

8. Lu, J. *et al.* Breast Cancer Chemo-immunotherapy through Liposomal Delivery of an Immunogenic Cell Death Stimulus Plus Interference in the IDO-1 Pathway. *ACS Nano* **12**, 11041–11061 (2018).

9. Ramesh, A., Kumar, S., Nandi, D. & Kulkarni, A. CSF1R- and SHP2-Inhibitor-Loaded Nanoparticles Enhance Cytotoxic Activity and Phagocytosis in Tumor-Associated Macrophages. *Advanced Materials* **31**, 1–11 (2019).

10. Pauli, G., Tang, W. L. & Li, S. D. Development and characterization of the solvent-assisted active loading technology (SALT) for liposomal loading of poorly water-soluble compounds. *Pharmaceutics* **11**, (2019).

11. Gubernator, J. Active methods of drug loading into liposomes: Recent strategies for stable drug entrapment and increased in vivo activity. *Expert Opinion on Drug Delivery* **8**, 565–580 (2011).

12. Zucker, D., Marcus, D., Barenholz, Y. & Goldblum, A. Liposome drugs ' loading efficiency : A working model based on loading conditions and drug's physicochemical properties. *Journal of Controlled Release* **139**, 73–80 (2009).

13. Alyane, M., Barratt, G. & Lahouel, M. Remote loading of doxorubicin into liposomes by transmembrane pH gradient to reduce toxicity toward H9c2 cells. *Saudi Pharmaceutical Journal* **24**, 165–175 (2016).

14. Gubernator, J. Active methods of drug loading into liposomes: recent strategies for stable drug entrapment and increased in vivo activity. *Expert Opinion on Drug Delivery* **8**, 565–580 (2011).

15. Cern, A. *et al.* Quantitative structure - Property relationship modeling of remote liposome loading of drugs. *Journal of Controlled Release* **160**, 147–157 (2012).

16. Cern, A., Marcus, D., Tropsha, A., Barenholz, Y. & Goldblum, A. New drug candidates for liposomal delivery identified by computer modeling of liposomes' remote loading and leakage. *Journal of Controlled Release* **252**, 18–27 (2017).

17. Haran, G., Cohen, R., Bar, L. K. & Barenholz, Y. Transmembrane ammonium sulfate gradients in liposomes produce efficient and stable entrapment of amphipathic weak bases. *Biochimica et Biophysica Acta - Biomembranes* **1190**, 197 (1994).

18. Duong, A. D., Collier, M. A., Bachelder, E. M., Wyslouzil, B. E. & Ainslie, K. M. One Step Encapsulation of Small Molecule Drugs in Liposomes via Electrospray-Remote Loading. *Molecular Pharmaceutics* **13**, 92–99 (2016).

19. Engudar, G. *et al.* Remote loading of liposomes with a 124I-radioiodinated compound and their in vivo evaluation by PET/CT in a murine tumor model. *Theranostics* **8**, 5828–5841 (2018).

20. Kobold, S., Wiedemann, G., Rothenfußer, S. & Endres, S. Modes of action of TLR7 agonists in cancer therapy. *Immunotherapy* (2014) doi:10.2217/imt.14.75.

21. Ma, F., Zhang, J., Zhang, J. & Zhang, C. The TLR7 agonists imiquimod and gardiquimod improve DC-based immunotherapy for melanoma in mice. *Cellular and Molecular Immunology* **7**, 381–388 (2010).

22. Howell, B. A. & Chauhan, A. Interaction of Cationic Drugs with Liposomes. *Langmuir* **25**, 12056–12065 (2009).

23. Campbell, R. B., Balasubramanian, S. v. & Straubinger, R. M. Phospholipid-cationic lipid interactions: Influences on membrane and vesicle properties. *Biochimica et Biophysica Acta - Biomembranes* **1512**, 27–39 (2001).

24. Wang, Y. *et al.* Cooperative Self-Assembled Nanoparticle Induces Sequential Immunogenic Cell Death and Toll-Like Receptor Activation for Synergistic Chemo-immunotherapy. *Cite This: Nano Lett* **21**, 4380 (2021).

25. Yuan, X. *et al.*. Recent Advances of SHP2 Inhibitors in Cancer Therapy: Current Development and Clinical Application. *J. Med. Chem.* **63**, 11368–11396 (2020).

26. Marasco, M. *et al.* Molecular mechanism of SHP2 activation by PD-1 stimulation. *Sci. Adv.* **6**, (2020).

27. Chen, Y. N. P. *et al.* Allosteric inhibition of SHP2 phosphatase inhibits cancers driven by receptor tyrosine kinases. *Nature* **535**, 148–152 (2016).

28. Mainardi, S. *et al.* SHP2 is required for growth of KRAS-mutant non-small-cell lung cancer in vivo letter. *Nat. Med.* **24**, 961–967 (2018).

29. Ramesh, A. *et al.* CSF1R- and SHP2-Inhibitor-Loaded Nanoparticles Enhance Cytotoxic Activity and Phagocytosis in Tumor-Associated Macrophages. *Adv. Mater.* **31**, 1–11 (2019).

Chapter 3

Enhancing adoptive cell therapy by T cell loading of SHP2 inhibitor nanocrystals before infusion

Xin Li[1], Hólmfridur Halldórsdóttir[1], Sven Weller[1], Anna Colliander[1], Martin Bak[1], Paul Kempen[1,2], Gael Clergeaud[1*] & Thomas L. Andresen[1*].

[1] Department of Health Technology, Technical University of Denmark, 2800 Kgs. Lyngby, Denmark.
[2] National Centre for Nano Fabrication and Characterization, Technical University of Denmark, 2800 Kgs. Lyngby, Denmark.
*Corresponding authors. E-mail: gaecle@dtu.dk, tlan@dtu.dk

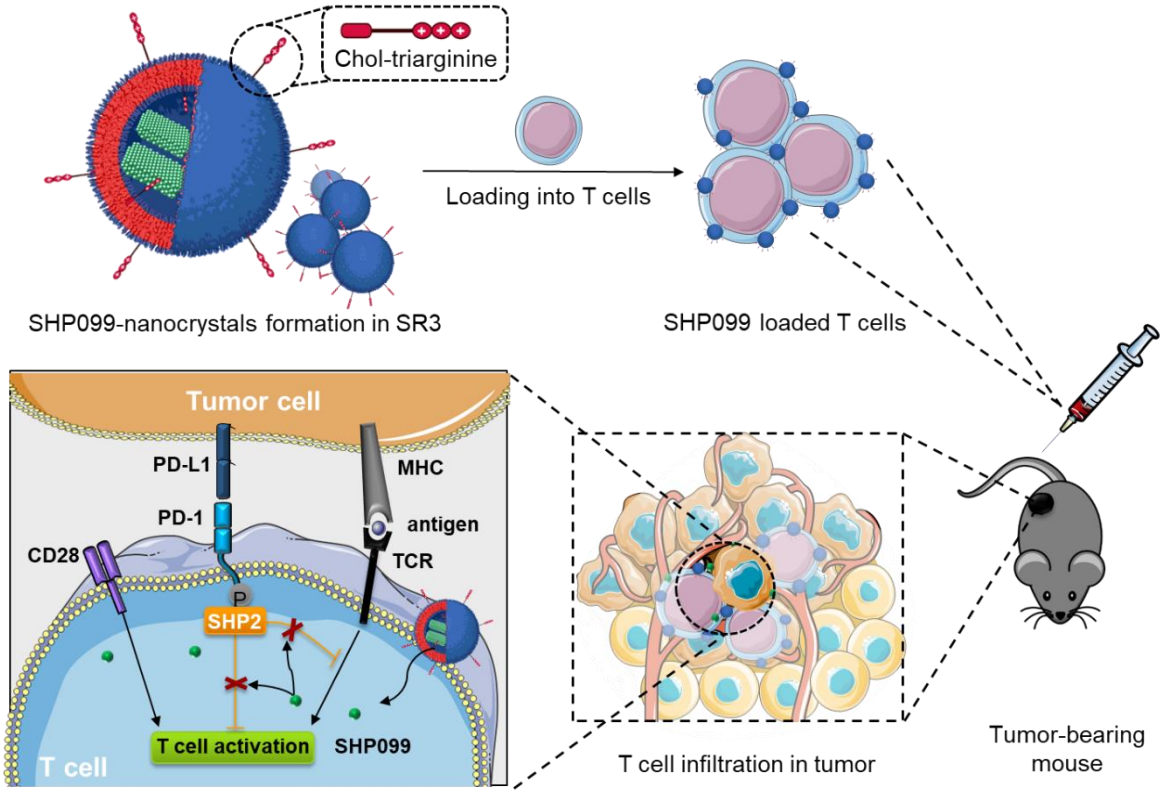

3.1 Abstract

Whereas adoptive T cell therapy has been extensively studied for cancer treatment, the response is still limited primarily due to immune dysfunction related to poor cell engraftment, tumor infiltration and engagement, and lack of target. In addition, the modification of therapeutic T cells often suffers from being complex and expensive. Here we present a strategy to load T cells with SHP099, an allosteric SHP2 inhibitor, to enhance the therapeutic efficacy of the T cells. Remote-loading of SHP099 into lipid nanoparticles decorated with tri-arginine motifs resulted in nanocrystal formation of SHP099 inside the lipid vesicles, and alloweding high loading efficiency and prolonged retention of SHP099 nanocrystals within T cells. Cell-loaded SHP099 enabled sustained inhibition of the PD-1/PD-L1 signaling and increased cytolytic activity of the T cells. We show in mice model that tumor-homing T cells can circulate with the cargos, improving their tumor accumulation compared to systemically administered lipid nanoparticles. On an established solid tumor model, adoptively transferred SHP099 loaded T cells induced complete tumor eradication and durable immune memory against tumor re-challenging on all of treated mice, achieving equivalent efficacy as repeated doses of the anti-PD-L1 antibody. We demonstrate that the combination of T cell therapy with SHP2 inhibition is a promising therapeutic strategy and the lipid nanocrystal platform could be generalized as a promising approach for T cell loading of immunomodulators.

3.2 Introduction

Adoptive transfer of expanded tumor-infiltrating lymphocytes (TILs), genetically modified T cells that are made to express tumor antigen-specific T cell receptors (TCRs), or chimeric antigen receptors (CARs) has demonstrated great success in the treatment of some established malignancies, especially for leukemia and lymphoma[1,2]. However, favorable conditions regarding target antigen presentation and immunostimulatory cytokines are absent in many solid tumors. Instead, multiple factors including loss of tumor antigens and heterogeneous immunosuppressive components in the tumor microenvironment (TME) limit the persistence and function of adoptive T cells[3,4]. Thus, to optimize the therapeutic outcomes, new treatments aimed at counteracting the immunosuppressive TME in combination with adoptive T cell therapy (ACT) have been intensively pursued. Combinations of checkpoint inhibitors (CPIs) with T cell therapies have shown advanced clinical benefits[5,6]. Several major checkpoints have been identified and studied in the past decades including PD-1, CTLA-4, LAG3, TIM3, TIGIT,

and BTLA. PD-L1 is often overexpressed on tumor cells and various host cells[7], and its engagement with PD-1 on T cells leads to exhaustion marked by decreased proliferation, production of type I cytokines, and poor cytolytic activity[8]. The dysfunctional state of T cells can be reversed by CPIs to counteract the immunosuppressive signal and thereby improve ACT efficacy[9]. So far, the success in immunotherapy using CPIs is limited to monoclonal antibodies, with anti-CTLA-4, anti-PD-1/PD-L1 authorized for several cancer types successively[10], however, the overall response rate remains quite low.

Src-homology domain-containing protein tyrosine phosphatase-2 (SHP2) is a major phosphatase involved in several key cellular processes that regulates cell survival and proliferation[11]. It serves as an important hub to connect multiple growth factors, cytokine, and extracellular-matrix receptor-induced signaling pathways, such as Jak/STAT, PI3K/AKT, RAS/Raf/MAPK, and PD-1/PD-L1 pathways, thus playing a major role for both cancer and immune cells. Upon binding to its ligand, PD-1 forms negative costimulatory microclusters that directly inhibit T cell receptor signaling by recruiting phosphatase SHP2[12]. Many other immune checkpoint pathways such as CLTA-4, BTLA, TIGIT, also recruit SHP2 in their cytoplasmic regions to suppress T cell function[13]. In $CD4^+$ T cells, knockout of SHP2 hyper-activated STAT1, resulting in increased Th1 differentiation and IFN-γ production, which in turn enhanced the activity of $CD8^+$ CTLs[14]. Targeting SHP2 has emerged as a promising strategy for cancer immunotherapy, and the discovery of allosteric inhibitors represented by SHP099 inspired a novel approach to selectively target SHP2[15]. SHP099 has shown encouraging preclinical results on various cancer types[16–19], however, multiple doses of up to 100mg/kg were required on mice models. The clinical translation at these dose levels seems unlikely. Moreover, to our knowledge, previous studies have mainly focused on targeting cancer cells with SHP2 inhibitors. The combination of SHP2 inhibition with adoptive T cell therapy remains to be thoroughly investigated.

Delivering therapeutic agents to specific tumor sites and cell subsets with minimal off-target distribution is crucial for cancer treatment[20]. For this reason, nanoparticle-based platforms have been explored for targeted delivery to tumors and immune cells[21,22]. However, a comprehensive review summarized that a median of only 0.7% of the administered nanoparticles could reach solid tumors[23], and targeting those nanomedicines to T cells remains an even bigger challenge due to the non-phagocytic nature of T cells. An alternative strategy to overcome the challenge is the use of cells as drug delivery vehicles[24]. Nanoparticles containing interleukins[25,26], small

molecule drugs[27], siRNA[28], or photothermal therapy[29] have been conjugated to T cells, to either improve the function of T cells or promote drug delivery to the tumor site. The strategy utilizes the natural properties of T cells to circulate for a long time, be able to cross endothelial barriers, and infiltrate into tumor tissue[30].

In this work, we developed a lipid platform for loading the small molecule checkpoint inhibitor, SHP099, as nanocrystals into T cells before *in vivo* infusion. The SHP099 nanocrystals can stay stably in T cells over days and filtrate into tumors together with T cells. Thus the T cells are equipped with a depot of supporting drugs against the immunosuppressive signals in the TME, exhibiting an enhanced persistence and anti-tumor efficacy (**Figure 3.1**). Active-loading of SHP099 using transmembrane gradients allowed the encapsulation of high concentrations of crystallized SHP099 into a novel lipid nanoparticle formulation decorated with tri-arginine motifs on the surface. We found that the nanoparticles remained in T cells for days, sustainably released SHP099, which acted as CPI in the carrier T cells. The T cells loaded with SHP099 nanocrystals showed an increased tendency to stay in the central memory phenotype and displayed enhanced cytotoxicity against target tumor cells. Using an EG.7-OVA tumor-bearing mice model, we demonstrated the improved tumor accumulation of nanoparticle cargos carried by T cells. Consequently, we observed improved antitumor efficacy of adoptive transferred SHP099 loaded T cells compared with unloaded T cells. Moreover, the efficacy of a single dose of SHP099-T cells was equivalent to the combination of T cell therapy with multiple dosages of anti-PD-L1. Considering the transferable remote-loading of drugs with similar physiochemical properties into the lipid nanoparticles, this lipid nanocrystal platform can be potentially applied to load T cells with various types of therapeutic agents, representing a new strategy for modifying cells for improved functionality.

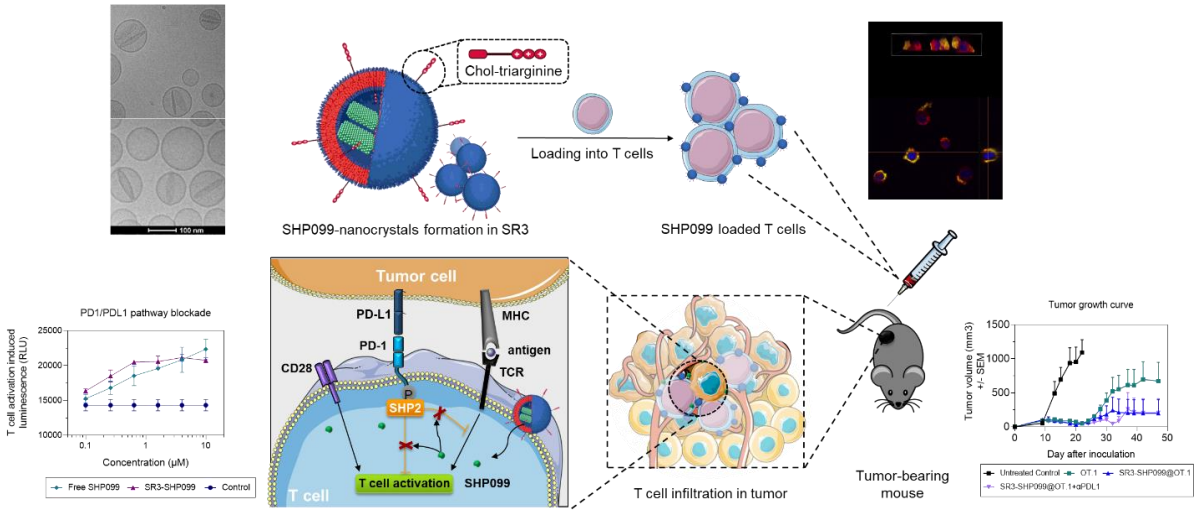

Figure 3.1 Schematic illustration of T cell loading of SHP2 inhibitor nanocrystals for adoptive T cell therapy.

3.3 Results

3.3.1 *Tri-Arginine conjugate increases lipid nanoparticles loading to murine T cells.*

To load T cells with the drug molecule and meanwhile prevent pre-mature release before arriving at the active sites, nanoparticles have been used as 'backpacks' to attach large therapeutic molecules to living cells[31]. Here, we designed a tri-arginine functionalized lipid nanoparticle (SR3) as a versatile platform for loading drugs into T cells (**Figure 3.1**). The tri-arginine conjugate consisted of the peptide sequence (Gly-Trp-Arg-Arg-Arg) synthesized by solid-phase peptide synthesis, and the sequence was linked to a cholesterol anchor in order to enable incorporation into the lipid membrane of the lipid nanoparticles (Supplementary Information). The cationic arginine-rich motifs exposed on the SR3 nanoparticle surface can exert strong interactions with the negatively charged cell membrane through electrostatic attraction and induce membrane deformation[32]. For comparison, we also tested saturated stealth (SS) lipid nanoparticles with a PEGylated shell and saturated cationic (SCat) lipid nanoparticles with a high positive charge provided by cationic lipid DSTAP. The lipid nanoparticles had similar hydrodynamic diameters (110-140 nm), with narrow PDI (~ 0.050), and both Scat and SR3 formulations were positively charged (~ +35 mV) (**Figure 3.2a**).

Flow cytometry analysis of fluorescently-labeled nanoparticles showed that only SR3 nanoparticles were efficiently loaded into activated murine cytotoxic $CD8^+$ T cells. Here,

almost 100% of T cells were loaded with SR3 nanoparticles, and the T cells displayed a much higher mean fluorescence intensity (MFI) signal compared to loading with the SS- and Scat formulations (**Figure 3.2b, Figure 3.7**). As expected, PEGylated SS formulation showed almost no T cell attachment, most likely due to the electrostatic repulsion and the non-phagocytic nature of T cells. Despite having a similar surface charge, the SR3 formulation yielded around a 20-folds higher MFI signal in the T cells than the Scat nanoparticles **(Figure 3.2c)**. We reasoned that the tri-arginine mimics the function of the polycationic cell-penetrating peptide[32], thus mediating high T cell loading efficiency. Confocal microscopy was used to confirm the attachment of the SR3 lipid nanoparticles to the surface of the T cells, showing them evenly distributed among the cells and forming a cap structure at the cytoplasmic face of the T cell membrane (**Figure 3.2d)**. To optimize the loading conditions, we investigated the effect of incubation time and observed that increasing incubation time could lead to higher loading efficiency but was accompanied by a slightly decreased cell viability after 3 h (**Figure 3.2e**). Since the structure and lipid compositions of the plasma membrane of T cells are dynamically changing during the activation process[33], cells activated with anti-CD3/CD28 at different times were tested for loading SR3. We found that the loading efficiency was significantly higher on day 5 of activation than on the other days (**Figure 3.2f**). Further screening of different ratios of tri-arginine and PEG content in the SR3 formulation revealed no significant differences in loading efficiency (**Figure 3.8)**. To conclude, these experiments confirmed that SR3 lipid nanoparticles containing 1.5% Cholesterol-GWR3 and 0.5% DSPE-PEG2k are efficiently loaded by T cells under the optimized conditions.

a

Formulation	Composition (mol%)	Size (nm)	PDI	ζ-Potential (mV)
Saturated Stealth (SS)	HSPC:Cholesterol:DSPE-PEG2000 (57:38:5)	117.8 ± 5.6	*0.053*	-12.6 ± 2.6
Saturated Cationic (SCat)	HSPC:Cholesterol:DSTAP (52:38:10)	134.1 ± 8.9	*0.043*	36.8 ± 3.0
Saturated TriArginine (SR3)	HSPC:Cholesterol:DSTAP: Chol-GWR3:DSPE-PEG2000 (50:38:10:1.5:0.5)	133.6 ± 12.1	*0.049*	34.9 ± 2.6

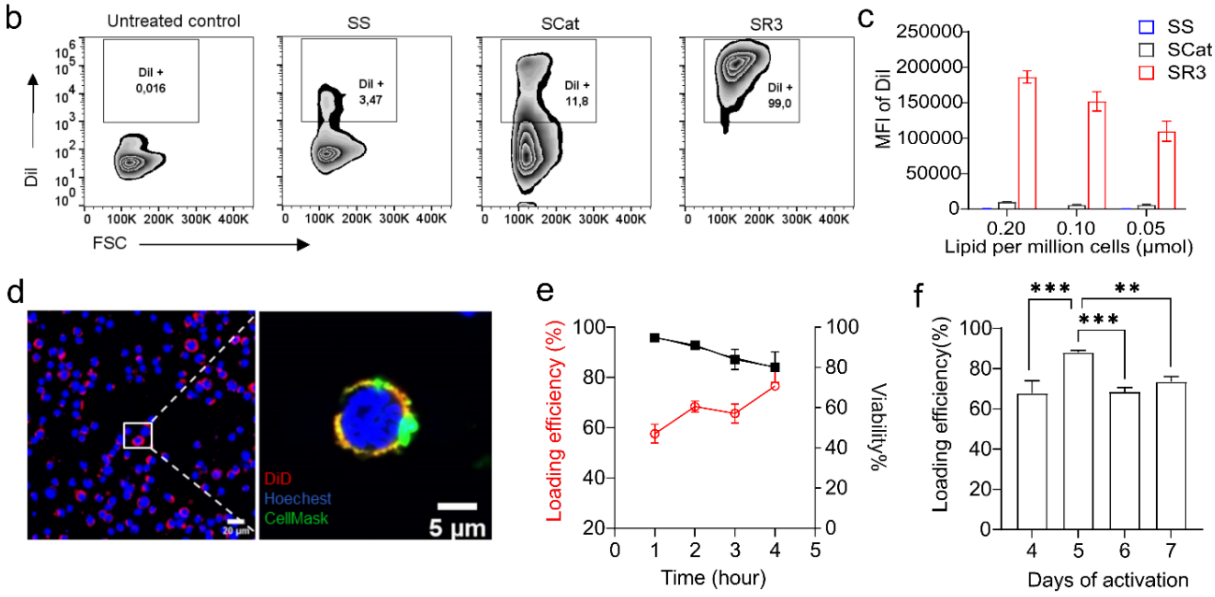

Figure 3.2 Formulation of lipid nanoparticles with tri-Arg enhances T cell loading**. a** Size, PDI, and Z-Potential distribution of lipid nanoparticle formulations. **b,** Representative flow cytometry plots depicting DiI labeled nanoparticle loading on T cells. **c,** MFI of each formulation from T cells at different concentrations. Data are represented as Mean ± SEM (n = 5). **d,** Confocal microscopy images of CD8+ effector T cells stained with Hoechest33258 (blue) and CellMask Green (green) following incubation with DiD-labeled nanoparticles (red). **e,** Nanoparticle loading efficiency, and cell viability as a function of incubation time in murine CD8+ effector T cells activated after 6 days. **f,** Effect of cell CD3/CD28 activation time prior incubation with nanoparticles during 2h on loading efficiency. Data are presented as means ± SD (n=3; ** = $p < 0.005$; *** = $p < 0.001$, two-tailed unpaired t-test with multiple comparison.).

3.3.2 *SHP099 nanocrystals are formed by remote loading of SHP099 into lipid nanoparticles.*

Having optimized the lipid formulation and T cells loading procedure, we next focused on loading the formulations with the therapeutic agent SHP099 which can promote T cells functions to improve anti-cancer efficacy. SHP099 is a small amphipathic molecule (clogP = 2.74) and has the characteristics of a weak base with the isoelectric point between 7-8. With its physicochemical nature like doxorubicin which can be loaded with transmembrane ammonium sulfate gradient, we hypothesized SHP099 could be remote loaded and crystalized into the lipid nanoparticles using a similar conditon[34]. As illustrated in **Figure 3.3a** uncharged species of

SHP099 upon diffusing into the nanoparticle core, where the compound gets protonated by the released hydrogen ion. In the charged state, the compound cannot diffuse out across the lipid bilayer and therefore remains trapped inside. After optimization of remote loading conditions, we were able to encapsulate high concentrations of SHP099 in SR3 with an average encapsulation efficiency (EE) of 91% and a high drug-to-lipid molar ratio of 0.23, without affecting the size, PDI, and zeta-potential of the lipid nanoparticles (**Figure 3.3b**). SHP099 formed precipitates inside the lipid shell as revealed by cryo-TEM (**Figure 3.3c**), resembling the crystallization of doxorubicin observed inside liposomes[35]. We reasoned the nanocrystal formation that the amphiphilic weak base SHP099, upon crossing the lipid membrane, is ionized and the ionized SHP099 further forms a complex with the sulfate counterion. In some cases, this complex exceeds its solubility in the nanoparticle core and precipitates as nanocrystals. This is an important finding as it is the first evidence of this class of SHP2 inhibitors forming nanocrystals inside lipid nanoparticles, which enables enhanced drug stability and sustained release rates. We next investigated the release profile of SHP099 by incubating the lipid nanocrystals at 37 ºC in PBS and a cell culture medium containing 10% FBS to mimic physiological conditions. In both conditions, SHP099 showed steady release over time. We observed that only 32% of the SHP099 was released in PBS and 51% was released in cell culture medium after 8 days (**Figure 3.3d**). The results demonstrated for the first time that SHP099 can be encapsulated in lipid nanoparticles as nanocrystals through remote loading methods to achieve very high drug encapsulation, high stability, and sustained release over days.

3.3.3 ***SHP099 nanocrystals can block the PD-1/PD-L1 axis.***

To test the ability of SHP099 nanocrystals to block the PD-1/PD-L1 interaction, we used a bioluminescent cell-based PD-1/PD-L1 blockade assay. Two genetically engineered cell lines, PD-1 effector cells, and PD-L1 aAPC/CHO-K1 cells, were co-cultured for six hours in the presence of various concentrations of free-SHP099, SR3-SHP099 nanocrystals, and anti-PD1 antibody as the positive control. The PD1/PD-L1 interaction inhibited TCR-mediated luminescence from the effector cells, thus disruption of the interaction released the inhibitory signal, reflected by the increase in luminescence. Free SHP099 and SR3-SHP099 nanocrystals induced a similar increase in luminescence **(Figure 3.3e)**, which was lower than the increase observed by the direct blockade with anti-PD1. However, after 24h, the effect of anti-PD1 quickly dropped to the same level as SHP099 and then completely back to the unblocked

control level (**Figure 3.3e**). Meanwhile, SHP099 mediated a sustained PD-1/PDL1 blockade longer than the antibody. This phenomenon may be one of the key hindrances to the efficacy of antibody-based CPIs, which can neutralize the equal amount of target ligands at the most, thus requiring frequent high doses if the cells express new checkpoint ligands on their surface[36]. In this case, prolonged downstream inhibition of the PD1/PD-L1 axis achieved by the SHP099 nanocrystals emerges as a promising alternative.

3.3.4 ***SHP099 nanocrystals can be efficiently loaded in T cells and sustainably released over days.***

Using the same conditions as with empty lipid nanoparticles, we investigated whether SR3 encapsulating SHP099 nanocrystals would load into T cells. After loading, the cells were washed thoroughly and lysed to measure the amount of SHP099 by HPLC. Depending on the feeding ratio, 60 to 90% of initial SHP099 were loaded by T cells (**Figure 3.3f**), corresponding to each T cell carrying up to 20 pg of SHP099 nanocrystals (**Figure 3.3g**), which provides a depot of SHP099 in the T cells. The loaded SHP099 nanocrystals exhibited a sustained release profile from the T cells over 5 days and the release was concentration-dependent. T cells loaded with a high dose of SR3-SHP099 (0.1μmol nanoparticles per million cells) showed longer retention of SHP099 and slower percentage release than the ones loaded with the lower dose (0.05μmol nanoparticles per million cells) (**Figure 3.3h**).

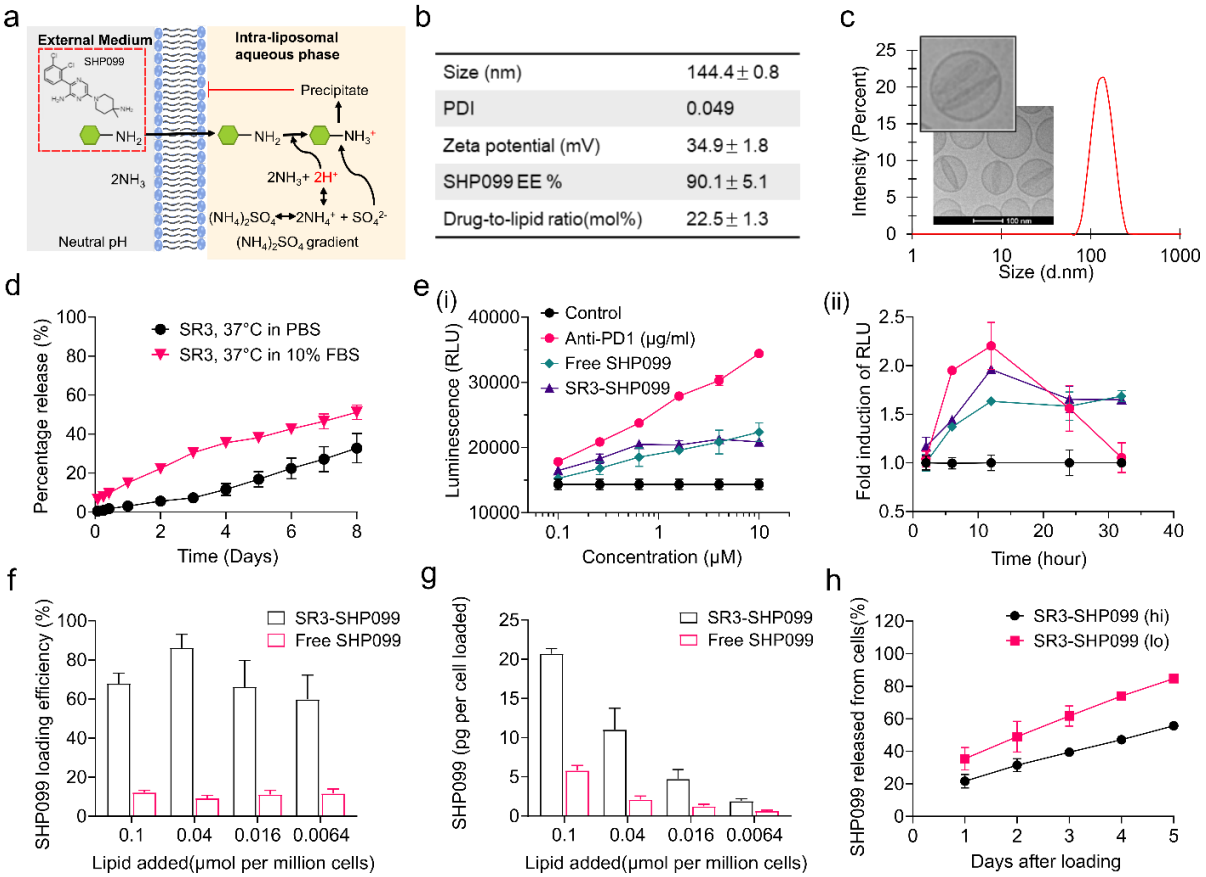

Figure 3.3 T cell loading of SHP099 nanocrystals. **a,** Remote loading of the amphipathic weak base SHP099 into SR3 formulation using transmembrane ammonium sulfate gradient. **b,** Characteristics of the SR3-SHP099 nanocrystals**.** Data are presented as means ± SD (n=3). **c,** Size distribution, and cryo–TEM image of SR3 lipid nanoparticles encapsulating SHP099 nanocrystals. Scale bar = 100nm. **d,** The release profile of SHP099 from SR3 formulation in PBS or cell culture medium containing 10% serum (37 ºC, pH=7.4). **e,** PD-1/PD-L1 Blockade Bioassay showing the inhibitory activity of SHP099 and anti-PD-1 antibodies (i) for six hours at escalating concentrations and (ii) for different incubation times using 2μM of SHP099 and 2μg/ml of anti-PD1. Data are presented as means ± SEM of triplicate samples. **f,** Loading of free SHP099 or SR3 encapsulated SHP099 to CD8+ T cells at various concentrations expressed as loading efficiency or **g,** amount of SHP099 loaded per million T cells. **h,** Release rates of SHP099 from T cells loaded with 0.1μmol per million cells (hi) or 0.05μmol/million cells (lo) of SHP099. Data are presented as means ± SEM of two independent experiments conducted in duplicate.

3.3.5 *Loading T cells with SHP099 nanocrystals does not affect cell viability and proliferation.*

Once we had demonstrated that SHP099 nanocrystals could be loaded to T cells we next investigated if the T cell function was hampered. We evaluated the effect of loading SR3-SHP099 on the key characteristics of T cells including viability, proliferation, phenotype, and cytotoxic function. Neither empty SR3 nanoparticles nor SR3-SHP099 nanocrystals affected cell viability compared with untreated cells, and the cell viability was preserved at higher than 95% after loading (**Figure 3.4a**). The T cells stimulated with anti-CD3/CD28 expanded 6-10-fold on day 5 and kept proliferating after SR3-SHP099 loading, achieving an extra 4-fold expansion after three days (**Figure 3.4b**). These results show that loading with SR3-SHP099 has no immediate or prolonged toxicity on T cells and that their proliferation capacity is maintained.

3.3.6 *SHP099 drives T cells into central memory phenotype and prevented T cell exhaustion.*

The phenotype change of T cells after loading was further investigated by measuring the expression levels of the phenotypic markers CD44 and CD62L. At 24 hours and 72 hours after loading with SHP099 nanocrystals, which correspond to day 6 and day 8 of initial antibody activation, more than 86% of loaded T cells differentiated into the central memory subpopulation ($CD44^+$, $CD62L^+$) (**Figure 3.4c**). This is remarkably higher than the proportion of unloaded T cells with the central memory phenotype (60% at 24h, 31% at 72h). Most of the unloaded T cells already lost the effector or memory markers on day 6 and were more pronounced on day 8, showing a sign of dysfunction. The SR3-SHP099 nanocrystals induced a similar phenotypic change of T cells as the free SHP099, thus showing preserved SHP2 inhibitor activity of the nanocrystals. The dominance of memory phenotypes arises from diminished T cell exhaustion. Persistent antigen exposure often leads to T cell exhaustion, in which state T cells lose effector functions and thus fail to exert sufficient tumor control[37]. Memory $CD8^+$ T cells persist in greater numbers and have higher proliferation potential upon antigen re-encounter than naïve T cells and effector T cells[38,39]. Down-regulation of CD44 expression is one of the key markers distinguishing exhausted T cells from effector/memory T cells[8]. As shown in **Figure 3.4d,e,** SHP099 loaded T cells maintained a dramatically higher level of CD44 expression than unloaded T cells 24h and 72h after loading.

However, CD44 and CD62L only provide a basic insight into the state of the $CD8^+$ T cells, and memory $CD8^+$ T cells comprise a heterogeneous pool of cells differing in phenotype and function. Extended mechanistic understanding of the effect of loading SHP099 on $CD8^+$ T cells still requires more in-depth investigation.

3.3.7 *Loading SHP099 nanocrystals into CD8+ T cells improves their cytotoxic function*

The main therapeutic function of cytotoxic T cells is to specifically recognize and kill target cells. To evaluate the effects of SR3-SHP099 nanocrystals on the cytotoxic function of T cells, ovalbumin (OVA)-specific T cell receptor-transgenic OT-1 $CD8^+$ T cells were co-cultured with OVA pulsed B16-OVA target tumor cells or the isogenic control cells B16-F10 at various effector-to-target (E: T) ratios for 5h and 24h, respectively. To better address the biological effect of SHP099 in blocking the PD-1/PD-L1 downstream signal transduction, tumor cells were stimulated with IFN-γ before co-culture to upregulate the PD-L1 expression (**Figure 3.9a**)[40]. After 5 h, we observed that SHP099 loaded T cells exerted significantly higher tumor cell killing than unloaded T cells. At an E: T ratio of 20:1, SR3-SHP099 loaded T cells lysed 62% of the B16-OVA cells compared to 45% by the unloaded T cells. When the co-culture time was prolonged to 24h, loaded T cells showed further enhanced tumor cell lysis with 100% of B16-OVA cells lysed at a 20:1 ratio, while only 60% were lysed by unloaded T cells (**Figure 3.4f**). At both time points, OVA-negative B16-F10 cells remained unaffected (**Figure 3.9b**), meaning that SHP099 at these concentrations did not have a direct cytotoxic effect on tumor cells. The SHP099 nanocrystals equipped T cells with a depot of CPIs that counteract the immunosuppression and strengthen the specific recognition and killing function of $CD8^+$ T cells.

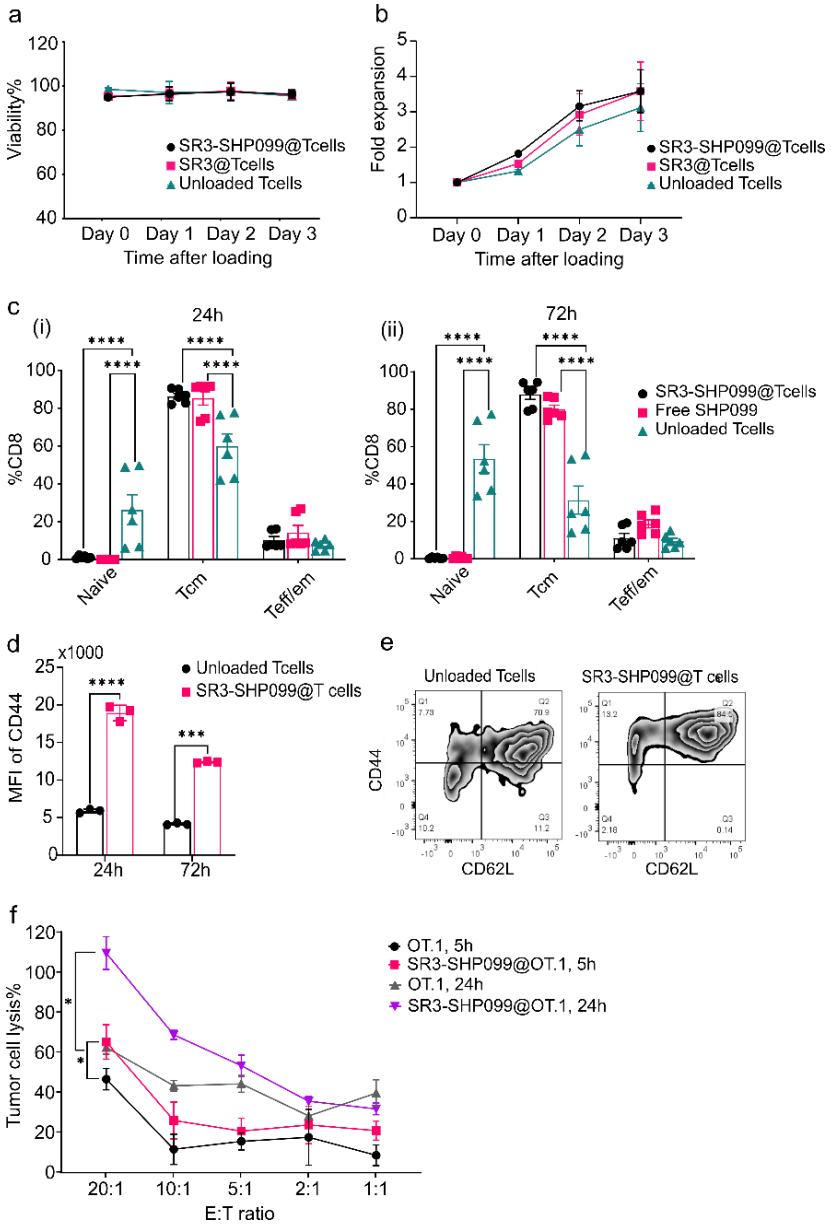

Figure 3.4 T cell viability and function after loading with SHP099. **a,** Cell viability of CD8+ T cells loaded with either empty SR3 or SHP099 nanocrystals measured over 3 days using DAPI staining. **b,** Fold expansion of CD8+ T cells after loading empty SR3 or SHP099 nanocrystals. **c,** Effects of SHP099 on the phenotype of CD8+ T cells. T cells were loaded with SHP099 on day 5 of activation and the phenotypes were determined 24 hours and 72 hours after loading by measuring the expression of CD44 and CD62L. Naïve T cells (CD44-/CD62L+), Tcm: Central memory T cells (CD44+/CD62L+), Teff/em: Effector and Effector memory T cells (CD44+/CD62L-). Data are presented as means ± SEM of two independent experiments conducted in triplicate. **d,** CD44 expression at 24h after loading. MFI ± SD, n=3. P values were determined by two-way ANOVA with the Bonferroni test. ***P<0.001, ****P<0.0001 **e,** Representative histograms of CD44 and CD62L 24h after loading. **f,** Co-culture of SR3-SHP099 loaded OT.1 cells and OVA-pulsed B16 (B16-OVA) cells at different effector: target (E: T) ratios. Specific tumor lysis was measured by LDH assay. Data are presented as means ± SEM of two independent experiments conducted in duplicate. *P<0.01 by two-way ANOVA with Tukey test at the E: T ratio of 20:1.

3.3.8 ***Unmodified T cell biodistribution and increased delivery of the payload to tumors by SR3-loaded T cells.***

We next evaluated the potential of harnessing the loaded T cells to transport the cargo *in vivo* using OT.1 $CD8^+$ T cells and EG.7-OVA tumor-bearing mice. We first investigated if loading the T cells with SHP099 nanocrystals would have an impact on their *in vivo* biodistribution and proliferation by tracking the cells with cell trace violet (CTV) in major organs and tumors after intravenous injection. On day 1 and day 3 after T cell infusion, flow cytometry of cell suspensions from the lung, spleen, and tumor revealed no major changes in T cells distribution upon loading with SHP099 nanocrystals (**Figure 3.5a**). Both SR3-loaded T cells and unloaded T cells accumulated predominantly in the spleen. Compared to day 1 when only a few transferred T cells were observed in the tumor, homing of T cells to the tumor increased by over 100 times on day 3 (**Figure 3.5a**). This increase was also observed in the tdLN. These results are in line with previous studies that showed adoptive T cells remained in circulation on day 1 and gradually trafficked to tumors and immune organs from day 2[41,42]. The increased number of CTV+ cells and dilution of CTV signals for 3 days demonstrated that the SR3-loaded T cells held great capability of proliferation and persistence *in vivo* (**Figure 3.10)**.

To confirm whether the loaded T cells could transport the SR3 nanoparticles into tumors, the DSPE-DOTA construct was chelated with gadolinium (Gd), formulated in the SR3 nanoparticles, and the Gd accumulation from systemically injected SR3-Gd nanoparticles or SR3-Gd loaded T cells was analyzed in major organs and tumors by ICP-MS. As expected from the low tumor accumulation of the transferred T cells on day 1 (**Figure 3.5a**), no difference in the Gd signal was observed in the tumors (**Figure 3.5b**). However, upon T cell homing on day 3, T cells loaded with SR3-Gd accumulated 3.3-fold more in tumor tissues than systemically injected SR3-Gd nanoparticles, whose levels reduced from 24h to 72h. While most Gd signal was in the liver and spleen, we observed significantly different distribution profiles as the T cell-loaded SR3-Gd showed a higher accumulation in the spleen while the SR3-Gd nanoparticles were preferentially accumulating in the liver (**Figure 3.5b**).

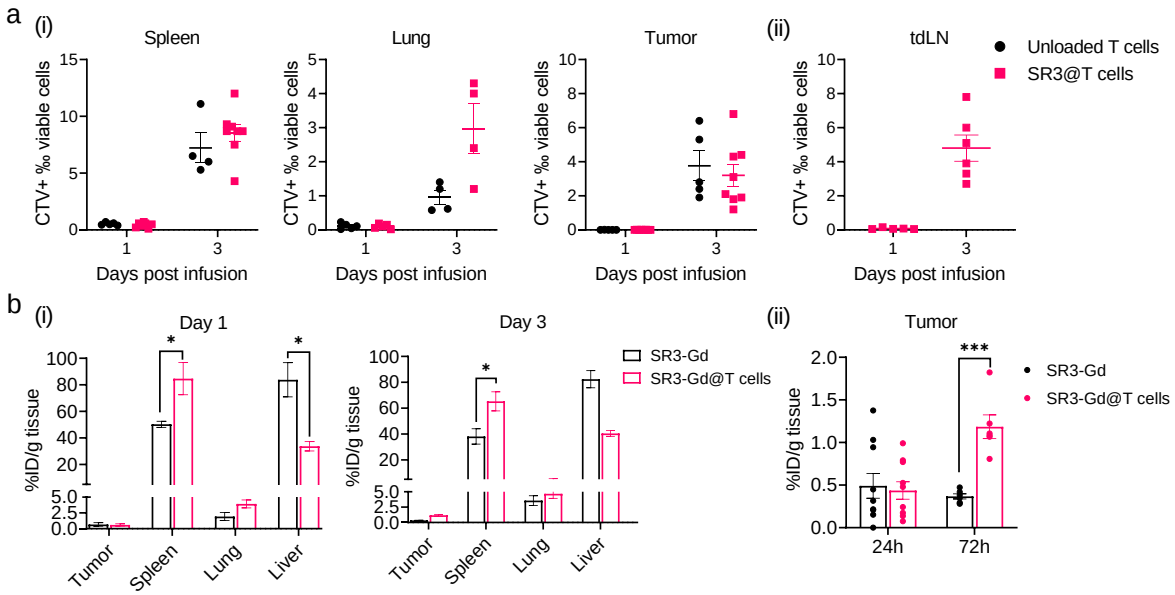

Figure 3.5 Biodistribution of T cells and SR3 loaded in T cells on an EG.7-OVA tumor-bearing mice model. **a, (i)** The ratio of Cell Trace Violet (CTV) labeled T cells, either unloaded or loaded with SR3 nanoparticles, in the total cells from spleen, lung, and tumor on day 1 and day 3 after adoptive transfer. **(ii)** Change of T cell number in tumor-draining lymph node (tdLN) from day 1 to day 3. Tissues were harvested and prepared into single cells and run on a flow cytometer for CTV-positive cells. Data are presented as Mean ± SEM, n=4-8. **b, (i)** Biodistribution of free SR3-Gd and SR3-Gd@T cells in tumor, spleen, lung, and liver. **(ii)** Individual %ID values in tumors. Values are the percentage of injected dose per gram of tissue (%ID/g) and were measured by ICP-MS. Data are presented as Mean ± SEM pooled from two independent experiments. ; * = $p < 0.05$; *** = $p < 0.001$, by two-tailed unpaired t-test.).

3.3.9 *Loading SHP099 nanocrystals on T cells before infusion results in clearance of pre-existing tumors and induces a durable protective immune response.*

The therapeutic efficacy of the T cells loaded with SHP099 nanocrystals and their combination with other therapies was investigated in C57BL/6J mice bearing EG7-OVA tumors (**Figure 3.6a**). Mice were pre-treated with CPX for lymphodepletion before T cell transfer. Compared with the untreated mice (median survival = 16 days), CPX treatment halted tumor growth at the early stage but completely lost control of tumor growth after that (**Figure 3.6b, d**), prolonging the median survival to 33 days (**Figure 3.6c**). Likewise, despite the early slowing of tumor growth by OT.1 $CD8^+$ T cells, tumor relapse happened fast and only two out of six mice showed complete response to the therapy (**Figure 3.6b, c, d**). In contrast, treatment with OT.1 CD8+ T cells loaded with SHP099 nanocrystals provided inhibition of tumor growth and relapse in all groups **(Figure 3.6c)** as well as increased survival rates compared to OT.1

treatment alone (**Figure 3.6d**). After a single dose of SR3-SHP099 loaded T cell treatment, five out of six mice were completely tumor-free 34 days after tumor inoculation without tumor recurrence (**Figure 3.6b**). Similar response rates were observed by combining SR3-SHP099@OT.1 with anti-PD-L1 therapy. Moreover, we found that loading SHP099 nanocrystals in a mixture of $CD8^+$ T cells and $CD4^+$ T cells delayed the tumor relapse in one mouse, but there were no differences in response rate and survival in the group treated with SR3-SHP099@$CD8^+$ OT.1 alone. Overall, the mice tolerated all treatments well, as indicated by the negligible changes in body weight (**Figure 3.6e**).

In order to demonstrate if this novel therapeutic strategy induced long-term immunity, we re-challenged the cured mice by subcutaneously injecting EG7-OVA tumor cells into the opposite flank of the primary tumor. We show that all mice cured by SHP099 loaded T cells rejected the secondary tumors (**Figure 3.11a**), resulting in 100% survival on day 30 after inoculation when all mice from the untreated control group reached the endpoint regarding tumor size (**Figure 3.6f**). Tumor recurrence also happened in OT.1 cured mice by day 30. Analysis of the T cell populations in the spleen of the cured mice revealed an increased ratio of central memory $CD8^+$ and $CD4^+$ T cells, indicating that the immune memory was established after the eradication of the primary tumors (**Figure. 3.11b**). Thereby loading SHP099 nanocrystals in T cells not only increased the anti-tumor efficacy by rejecting the established primary tumors but also induced a stronger long-term immunity compared with unloaded T cells.

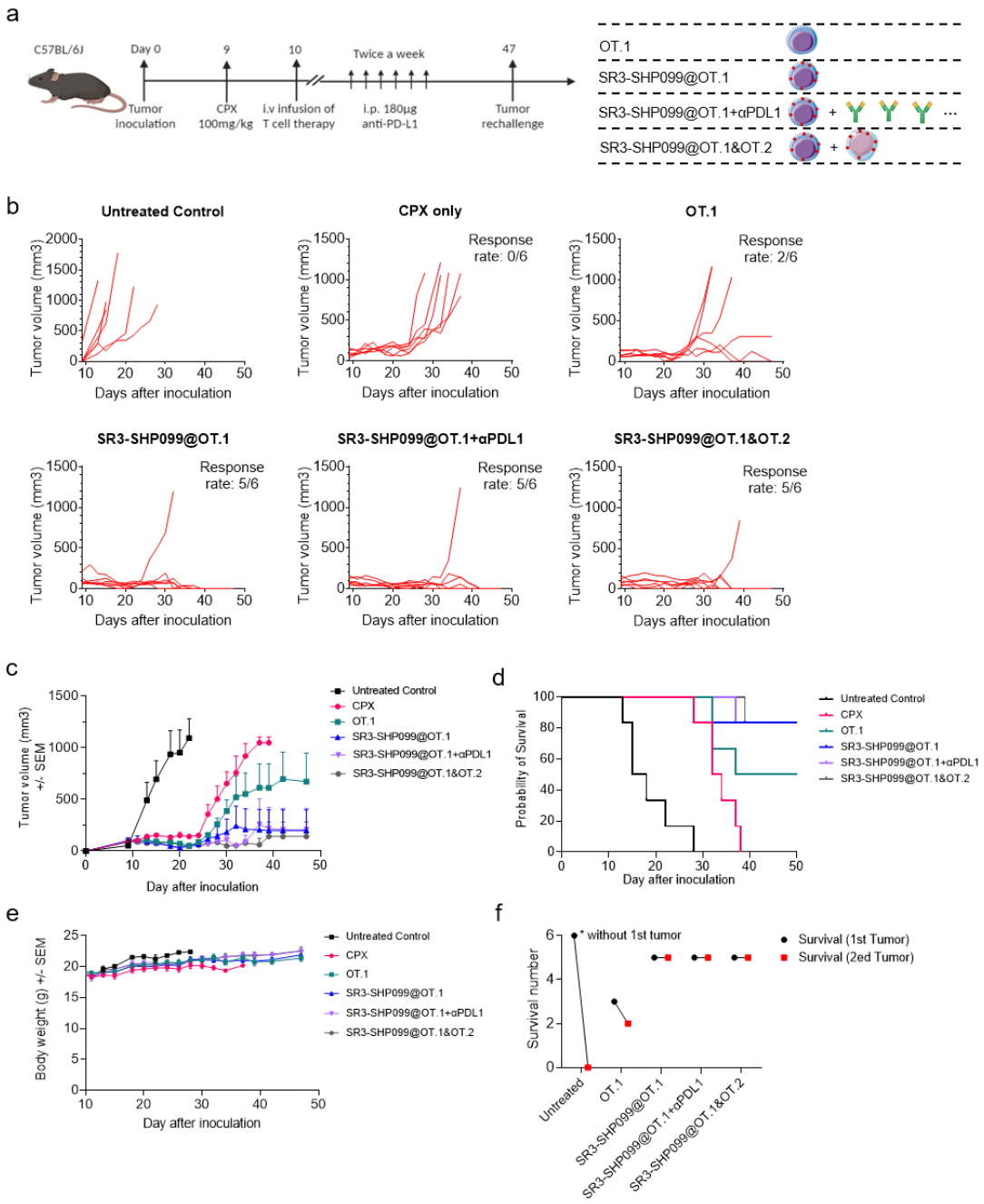

Figure 3.6 Enhanced antitumor activity of OT.1 T cells loaded with SHP099 nanocrystals**.** C57BL/6J mice were inoculated with 5×10^5 EG7-OVA cells injected subcutaneously into the right flanks on day 0. On day 9 after inoculation, mice were randomized according to tumor size (mean tumor size at inclusion=93±43mm^3) and divided into treatment groups (n=6). Immediately after, mice received an i.p. injection of CPX (100mg/kg). On day 10, mice received i.v. unloaded OT.1 (1x10^6), SR3-SHP099 loaded OT.1 (1x10^6) alone or in combination with anti-PDL1 (180ug/mouse, i.p, b.i.w), SR3-SHP099 loaded OT.1+OT.2 (1:1 mixture of 1x10^6 cells in total). **a,** Experimental timeline of the efficacy study. **b,** Individual tumor growth curves from each mouse. **c,** Average tumor growth curves, and **d,** survival rates in control and treated groups. **e,** Bodyweight of mice. Data with error bars were presented as mean ± SD (n=6). **f,** Survival number of mice receiving a second tumor inoculation in the opposite flank after curing of primary tumors.

3.4 Discussion

The emerging new insights into the key mechanisms that regulate T cell functions have provoked intensive efforts to improve their therapeutic potential, including the direct genetic engineering of T cells or applying adjuvant drugs to enhance the cell function, phenotype, and persistence.

Here we described a novel strategy to enhance the anti-tumor performance of T cell therapy by loading a small-molecule CPI into T cells using a lipid nanoparticle platform encapsulating drug nanocrystals. We report for the first time the remote-loading of an allosteric SHP2 inhibitor, SHP099, into lipid nanoparticles as nanocrystals. The nanocrystals formation allows for high drug encapsulation efficiency and stability in the nanoparticle. A tri-arginine motif was incorporated in the formulation to enable high loading of SHP099 nanocrystals by T cells, which were steadily released to improve T cell activity mainly by blocking PD-1/PD-L1 interaction (**Figure 3.3**). Although nanoparticles have been used for loading T cells with drugs, most nanoparticles in previous studies were covalently conjugated to T cells by reacting with thiols or bound to receptors exposed on the cell surface[25,27,28,43]. These conjugation strategies occur on cell membrane proteins, which can negatively influence key functions of cells, and the loading capacity is limited by the steric hindrances or lack of presence of binding sites by cells. With the tri-arginine modified SR3 nanoparticles, we exploit electrostatic interactions to obtain the high loading capacity of SHP099 nanocrystals, allowing the drug to be sustainably released from the cell over more than 5 days. The prolonged retention of SHP099 in T cells can increase the chances for the inhibitor to travel with T cells and exert its effect at the relevant place of action. This is highly important since data from the *in vivo* model of established EG.7-OVA tumor-bearing mice showed that adoptively transferred antigen-specific cytotoxic $CD8^+$ T cells started infiltrating into tumors after 2-3 days post-injection[41]. Hence, the drug inhibitor needs to remain associated with the T cells and block the PD1-SHP2 interaction upon PD-L1/L2 binding, eluding T cell inactivation by the immunosuppressive tumor environment.

Current research suggests that ACT with an early memory phenotype absent of exhaustion markers would be an ideal phenotype for cancer treatment[44]. We show that SHP099 drives more T cells into the central memory phenotype and prevented T cell exhaustion. Moreover, the SHP099 loaded T cells exerted improved cytotoxicity against target tumor cells, particularly when tumor cells upregulated PD-L1 expression (**Figure 3.4**). Because the SHP099 works by blocking PD-1/PD-L1 interaction upon T cells encounter with tumor cells,

it is crucial to have the drug and T cells synchronized temporally and spatially. T cells have natural drug delivery abilities to target tumor sites and penetrate through biological barriers apart from the adaptive immune response. We demonstrate that migration of loaded T cells into tumors resulted in increased tumor accumulation of the cargo from day 1 to day 3, with the tendency of continuous increase afterward, while the number of free SR3 nanoparticles at tumor sites already began to decrease after day 1. In addition, we confirmed that loading the SR3 nanoparticles did not affect the cell distribution since it correlated with the unloaded T cell distribution (**Figure 3.5**).

Many challenges limit the therapeutic efficacy of T cells in solid tumors. Since T cell therapy often targets a single antigen, the heterogeneous and immunosuppressive TME imposes a selection of resistant clones of tumors with decreased or absent antigen expression, ultimately leading to the loss of responsiveness[45,46]. The combination immunotherapy of CAR T cells and anti-PD-1 or PD-L1 antibodies has been investigated to overcome this challenge, which has shown increased efficacy compared to each agent alone in preclinical and clinical studies[5,6]. In our study, a single administration of T cells loaded with SHP099 nanocrystals achieved the same efficacy as the combination of T cells with repeated doses of anti-PD-L1 (**Figure 3.6**), providing evidence that the targeted delivery of SHP099 could block the inhibitory signal downstream at the same level as the systemically administrated anti-PD-L1 antibody. While the optimal doses of 100-200 mg/kg of SHP099 were used in previous monotherapy studies[15,18], we demonstrated enhanced anti-tumor efficacy with only around 1% of that SHP099 dose in combination with T cell therapy. *In vitro* cytotoxicity studies on various cell lines indicated that such low concentrations of SHP099 did not have direct inhibition of cancer cell growth (**Figure 3.12**). Previous studies have reported that SHP2 inhibition evokes meaningful anti-tumor T cell responses[19,47], and its anti-tumor effects were reduced in mice lacking T cell populations. But SHP099 can also induce immigration of MDSCs, which suppress T cell activation, proliferation, and cytolytic differentiation[48]. Thus, precise delivery of SHP099 with the adoptively transferred T cells may leverage its effect on T cells, and reduce the potential "side-effect" of RAS/ERK pathway inhibition by SHPi.

In summary, we developed a novel strategy for inhibiting SHP2 to enhance T cell therapy by loading SHP099 nanocrystals into T cells to form a depot of CPIs. The SHP099 loaded T cells induced complete and durable eradication of solid tumors and showed enhanced antitumor efficacy to the same degree as the combination of adoptive T cells and repeated doses of the

anti-PD-L1 antibody. These results demonstrated the combination of SHP2 inhibition and adoptive T cell therapy is a promising therapeutic approach. In addition, this lipid nanoparticle platform provides an efficient and versatile technique for loading immunomodulatory drugs to T cells to further improve their anticancer activity.

3.5 Materials and Methods

3.5.1 *Materials for formulation*

Hydrogenated phosphatidylcholine (HSPC), 1,2-stearoyl-3-trimethylammonium-propane (DSTAP), Cholesterol, 1,2-distearoyl-sn-glycero-3-phosphoethanolamine-N-[amino(polyethylene glycol)-2000] (DSPE-PEG2000) were purchased from Avanti Polar lipids (Alabaster, AL, USA). Fluorescent 1,10-dioctadecyl-3,3,30,30-tetramethylindodicarbocyanine (DiD) and 1,1'-Dioctadecyl-3,3,3',3'-Tetramethylindocarbocyanine Perchlorate (DiI) was purchased from Thermo Fischer Scientific. SHP099 and Cholesterol-Carbamate-Gly-Trp-Arg-Arg-Arg-NH_2 (Chol-GWR_3) were synthesized and characterized as stated in the supplementary information. Unless specifically stated, all other chemicals were from Sigma Aldrich (Brøndby, Denmark) and of analytical grade.

3.5.2 *Preparation of lipid nanocrystals*

Empty lipid nanoparticles

Lipids were dissolved in tert-butanol: Milli-Q water (9:1), mixed to the desired lipid composition, snap-frozen in liquid nitrogen, and freeze-dried overnight. Three main lipid formulations were investigated with the following lipid molar ratios: Saturated stealth (SS, HSPC: Cholesterol: DSPE-PEG2000, 57:38:5), Saturated cationic (Scat, HSPC:Cholesterol:DSTAP, 52:38:10), Saturated tri-arginine (SR3, HSPC:Cholesterol:DSTAP:Chol-GWR_3:DSPE-PEG2000, 50:38:10:1.5:0.5). To produce DiD or DiI fluorophore-labeled lipid nanoparticles a 0.2% molar ratio was added to the composition. Mixed lipid powder was hydrated with HEPES buffered saline (25mM HEPES, 150mM NaCl, pH 7.4) to a lipid concentration of 20-50 mM and placed stirring at 70°C for 1 hour. The resulting lipid nanoparticles were homogenized by extruding two times through a 200 nm polycarbonate filter (Whatman, Maidstone, 356 UK) followed by six times through two stacked 100 nm filters with a high-pressure extruder (Northern lipids Inc. Burnaby, 355 Canada). For

smaller preparations, the lipid nanoparticles were extruded 21 times through a 100 nm polycarbonate filter using a mini-extruder (Avanti Polar Lipids, Alabaster, 358 AL, USA). The temperature was maintained at 65 °C during the extrusion process.

Remote loading of SHP099 nanocrystals

lipid vesicles were prepared following the procedure described above, with the exception that the lipids were hydrated with ammonium sulfate solution (250mM, pH~5.3). After extrusion, lipid nanoparticles were then dialyzed for 48 hours against HEPES buffered saline (25mM HEPES, 150mM NaCl, pH 7.4) in Slide-A-Lyzer dialysis cassettes (10K MWCO), with two times buffer exchanges. Subsequently, the lipid nanoparticles suspension was added to SHP099 in powder form at a drug/lipid mol ratio of 1:4. The solution was incubated at 60°C for 3 hours under stirring conditions. After cooling down, the non-encapsulated SHP099 was removed by dialysis (Slide-A-Lyzer, 10K MWCO). Before and after purification, the lipid and SHP099 concentrations were measured by ICP-MS and HPLC, respectively, to determine the final drug/lipid ratio. The encapsulation efficiency (EE) of SHP099 was calculated according to the following equation:

$$\text{Encapsulation efficiency (\%)} = \frac{\mathbf{C}\,(\text{loaded SHP099})\,/\mathbf{C}\,(\text{lipid})}{\mathbf{C}\,(\text{total SHP099})\,/\mathbf{C}\,(\text{total lipid})} \times 100\%$$

3.5.3 ***Physicochemical characterization of SR3-SHP099 nanocrystals***

The size distribution and zeta potential of SR3-SHP099 were measured by dynamic light scattering (DLS) using a ZetaSizer Nano ZS (Malvern, UK). The morphology was examined by cryogenic transmission electron microscopy (cryo-TEM) using a Tecnai T20 G2 (Thermo Fisher Scientific, Waltham, USA). Lipid concentration was determined using Inductively Coupled Plasma Mass Spectrometry (ICP-MS). Detailed information on the methods can be found in Supplementary Information. The release of SHP099 from nanocrystals was analyzed by analytical reversed-phase (RP)-HPLC in PBS or PBS containing 10% fetal bovine serum (FBS). Briefly, 100 μL of SR3-SHP099 were added in Slide-A-Lyzer MINI dialysis devices (Thermo Scientific) with molecular weight cut-offs of 10K. Then, the dialysis devices were put into conical tubes containing 1.6 mL of release medium at 37 °C. At specific time points, 100 μL of the release medium was drawn, and the same volume of fresh solution was added. The amount of SHP099 released at each time point was determined by HPLC.

3.5.4 *Cell culture*

$CD8^+$ T cells were isolated from the spleens of OT.1 or C57BL/6 mice via magnetic negative selection using an EasySep mouse $CD8^+$ T cell isolation kit (STEMCELL Technologies). T cells were activated using anti-CD3/CD28 antibodies (eBioscience MA, USA) at a density of 2×10^6 cells/well in a pre-coated 6-well plate. The cells were cultured in RPMI 1640 medium containing 10% (v/v) fetal bovine serum (FBS; Gibco-Invitrogen), 1% penicillin/streptomycin (Gibco-Invitrogen), 1% (v/v) Insulin-Transferrin-Selenium (ITS, Thermo Fisher), recombinant mouse IL-2 (20 ng/ml) and IL-7 (5 ng/ml) at 37 °C. After two days of incubation, the activated T cells were removed from the coated plate and cultured in the presence of a culture medium containing mouse IL-2 (4 ng/ml) and IL-7 (0.5 ng/ml).

Murine thymoma cell lines E.G7-OVA and melanoma cell line B16-OVA, B16-F10 (syngeneic with C57BL/6) were cultured in RPMI 1640 supplemented with 10% FBS, 400 μg/ml G418, and 1% penicillin/streptomycin at 37 °C in a humidified incubator containing 5% CO_2.

3.5.5 *Preparation and characterization of SR3 loaded $CD8^+$ T cells*

Unless specifically stated, T cells on day 5 of activation were harvested for loading. T cells were suspended at a density of 2×10^7 cells per mL in the serum-free RPMI1640 medium. An equal volume of the lipid nanoparticles diluted in serum-free RPMI medium was added to the cells at 0.1 μmol total lipids per million T cells and incubated at 37 °C for 2 hours with gentle agitation every 20 min. Subsequently, the cells were thoroughly washed 3 times with PBS and the number of lipid nanoparticles attached to T cells was evaluated by flow cytometry on a Beckman Gallios flow cytometer by measuring the DiI or DiD positive ratio of T cells and the mean fluorescence intensity (MFI). The loading efficiency was further quantified by measuring DiI or SHP099 amount in T cell lysis. 1×10^6 T cells loaded with SR3-SHP099 were lysed in 100μL Triton X-100 solution (1%, w/v), followed by adding 400 μL of ethanol, and after centrifugation at 15000 g, for 20 min to remove the cell debris, DiI was quantified using a TECAN Spark microplate reader (TECAN) along with serial standard solutions processed in the same manner. For SHP099 quantification, 400 μL of acetonitrile was added to the cell lysis to precipitate the proteins, and after centrifugation, SHP099 in the supernatant was measured by HPLC. T cells loaded with liposomal SHP099 were put back in culture in complete RPMI medium supplemented with IL-2 at 1×10^6 cells per ml at 37 °C to investigate the drug retention.

From day 1 to day 5, cells were collected and lysed to determine the remaining SHP099 ratio compared with the initial amount.

Confocal microscopy was used to visualize the T cells loading with SR3 nanoparticles. Briefly, T cells loaded with DiD-labelled SR3 were stained with the cell nucleus dye Hoechst33342 (10μg/ml) and CellMask green for 30min on ice according to the manufacturer's protocol and washed three times with live-cell imaging solution (Invitrogen), transferred to a poly-L-lysine precoated μ-Slide well (Ibidi GmbH, Germany), and imaged using TEM

3.5.6 *Functional study of $CD8^+$ T cells after loading*

$CD8^+$ T cells were loaded with empty lipid nanoparticles and SHP099 nanocrystals as previously described. Following SR3 loading, T cells were put back to the culture in 96-well round-bottom plates at 2×10^5 cells per well in the complete RPMI medium containing IL-2. Cell viability and proliferation were determined using cell counting and viability assay on a NucleoCounter® NC-200™ automated cell counter mounted with Via1-Cassettes (ChemoMetec A/S, Denmark) at varying time points (0h, 24h, 48h, and 72h). At the same time, the activation state of T cells was measured by CD44 and CD62L expression via flow cytometry. T cells were stained with FITC anti-mouse CD8, Brilliant Violet 42 anti-mouse CD44 (BioLegend), and APC anti-mouse CD62L antibodies (BD Biosciences), followed by analysis on LSR Fortessa X20 flow cytometer (BD Biosciences) and data followed by data processing with Flowjo software.

Furthermore, the effect of SHP099 liposomal loading on the cytotoxic properties of the T cells was assessed using OT.1 T cells and the target cells B16-OVA, with the OVA-negative B16-F10 cells as control. Tumor cells were seeded in a 96-well plate in complete medium containing 20ng/ml of IFN-γ and incubated for 24 hours in a 37°C incubator with 5% of CO_2. After removing the medium, SHP099 loaded and unloaded OT.1 $CD8^+$ T cells were added in triplicates to B16-OVA and B16-F10 cells at effector: target (E: T) cell ratios of 20:1, 10:1, 5:1, 2:1, and 1:1. After 5 h and 24 h of incubation, cells were spun down, and 50 μl of each sample medium was transferred to a new plate for measuring the cell lysis using a CyQUANT™ LDH Cytotoxicity Assay Kit according to the manufacturer´s instruction. Target cells completely lysed with the lysis buffer were used as maximum LDH release control, and medium from untreated target cells and the T cells at each ratio was used for measuring background LDH activity. % Tumor cell lysis was calculated by using the following formula:

$$\% \text{ Tumor cell lysis} = \left[\frac{\text{Treated LDH activity} - \text{Spontaneous LDH activity}}{\text{Maximum LDH activity} - \text{Spontaneous LDH activity}}\right] \times 100\%$$

3.5.7 *In vivo biodistribution of SR3 nanoparticle loaded T cells*

E.G7-OVA tumors were established in C57BL/6 mice by *s.c.* injection of 5×10^5 cells in the right flanks. Tumors were allowed to grow for 10 days before administration of Gadolinium-labelled SR3 nanoparticles (SR3-Gd) and 2×10^6 OT.1 $CD8^+$ T cells loaded with SR3-Gd (SR3-Gd@T cells) through tail vein injection at a dose of 190ng Gadolinium per mouse. Gadolinium labeled SR3 nanoparticles were prepared by including 1mol% of DSPE-DOTA-Gd (Supplementary information). After 24 h and 72 h, mice were sacrificed by cervical dislocation, and lung, spleen, liver, tumor-draining lymph node (tdLN) and tumor were harvested and weighed, followed by digestion with 65% nitric acid, 37% hydrochloric acid, and 30% Hydrogen peroxide at the ratio (v/v) of 50:5:30 added in sequence overnight at 65°C. Digested tissue solution was further diluted for quantifying Gd on ICP-MS and calculated the percentage of injected dose per gram of tissue (%ID/g) as the final readout.

For evaluating the *in vivo* distribution and proliferation of adoptively transferred T cells, cells were stained with CellTrace™ Violet (CTV, Thermo Fisher). SR3 nanoparticles loaded OT.1 $CD8^+$ T cells (SR3-T cells) and unloaded OT.1 $CD8^+$ T cells were washed and incubated at a density of 5×10^6 cells/ml with 2.5 µM CTV dye in warm PBS for 20 min at 37 °C followed by washing with complete medium and PBS. When the average tumor size reached 58 mm3, 2×10^6 of CTV labeled cells were injected into C57BL/6 mice bearing EG7-OVA tumors through the tail vein. Mice were sacrificed after 24 h and 72 h, from which the lung, spleen, and tumor were harvested for detecting the CTV positive cells on a flow cytometer. Single-cell suspensions were obtained by mechanical disruption (spleens) or enzyme digestion (lungs and tumors) before passing the tissue suspension 2 times through a 70 µM cell strainer.

3.5.8 *In vivo antitumor efficacy*

Female 6 weeks old C57BL/6 mice were obtained from Janvier Labs (France). E.G7-OVA subcutaneous tumor model was established as described above. Mice were randomized into six groups (n = 6 per group) with the average tumor volume reaching around 90 mm^3 on day 9 after tumor inoculation. One day before T cells infusion, mice were treated with intraperitoneal (*i.p.*) injection of 100mg/kg cyclophosphamide (CPX). Subsequently on day 10, the mice were administrated with Saline (Untreated control and CPX), OT.1 $CD8^+$ T cells (OT.1), OT.1 $CD8^+$

T cells loaded with liposomal SHP099 (SR3-SHP099@OT.1) alone and in combination with anti-PD-L1 antibodies (SR3-SHP099@OT.1+αPDL1) or OT.2 $CD4^+$ T cells loaded with liposomal SHP099 (SR3-SHP099@OT.1&OT.2), respectively. A single infusion of 1×10^6 T cells was given to the mice, corresponding to the SHP099 dose of 0.5-1 mg/kg. Anti PD-L1 antibody was administered through *i.p.* injection at the dosage of 180μg per mouse (~9 mg/kg) twice a week until day 10, and 1080μg was given in total. The body weight and tumor length (L) and width (W) were measured every 3 days starting from day 9 after tumor inoculation, and the tumor volume (V) was calculated using the equation: $V= 0.5 \times L \times W^2$.

The tumor re-challenge study was conducted on tumor-free cured mice from the initial treatments. On day 47 after the first tumor inoculation, the mice without visible tumors were inoculated on the opposite flank with 5×10^5 EG.7-OVA cells. At least 3 mice were included in each group, and untreated C57BL/6 mice at 12 weeks of age were inoculated as control. The body weight and both initial and second tumor volume were measured every third day.

The animal studies reported in this article were approved by the Danish Animal Experiments Inspectorate and all animal experiments were performed in compliance with the relevant guidelines and regulations as stated by Danish Animal Experiments Inspectorate.

3.5.9 ***Statistical analysis***

Statistical analysis of data was performed using Prism 9 (GraphPad Software). Survival data were analyzed by the Log-rank (Mantel-Cox) test. Comparison between groups was performed with One-Way ANOVA variance analysis with Tukey post hoc test for multiple comparisons. All of the results are presented as mean ± standard error of the mean (SEM) unless otherwise stated. A p-value < 0.05 was considered statistically significant.

3.6 References

1. June, C. H., O'Connor, R. S., Kawalekar, O. U., Ghassemi, S. & Milone, M. C. CAR T cell immunotherapy for human cancer. *Science* **359**, 1361–1365 (2018).

2. Restifo, N. P., Dudley, M. E. & Rosenberg, S. A. Adoptive immunotherapy for cancer: Harnessing the T cell response. *Nature Reviews Immunology* **12**, 269–281 (2012).

3. Vignali, D. & Kallikourdis, M. Improving homing in T cell therapy. *Cytokine and Growth Factor Reviews* (2017) doi:10.1016/j.cytogfr.2017.06.009.

4. Labani-Motlagh, A., Ashja-Mahdavi, M. & Loskog, A. The Tumor Microenvironment: A Milieu Hindering and Obstructing Antitumor Immune Responses. *Frontiers in Immunology* **11**, 1–22 (2020).

5. Grosser, R., Cherkassky, L., Chintala, N. & Adusumilli, P. S. Combination Immunotherapy with CAR T Cells and Checkpoint Blockade for the Treatment of Solid Tumors. *Cancer Cell* **36**, 471–482 (2019).

6. Wang, Z. *et al.* Phase I study of CAR-T cells with PD-1 and TCR disruption in mesothelin-positive solid tumors. *Cellular and Molecular Immunology* **18**, 2188–2198 (2021).

7. Nazareth, M. R. *et al.* Characterization of Human Lung Tumor-Associated Fibroblasts and Their Ability to Modulate the Activation of Tumor-Associated T Cells. *The Journal of Immunology* **178**, 5552–5562 (2007).

8. Wherry, E. J. *et al.* Molecular Signature of CD8+ T Cell Exhaustion during Chronic Viral Infection. *Immunity* **27**, 670–684 (2007).

9. Jing, W. *et al.* Adoptive cell therapy using PD-1+ myeloma-reactive T cells eliminates established myeloma in mice. *Journal for ImmunoTherapy of Cancer* **5**, 1–11 (2017).

10. Robert, C. A decade of immune-checkpoint inhibitors in cancer therapy. *Nature Communications* **11**, 10–12 (2020).

11. Chan, G., Kalaitzidis, D. & Neel, B. G. The tyrosine phosphatase Shp2 (PTPN11) in cancer. *Cancer and Metastasis Reviews* **27**, 179–192 (2008).

12. Patsoukis, N. *et al.* Interaction of SHP-2 SH2 domains with PD-1 ITSM induces PD-1 dimerization and SHP-2 activation. *Communications Biology* (2020) doi:10.1038/s42003-020-0845-0.

13. Gavrieli, M., Watanabe, N., Loftin, S. K., Murphy, T. L. & Murphy, K. M. Characterization of phosphotyrosine binding motifs in the cytoplasmic domain of B and T lymphocyte attenuator required for association with protein tyrosine phosphatases SHP-1 and SHP-2. *Biochemical and Biophysical Research Communications* **312**, 1236–1243 (2003).

14. Li, J. *et al.* PD-1/SHP-2 inhibits Tc1/Th1 phenotypic responses and the activation of t cells in the tumor microenvironment. *Cancer Research* (2015) doi:10.1158/0008-5472.CAN-14-1215.

15. Chen, Y. N. P. *et al.* Allosteric inhibition of SHP2 phosphatase inhibits cancers driven by receptor tyrosine kinases. *Nature* **535**, 148–152 (2016).

16. Dardaei, L. *et al.* SHP2 inhibition restores sensitivity in ALK-rearranged non-small-cell lung cancer resistant to ALK inhibitors. *Nature Medicine* **24**, 512–517 (2018).

17. Mainardi, S. *et al.* SHP2 is required for growth of KRAS-mutant non-small-cell lung cancer in vivo letter. *Nature Medicine* **24**, 961–967 (2018).

18. Wong, G. S. *et al.* Targeting wild-type KRAS-amplified gastroesophageal cancer through combined MEK and SHP2 inhibition letter. *Nature Medicine* **24**, 968–977 (2018).

19. Quintana, E. *et al.* Allosteric inhibition of SHP2 stimulates antitumor immunity by transforming the immunosuppressive environment. *Cancer Research* **80**, 2889–2902 (2020).

20. Jiang, W. *et al.* Designing nanomedicine for immuno-oncology. *Nature Biomedical Engineering* **1**, 1–11 (2017).

21. Schmid, D. *et al.* T cell-targeting nanoparticles focus delivery of immunotherapy to improve antitumor immunity. *Nature Communications* **8**, 1–11 (2017).

22. Smith, T. T. *et al.* In situ programming of leukaemia-specific t cells using synthetic DNA nanocarriers. *Nature Nanotechnology* **12**, 813–822 (2017).

23. Stefan Willhelm *et al.* Analysis of nanoparticle delivery to tumours. *Nature Reviews Materials* **1**, 16014 (2016).

24. Steinfeld, U., Pauli, C., Kaltz, N., Bergemann, C. & Lee, H. H. T lymphocytes as potential therapeutic drug carrier for cancer treatment. *International Journal of Pharmaceutics* **311**, 229–236 (2006).

25. Tang, L. *et al.* Enhancing T cell therapy through TCR-signaling-responsive nanoparticle drug delivery. *Nature Biotechnology* **36**, (2018).

26. Stephan, M. T., Moon, J. J., Um, S. H., Bersthteyn, A. & Irvine, D. J. Therapeutic cell engineering with surface-conjugated synthetic nanoparticles. *Nature Medicine* **16**, 1035–1041 (2010).

27. Huang, B. *et al.* Active targeting of chemotherapy to disseminated tumors using nanoparticle-carrying T cells. *Science Translational Medicine* **7**, (2015).

28. Wayteck, L. *et al.* Hitchhiking nanoparticles: Reversible coupling of lipid-based nanoparticles to cytotoxic T lymphocytes. *Biomaterials* **77**, 243–254 (2016).

29. Sanz-Ortega, L. *et al.* T cells loaded with magnetic nanoparticles are retained in peripheral lymph nodes by the application of a magnetic field. *Journal of Nanobiotechnology* **17**, 1–20 (2019).

30. Pittet, M. J. *et al.* In vivo imaging of T cell delivery to tumors after adoptive transfer therapy. *Proceedings of the National Academy of Sciences of the United States of America* **104**, 12457–12461 (2007).

31. Ayer, M. & Klok, H. A. Cell-mediated delivery of synthetic nano- and microparticles. *Journal of Controlled Release* **259**, 92–104 (2017).

32. Schmidt, N., Mishra, A., Lai, G. H. & Wong, G. C. L. Arginine-rich cell-penetrating peptides. (2009) doi:10.1016/j.febslet.2009.11.046.

33. Wu, W., Shi, X. & Xu, C. Regulation of T cell signalling by membrane lipids. *Nature Publishing Group* (2018) doi:10.1038/nri.2016.103.

34. Cern, A. *et al.* Quantitative structure - Property relationship modeling of remote liposome loading of drugs. *Journal of Controlled Release* **160**, 147–157 (2012).

35. Fritze, A., Hens, F., Kimpf, A., Schubert, R. & Peschka-süss, R. Remote loading of doxorubicin into liposomes driven by a transmembrane phosphate gradient. **1758**, 1633–1640 (2006).

36. Kroetsch, A. *et al.* mAbs Engineered pH-dependent recycling antibodies enhance elimination of Staphylococcal enterotoxin B superantigen in mice Engineered pH-dependent recycling antibodies enhance elimination of Staphylococcal enterotoxin B superantigen in mice. (2018) doi:10.1080/19420862.2018.1545510.

37. John Wherry, E. & Kurachi, M. Molecular and cellular insights into T cell exhaustion. (2015) doi:10.1038/nri3862.

38. Cui, W., Schluns, K. S., Badovinac, V. P. & Martin, M. D. Defining Memory CD8 T Cell. *Frontiers in Immunology | www.frontiersin.org* **9**, 2692 (2018).

39. Veiga-Fernandes, H., Walter, U., Bourgeois, C., McLean, A. & Rocha, B. Response of naïve and memory CD8+ T cells to antigen stimulation in vivo. *Nature Immunology* **1**, 47–53 (2000).

40. Lin, H. *et al.* Host expression of PD-L1 determines efficacy of PD-L1 pathway blockade–mediated tumor regression. *Journal of Clinical Investigation* **128**, 805–815 (2018).

41. Kim, W. *et al.* In vivo tracking of bioorthogonally labeled T-cells for predicting therapeutic efficacy of adoptive T-cell therapy. *Journal of Controlled Release* **329**, 223–236 (2021).

42. Man, F. *et al.* In Vivo PET Tracking of 89 Zr-Labeled Vγ9Vδ2 T Cells to Mouse Xenograft Breast Tumors Activated with Liposomal Alendronate. *Molecular Therapy* **27**, 219–229 (2019).

43. Liu, S. *et al.* Adoptive CD8 + T-cell grafted with liposomal immunotherapy drugs to counteract the immune suppressive tumor microenvironment and enhance therapy for melanoma . *Nanoscale* **13**, 15789–15803 (2021).

44. Tantalo, D. G. M. *et al.* Understanding T cell phenotype for the design of effective chimeric antigen receptor T cell therapies. *Journal for ImmunoTherapy of Cancer* **9**, 1–10 (2021).

45. Jæhger, D. E. *et al.* Enhancing adoptive CD8 T cell therapy by systemic delivery of tumor associated antigens. *Scientific Reports* **11**, 1–19 (2021).

46. Junttila, M. R. & De Sauvage, F. J. Influence of tumour micro-environment heterogeneity on therapeutic response. *Nature* **501**, 346–354 (2013).

47. Chen, H. *et al.* SHP2 is a multifunctional therapeutic target in drug resistant metastatic breast cancer. *Oncogene* **39**, 7166–7180 (2020).

48. Zhang, T. *et al.* Loss of SHP-2 activity in CD4 + T cells promotes melanoma progression and metastasis. *Scientific Reports* **3**, (2013).

3.7 Supplementary Information to chapter 3

3.7.1 *Materials and Methods*

All solvents for chemical syntheses were bought in HPLC grade from Sigma-Aldrich Inc. (Broendby, Denmark). All chemicals were purchased from Sigma-Aldrich Inc. (Broendby, Denmark) unless otherwise stated. 3-Bromo-6-chloro-pyrazin-2-amine was purchased from Manchester organics (Runcorn, United Kingdom). 2,3-dichlorophenyl) boronic acid was purchased from Thermo Fisher Scientific (New Jersey, USA). tert-butyl (4-methylpiperidin-4-yl) carbamate was purchased from Advanced ChemBlock Inc. (Burlingame, CA, USA).

Synthesis of SHP099.HCl

The protocol for synthesis of SHP099 was modified from: Garcia Fortanet J et al. Allosteric Inhibition of SHP2: Identification of a Potent, Selective, and Orally Efficacious Phosphatase Inhibitor. J Med Chem. **2016** Sep 8;59(17):7773–82.

6-chloro-3-(2,3-dichlorophenyl) pyrazin-2-amine

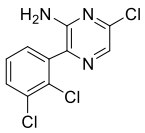

To a solution of 3-bromo-6-chloropyrazin-2-amine (1 eq.) in dioxane was added (2,3-dichlorophenyl) boronic acid as a powder (1 eq.), and a solution of K_3PO_4 (3 eq.) in H_20. The solution was degassed with argon for 5min and $Pd(dppf)Cl_2$ (0.05 eq.) was added. The reaction mixture was warmed to 110 °C and stirred for 4h. After cooling to room temperature, the reaction mixture was filtered through a pad of Celite followed by EtOAc wash. The solvent was removed *in vacuo* to give a dark brown solid, which was purified with Silica column chromatography on a Reveleris® PREP Purification System, using a Reveleris® HP Flash Cartridge (60Å, 20µm) and 0-30% EtOAc in n-Heptane. This gave the pure product as a yellow solid (1.53g, 77.5%). TLC R_f = 0.4 (3:7, EtOAc:*n*-heptane, v:v). LC-MS (ESI-MS) found: 273.9 $[M+H]^+$, calculated mass for $C_{10}H_7Cl_3N_3^+$ $[M+H]^+$: 273.97.

^{1}H NMR (400 MHz, Chloroform-d) δ 8.02 (s, 1H), 7.59 (dd, J = 7.8, 1.8 Hz, 1H), 7.36 (t, J = 7.7 Hz, 1H), 7.32 (dd, J = 7.6, 1.8 Hz, 1H), 4.66 (s, 2H). ^{13}C NMR (101 MHz, Chloroform-d) δ 151.72, 146.81, 136.75, 136.45, 134.38, 132.30, 131.93, 131.67, 129.47, 128.43.

tert-butyl (1-(6-amino-5-(2,3-dichlorophenyl) pyrazin-2-yl)-4-methylpiperidin-4-yl) carbamate

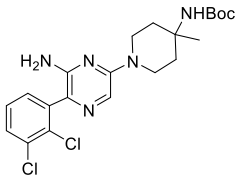

6-chloro-3-(2,3-dichlorophenyl) pyrazin-2-amine (1eq.), K_3PO_4 (1eq.) and tert-butyl (4-methylpiperidin-4-yl) carbamate (2eq.) was dissolved in DMF (3.3mL). The reaction was stirred for 39 h at 140 °C. After cooling to room temperature, the mixture was poured into a separation funnel containing saturated aqueous NH_4Cl (10ml) and it was extracted with EtOAc (4 × 10 ml). The combined organic phases were dried over Na_2SO_4, filtered and the solvents were removed under reduced pressure to give a brown oil. The resulting residue was purified by silica chromatography on a Reveleris® PREP Purification System, using a Reveleris® HP Flash Cartridge (60Å, 20µm) (5 to 60% gradient of EtOAc in n-heptane) to give tert-butyl (1-(6-amino-5-(2,3-dichlorophenyl) pyrazin-2-yl)-4-methylpiperidin-4-yl)carbamate as a yellow solid (477.7mg, 71.7% yield). TLC R_f = 0.4 (4:7, EtOAc:*n*-heptane, v:v). LC-MS (ESI-MS) found: 452.1 $[M+H]^+$, calculated mass for $C_{21}H_{28}Cl_2N_5O_2$ $[M+H]^+$: 452.16.

^{1}H NMR (400 MHz, Chloroform-d) δ 8.02 (s, 1H), 7.59 (dd, J = 7.8, 1.8 Hz, 1H), 7.36 (t, J = 7.7 Hz, 1H), 7.32 (dd, J = 7.6, 1.8 Hz, 1H), 4.66 (s, 2H). ^{13}C NMR (101 MHz, Chloroform-d) δ 151.72, 146.81, 136.75, 136.45, 134.38, 132.30, 131.93, 131.67, 129.47, 128.43.

6-(4-amino-4-methylpiperidin-1-yl)-3-(2,3-dichlorophenyl) pyrazin-2-amine (SHP099)

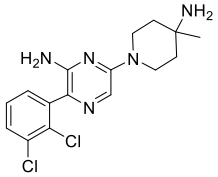

A solution of tert-butyl (1-(6-amino-5-(2,3-dichlorophenyl) pyrazin-2-yl)-4-methylpiperidin-4-yl)carbamate (1 eq.) in THF/H2O (4:1, v:v, 5 mL) was treated with HCl (4M in dioxane, 3.7 eq.). The resulting mixture was stirred for 2 h at 140 °C. After cooling to RT, the volatiles were removed under reduced pressure and the resulting residue was diluted in HPLC buffers. The mixture was then purified by reverse phase HPLC by employing a Phenomenex Gemini C18 column (110Å, 5µm, 250x30mm). Eluent: (A) 0.1 % TFA in H_2O, (B) 0.1 % TFA in CH_3CN. Gradient profile: 10% B to 35% B over 25 min to give the compound (SHP099) as a TFA salt (458.9mg, 94% yield). TLC R_f = 0.46 (9:3, DCM:MeOH, v:v + 0,1% HCl). HPLC R_T: 3.65min (Waters XTerra C18 column, 5 µm, 125Å (4.6×150 mm); Eluents: (A) 0.1% TFA and 5% MeCN in H2O (v/v/v); (B): 0.1% TFA in MeCN (v/v). Column temperature: 40ºC. Gradient: 0-60% buffer B over 10

min). LC-MS (ESI-MS) found: 352.0 $[M+H]^+$, calculated mass for $C_{16}H_{19}Cl_2N_5$ $[M+H]^+$: 352.16.

^{1}H NMR (400 MHz, Methanol-d4) δ 7.69 (dd, J = 7.9, 1.7 Hz, 1H), 7.54 (s, 1H), 7.45 (t, J = 7.8 Hz, 1H), 7.40 (dd, J = 7.7, 1.8 Hz, 1H), 4.17 (dt, J = 14.0, 4.7 Hz, 2H), 3.41 (dt, J = 14.0, 6.9 Hz, 2H), 1.91 – 1.83 (m, 4H), 1.51 (s, 3H). ^{13}C NMR (101 MHz, Methanol-d4) δ 155.52, 154.35, 136.28, 134.88, 134.03, 132.74, 131.58, 129.58, 122.48, 113.57, 53.76, 41.50, 35.60, 22.42.

SHP099.HCl

The TFA salt of SHP099 was converted into an HCl salt by using the following procedure: The AC046 TFA salt was loaded on a manually packed column with C18-reversed phase silica gel (Sigma Aldrich, 90Å, 230-400 mesh, 40-63 μm). The column was then washed with Water+5% MeCN and then the compound was eluted by washing the column with 25%MeCN+0.1HCl in MQ. The fractions containing the compound were combined and freeze dried to give the pure compound as a yellow HCl salt (258mg, 79% yield from tert-butyl (1-(6-amino-5-(2,3-dichlorophenyl) pyrazin-2-yl)-4-methylpiperidin-4-yl) carbamate). TLC R_f = 0.46 (9:3, DCM:MeOH, v:v + 0,1% HCl). HPLC R_T: 3.65min (Waters XTerra C18 column, 5 μm, 125Å (4.6×150 mm); Eluents: (A) 0.1% TFA and 5% MeCN in H2O (v/v/v); (B): 0.1% TFA in MeCN (v/v). Column temperature: 40ºC. Gradient: 0-60% buffer B over 10 min). LC-MS (ESI-MS) found: 352.1 $[M+H]^+$, calculated mass for $C_{16}H_{19}Cl_2N_5$ $[M+H]^+$: 352.16.

^{1}H NMR (400 MHz, Methanol-d4) δ 7.80 (dd, J = 5.4, 4.3 Hz, 1H), 7.64 – 7.61 (m, 1H), 7.56 – 7.51 (m, 2H), 4.30 – 4.18 (m, 2H), 3.56 – 3.44 (m, 2H), 1.96 – 1.90 (m, 4H), 1.55 – 1.52 (m, 3H). ^{13}C NMR (101 MHz, Methanol-d4) δ 155.02, 154.93, 133.90, 132.96, 132.86, 130.54, 130.05, 128.66, 115.05, 106.73, 52.29, 40.07, 34.23, 21.05.

Synthesis of Cholesterol-Carbamate-Gly-Trp-Arg-Arg-Arg (Chol-GWR3)

The peptide H-GWR_3-NH_2 was first synthesized by standard solid phase peptide synthesis (SPPS) on an automated BioTage Synthesizer with a Tentagel Rink Amide resin (Scale: 0.5 mmol; loading: 0.20 mmol/g) by standard Fmoc methodology. Each coupling was performed using 4.0 equiv. Fmoc protected amino acid, 3.95 equiv. HATU, and 8 equiv. 2,4,6-collidine in DMF for 30 min at room temperature (rt). Deprotection of the Fmoc-protection group was achieved by subjecting the resin to 2 x 5 min of 20 % Piperidine in DMF. The first glycine

residue was double-coupled first with 5 min 75 °C microwave (µW) and subsequently 30 min at rt. The resin was cleaved with TFA:Triisopropylsilane (TIPS):H_2O (95:2.5:2.5) for 3 h. The solvent was removed in *vacuo* and the crude peptide was precipitated in cold diethyl ether. The isolated white peptide powder was purified by semi-preparative HPLC by employing a Knauer Eurosphere 100-5 C18 (20 x 250mm) column. Eluent: (A) 5 % CH_3CN + 0.1 % TFA in H_2O, (B) 0.1 % TFA in CH_3CN. Gradient profile: 0% B for 10 min and 0% B to 20% B over 20 min. Rf-value = 10 min. Flow rate: 17 mL/min. UV detection at 220/280 nm. The solvent was removed in *vacuo* and the product lyophilized from a mixture of H_2O and CH_3CN to give a white fluffy powder (0.203 mmol, 41 %, purity 95 %). MALDI-TOF MS (m/z): Calc. mass $[M + H]^+$: 729.86, found mass $[M + H]^+$: 729.81.

A flamedried RB flask was fitted with a magnet, septum and N_2-atmosphere. The lyophilized peptide (0.101 mmol) was dissolved in dry DMF (75 mL) and added to the RB flask followed by adding DIPEA (441 µL, 2.533 mmol). Cholesteryl chloroformate (55 mg, 0.122 mmol) was dissolved in CH_2Cl_2 (25 mL) and added to the RB flask. The reaction was let to react overnight (o/n). The solvent was removed in *vacuo* and the crude cholesteryl-GWR_3-NH_2 was purified by semi-preparative HPLC by employing a Knauer Eurosphere 100-5 C18 (20 x 250 mm) column. Eluent: (A) 5 % CH_3CN + 0.1 % TFA in H_2O, (B) 0.1 % TFA in CH_3CN. Gradient profile: 50 % B to 100 % B over 20 min Rf-value = 12 min. Flow rate: 17 mL/min. UV detection at 220/280 nm. The solvent was removed in vacuo and the product lyophilized from a mixture of H_2O and CH_3CN to give a white fluffy powder (0.085 mmol, 84%, purity >98%). MALDI-TOF MS (m/z): Calc. mass $[M+H]^+$ = 1141.77; found mass $[M+H]^+$ = 1142.19. FT-IR, ν (cm-1): 3277.9, 3194.7, 2949.2, 1658.5, 1531.8, 1199.9, 1178.9, 1128.9, 835.4, 800.7, 720.6. This gives an overall isolated yield of 34%.

Chol-GWR3-NH_2

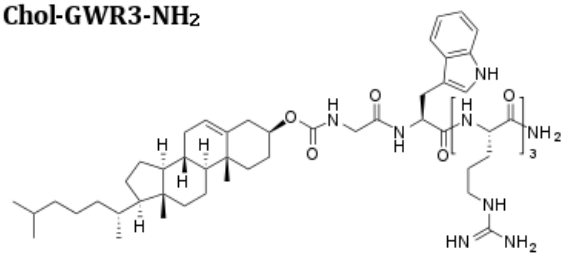

Molecular weight: 1141.52 g/mol

MALDI-TOF MS spectrum:

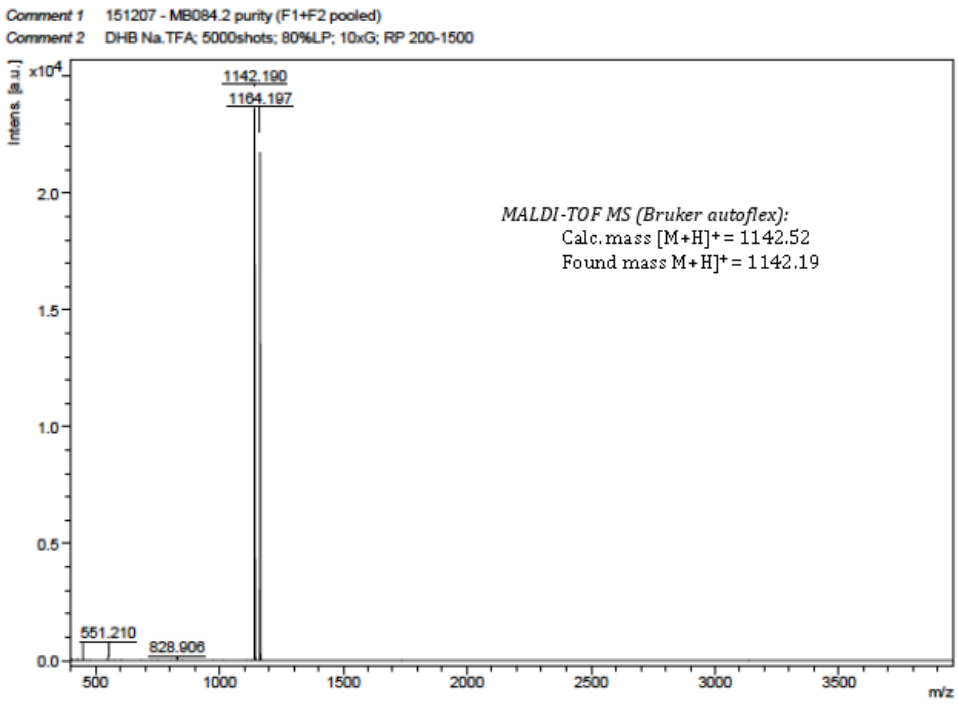

Determination of phospholipid concentration

The total lipid concentration was determined by measuring the phosphorus concentration using Inductively Coupled Plasma Mass Spectrometry (ICP-MS). Samples were diluted 2,000 - 5,000 times in an ICP-MS diluent (2% HCl, 10 ppb Ga) for measurement. The phosphorus content was measured on an ICAP-Q from Thermo Fisher Scientific. The total lipid concentration was calculated based on ratio of the lipids in formulations containing a phosphorus atom (HSPC, DSPE).

Determination of SHP099 concentration

Concentration of SHP099 was measured using analytical reversed-phase (RP)-HPLC on a LC-20AD liquid chromatograph (Shimadzu Corporation). A XBridge C8 (5 µm, 4.6x150 mm)

column (Waters) was used and SHP099 quantification was done by UV detection at 320 nm with an SPD-M20A Photodiode Array Detector fitted with a Deuterium Tungsten lamp (Shimadzu Corporation). Eluent: (A) 5% acetonitrile aqueous solution with 0.1% trifluoroacetic acid (TFA); (B) 0.1% TFA in acetonitrile. A gradient from 0% to 100% B over 15 minutes was applied (flow rate 1 ml/min). Lipid nanoparticles were diluted at least 20 times to fall into the standard concentration range.

Gd labelling of SR3 nanoparticles for biodistribution study

SR3 nanoparticles for biodistribution studies were formulated following the same procedure as described above, with 1% of HSPC replaced by DSPE-DOTA-Gd in the composition. To synthesize DSPE-DOTA-Gd, DSPE-DOTA was treated with an excess of Gadolinium (iii) chloride (molar ratio 1 : 2), dissolved in acetate buffer (pH = 6.0) at 50 °C for 24h. Resulting Gd–lipid complex was purified by extensive dialysis against water and was freeze dried to get dry powder. Phospholipid and Gd concentration in SR3 nanoparticles were measured by ICP-MS to determine the fraction of Gd in formulation.

3.7.2 *Results*

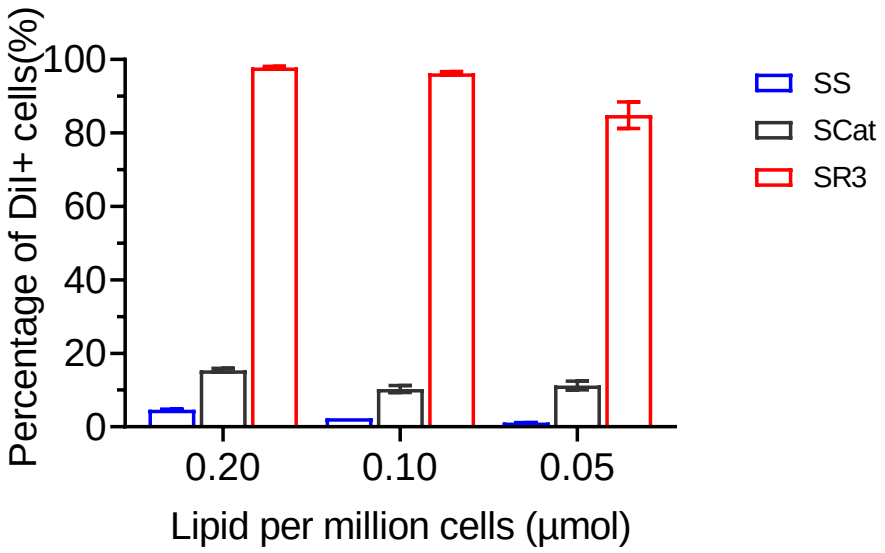

Figure 3.7 Quantification of lipid nanoparticle loading by flow cytometry. Percentage of T cells DiI+ (left) of each formulation at different concentrations. Data represent Mean ± SEM (n=3 or 5).

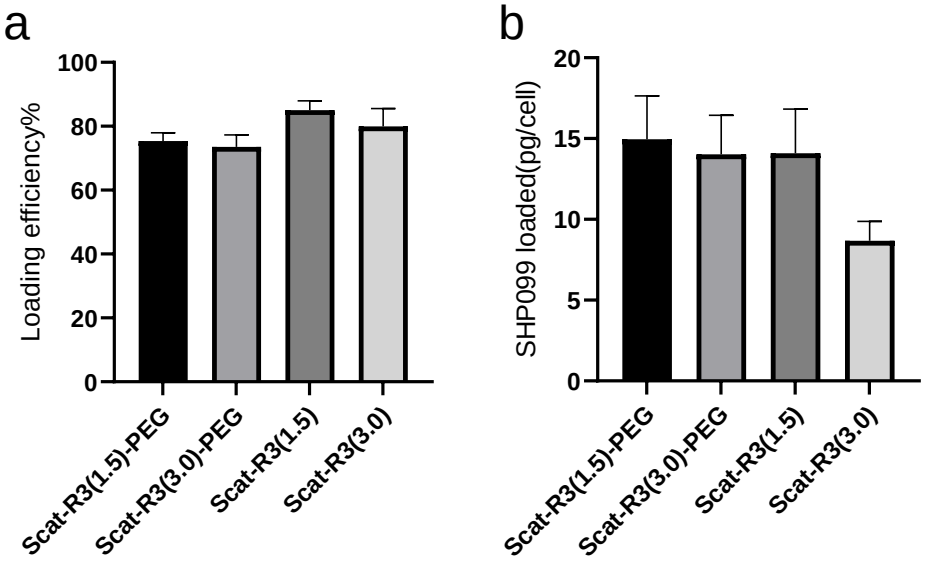

Figure 3.8 Quantification of cell-loaded SHP099 determined by HPLC. **a,** Loading efficiency and **b,** the SHP099 loading amount of SR3 formulations with different ratio of tri-arginine and PEG.

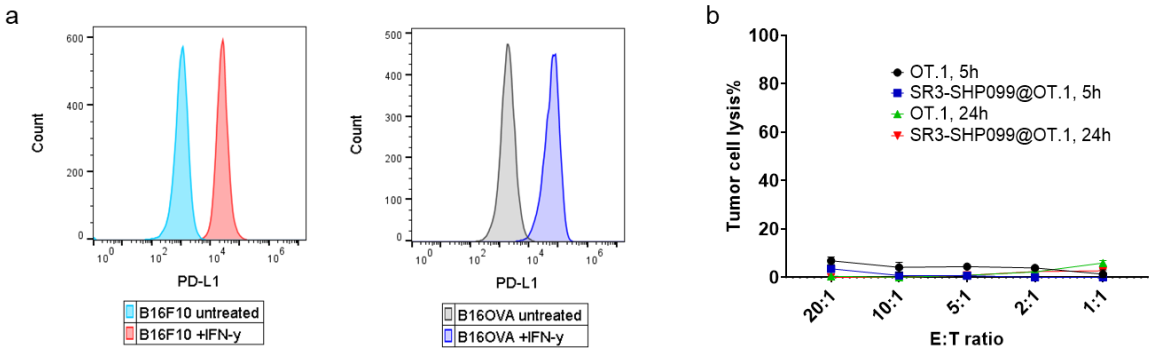

Figure 3.9 Cytotoxicity of SHP099 loaded OT.1 T cells. **a,** Upregulation of PD-L1 on B16-F10 (left) and B16-OVA (right) cells after stimulation by IFN-γ at 20ng/mL for 24 h before co-culture. **b**, Co-culture of SR3-SHP099 loaded OT.1 cells with B16-F10 control cells. Percentage of tumor lysis was measured by LDH assay. B16-F10 cells were not affected by adding unloaded or loaded OT.1 cells.

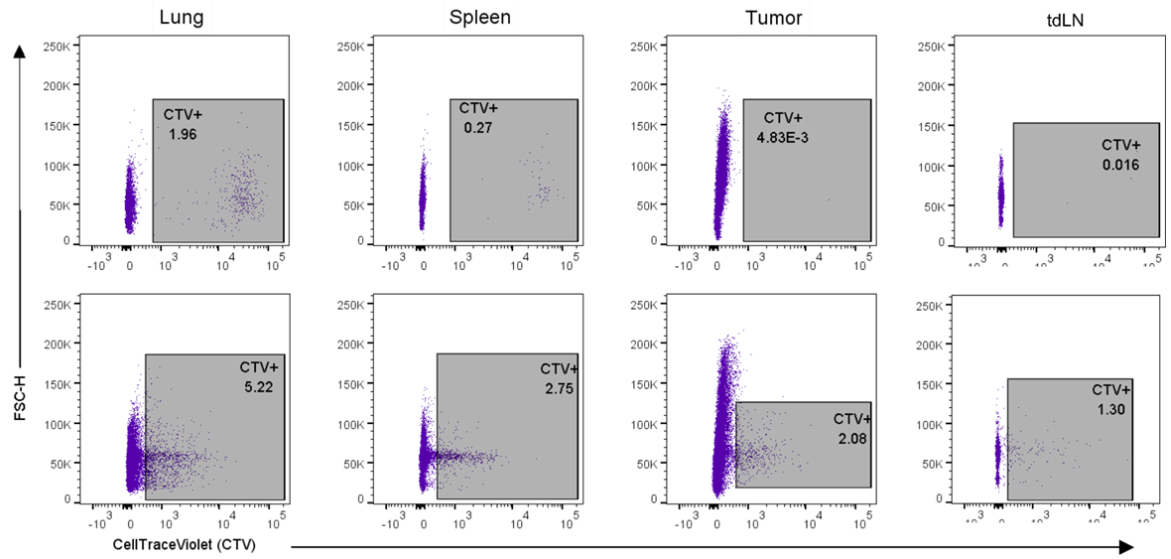

Figure 3.10 In vivo distribution and proliferation of SR3 nanoparticle loaded OT.1 T cells and unloaded OT.1 cells on EG.7-OVA tumor-bearing mice. Tissues were harvested and prepared to single cells and run on a flow cytometer for CellTrace Violet (CTV) positive cells. Representative plots from flow cytometry showing the dilution of CTV signal.

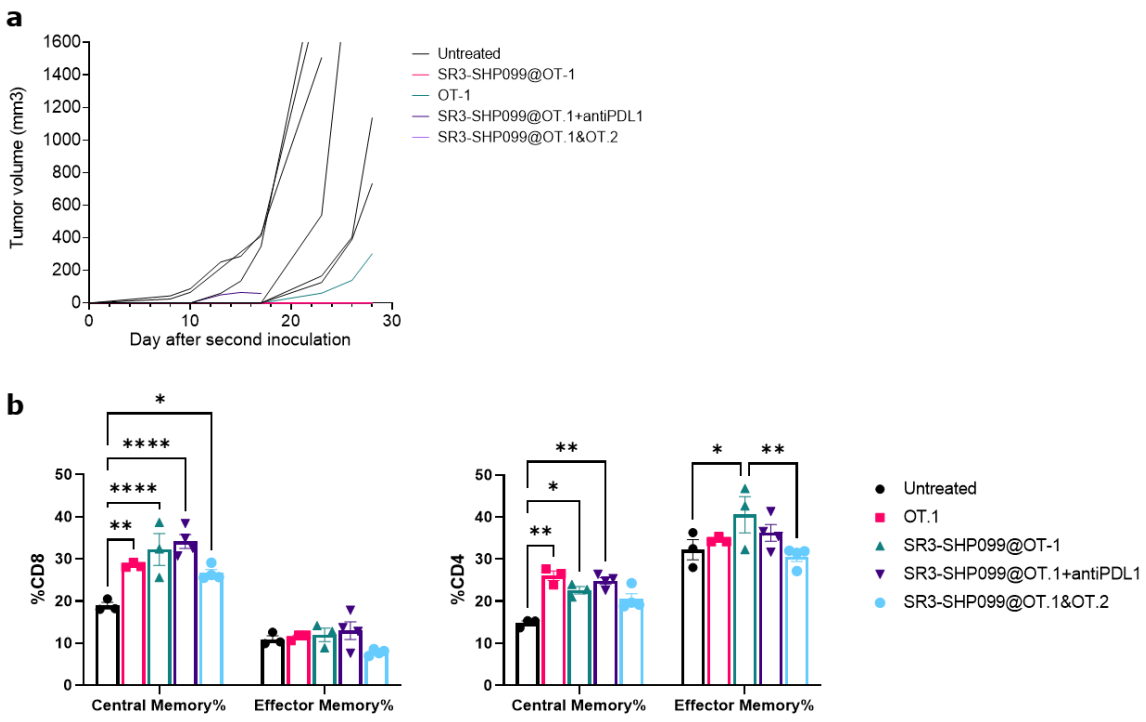

Figure 3.11 Tumor growth inhibition and immune memory formation in tumor re-challenge study. **a,** Individual tumor growth curves of the second tumor inoculated in the left flank of each mouse. **b,** Spleen T cells phenotype in re-challenged mice. At the end of the tumor re-challenge study, the mice from all groups were sacrificed and the spleens were harvested, and T cells phenotype were analyzed by flow-cytometry.

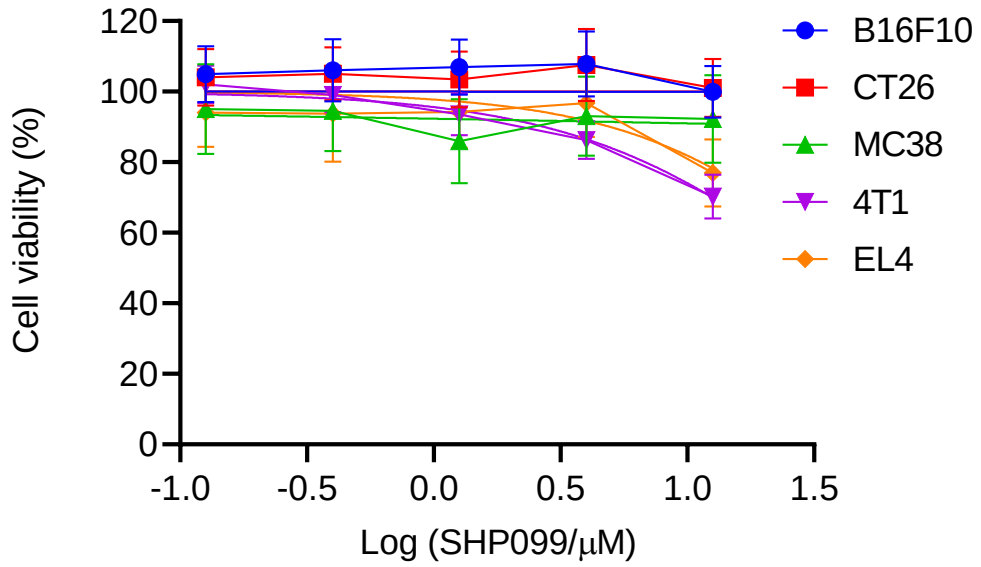

Figure 3.12 Quantification of SHP099 cytotoxicity in various murine cancer cells. Cytotoxicity assay was performed using the CellTiter 96® AQueous One Solution Cell Proliferation Assay (Promega). Cells were incubated with SHP099 (0.126 μM ~ 12.6 μM) for 48 hours at 37 ℃. Percentages are corrected based on the viability control (culture medium alone).

Chapter 4

Click conjugation of lipid-based nanoparticles on metabolic glycoengineered T cells

Xin Li[1], Sven Weller[1], Gael Clergeaud[1*] & Thomas L. Andresen[1*].

[1] Department of Health Technology, Technical University of Denmark, 2800 Kgs. Lyngby, Denmark.

*Corresponding authors. E-mail: gaecle@dtu.dk, tlan@dtu.dk

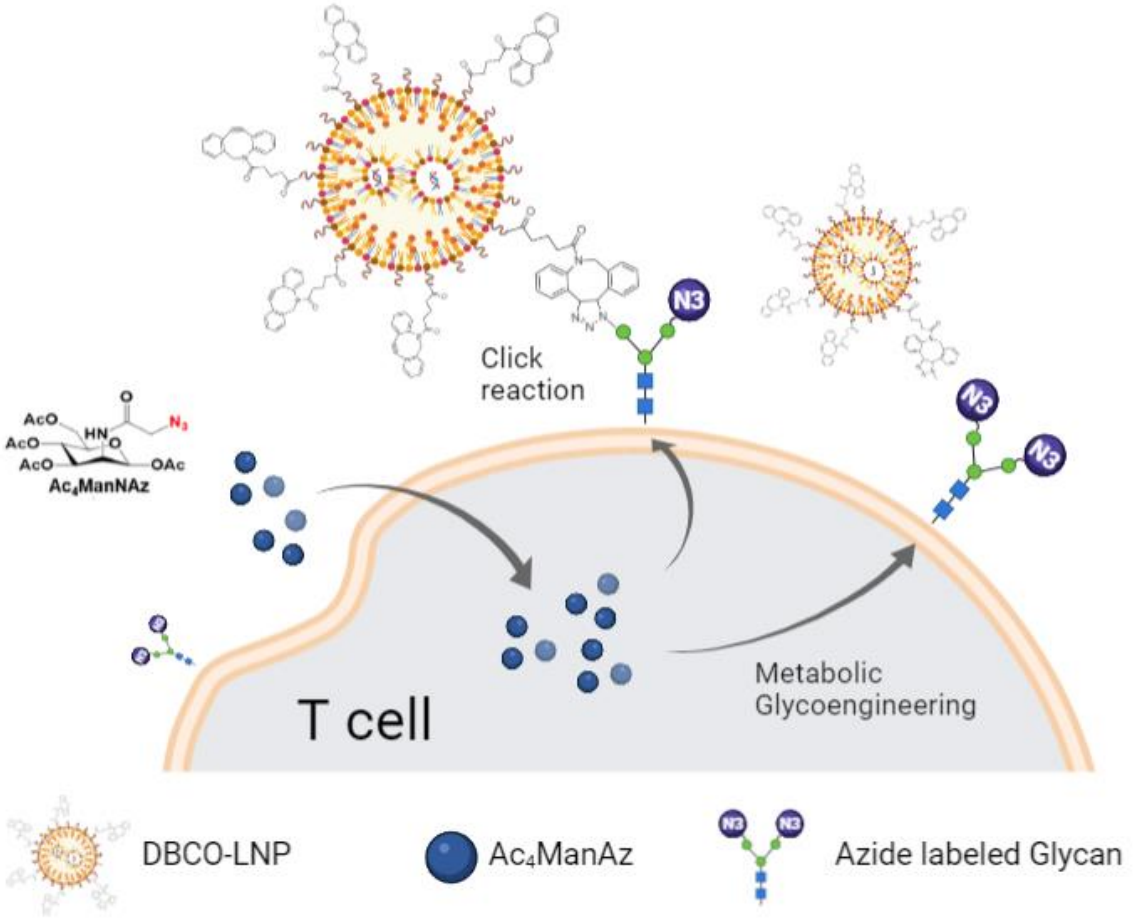

4.1 Abstract

Cell-mediated delivery of nanoparticles (NPs) by conjugating NPs to the surface of living cells is a promising strategy for targeted drug delivery, in terms of exploiting the tissue homing properties of the specific cell types to overcome *in vivo* barriers or directly putting the therapeutic payload in target cells to form a depot. Herein, we developed a bioorthogonal T cell conjugation strategy using SPAAC click chemistry, which allows controllable and highly efficient conjugation without affecting the viability and functions of the cytotoxic T lymphocytes. Azide groups were incorporated on the surface of T cells through metabolic glycoengineering, followed by reacting with dibenzylcyclooctyne (DBCO) modified lipid nanoparticles (LNPs). The results demonstrated highly specific and robust conjugation of liposomes to T cells, and the conjugation efficiency could be well-tuned by changing the presence of azide and DBCO liposomes. Based on the optimized procedure, we further developed DBCO functionalized mRNA-LNPs that can be conjugated to T cells and investigated the potential of the system to subsequently transfect the T cells with the encoded gene. The metabolic engineering and click reaction approach provide a simple and versatile strategy to conjugate NPs to living cells and engineer sophisticated therapeutic cell products.

4.2 Introduction

Cell-mediated delivery of nanoparticles (NPs) is an attractive strategy to take advantage of the natural drug delivery abilities of circulatory cells, which have long circulation time, can migrate across physical barriers and home to target tissues such as tumor[1]. Besides delivering the drugs, immune cells have unique therapeutic functions, and an example is the adoptive T cell therapy[2]. The cellular hitchhiked nanoparticles can be exploited for cell engineering to maximize the therapeutic performance of the cell therapy[3], such as backpacking supporting adjuvants to cells to enhance the in vivo persistence and activity[4].

The cell surface is composed of various biomolecules such as proteins, lipids, and polysaccharides that provide a range of functional receptors and groups to allow either non-covalent or covalent attachment of NPs[5]. Whereas non-covalent coupling that relies on the ligand-receptor interactions can be highly specific, it holds the risk of stimulating undesired cell responses. In addition, the surface receptor expression and function are unique to cell types, thus the method can hardly be versatile, and the manufacture of recombinant protein is at a high cost. Covalent approaches are considered as the most stable way, which mainly use the

amines from lysines or thiols from cysteines to react with activated esters, carboxylates, or maleimides[6,7]. Their principal disadvantages involve the uncontrolled reaction site introducing modifications of the proteins that can negatively affect the cell function, and the reaction can be very sluggish at low concentrations[8]. Thereby approaches that allow for efficient and selective cell surface conjugation without affecting cell functionalities are of high demand. Metabolic glycoengineering enables the chemical modification of the cell membrane to generate bioorthogonal functional groups on the cell-surface glycans through intrinsic biosynthetic pathways, which then undergo covalent reaction with exogenous reaction counterparts[9]. Cells can be surface-labeled with azide groups by the metabolism of an azido sugar (Ac4ManNAz)[10], and the azide groups can then be conjugated with cycloalkyne-modified NPs via the highly efficient and bioorthogonal click chemistry based on strain-promoted alkyne-azide cycloaddition (SPAAC) reaction[11,12]. This leads to the concept of our nanoparticle conjugation strategy that combines metabolic glycoengineering and SPAAC click chemistry. We first demonstrated the successful azide labeling on the T cells surface, and then used lipid-based nanoparticles as the model nanomedicine for proof-of-concept, showing high cell conjugation efficiency and selectivity as well as long persistence with the T cells.

Furthermore, we investigated the therapeutic application of this approach by conjugating mRNA-loaded LNPs to cytotoxic T cells. mRNA-LNP technology has been investigated to generate transient transcribed mRNA Chimeric Antigen Receptor T cells (Car T) *in vitro*[13] and *in vivo*[14]. The transient gene editing by mRNA accomplished 'hit-and-run' T cell modification to produce cytotoxicity for a limited duration, thus preventing the undesirable off-site side effects[3]. However, there are also limitations associated with transient mRNA transfection including the lack of sufficient longevity, poor tumor infiltration, and risks related to repeated doses. Herein we report a strategy with the potential to overcome these issues by conjugating mRNA-LNPs on T cells, which diminish the *ex vivo* incubation time and permit sustained transfection *in vivo*.

4.3 Results and discussion

4.3.1 *Generating azide groups on the surface of T cells*

For bioorthogonal conjugation of NPs to cells, two steps were required including the metabolic azide labeling of cells and subsequent click chemistry reaction. We first optimized the conditions to generate azide groups on T cells and the reactivity of the metabolically

incorporated azide with DBCO by strain-promoted azide-alkyne cycloaddition (SPAAC) reaction[15]. $CD8^+$ T cells, isolated from the spleen of mice and activated with anti-CD3 and anti-CD28 antibodies for 4 days, were incubated with various concentrations (0, 6, 12, 25, 50, 100 μM) of N-azidoacetylatedmannosamine-tetraacylated (Ac_4ManNAz) for 24 h. The presence of azide groups on the surface was confirmed by incubating with 50μM of DBCO-Cy5 for 1h and analyzed using flow cytometry for the Cy5 fluorescent signal. The Ac_4ManNAz treated T cells were successfully labeled with azide in a concentration-dependent manner, as the intensity of the Cy5 fluorescence signal increased with the Ac_4ManNAz feeding concentration (**Figure 4.1A**), and more than 90% of the cells were labeled with DBCO-Cy5 (**Figure 4.1B**) with low unspecific staining of the untreated T cells. The cell viability was not affected after incubation with Ac_4ManNAz at all concentrations for 24 h (**Figure 4.1C**), but the cell viability was significantly compromised when treated with 100 μM Ac_4ManNAz for 48 h. Since 50 μM of Ac_4ManNAz could yield a high azide label efficiency in T cells without affecting the cell viability, treatment with 50 μM of Ac_4ManNAz was selected for incorporating azide groups in the following study. At this condition, the Cy5 signal intensity also changed in proportion with the concentration of DBCO-Cy5 from 0 to 50 μM (**Figure 4.1D**), indicating an abundant amount of surface azide had been generated. We further investigated the persistence of azide-DBCO conjugates in 50 μM Ac_4ManNAz treated T cells after incubation with 50 μM of DBCO-Cy5 for 1 h followed by washing the cells three times. As shown in **Figure 4.1E**, the Cy5 fluorescence intensity underwent a fast decrease by 4.2-fold in the early phase from day 0 to day 3, and a stable phase of only 1.8-fold decrease from day 3 to day 7 post labeling. In contrast to the decrease in intensity, the ratio of T cells labeled with Cy5 remained at a high level of over 90% the whole time. The decrease in labeling intensity was assumed to be mainly caused by the signal dilution during T cell expansion, since the T cells also proliferate faster within 7-9 days after antibody activation, then become less active and halt the expansion, which correlates with the signal intensity change. In conclusion, the results establish that the T cells can be metabolically engineered to express azide groups on the surface, which can be further conjugated to DBCO functionalized fluorophore through SPAAC reaction with a high yield. The conjugation efficiency can be well-tuned by changing the concentration of the azide sugar or DBCO, and the azide-DBCO conjugation remains stable over time in cell culture.

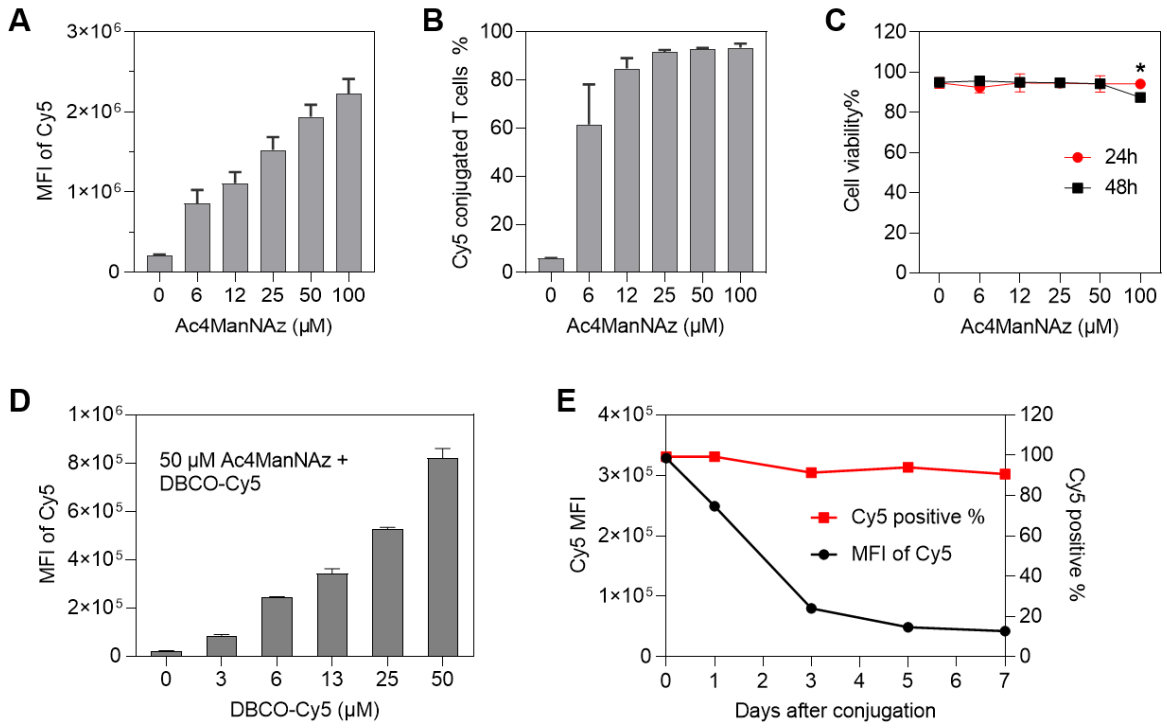

Figure 4.1 Azide groups were incorporated on the surface of CD8+ T lymphocytes via metabolic glycoengineering. **(A)** Flow cytometry analysis for mean fluorescence intensity (MFI) of Cy5 and **(B)** the Cy5 positive ratio of cells treated with various concentrations (0, 6, 12, 25, 50, 100 μM) of Ac4ManNAz for 24 h followed by incubating with 50μM of DBCO-Cy5 for 1 h. **(C)** Cell viability of T cells treated with various concentrations of Ac4ManNAz for 24 h and 48 h. **(D)** DBCO-Cy5 labeling efficiency of T cells after incubating with 50 μM of Ac4ManNAz for 24 h and incubated with various concentrations of DBCO-Cy5. **(E)** Persistence of azide conjugated DBCO-Cy5 in 50 μM Ac4ManNAz and 50 μM DBCO-Cy5 treated T cells over days, MFI of untreated cells was subtracted as the background signal. Data are shown as mean ± SD (n=3), Statistical analysis between groups was performed using the unpaired, two-tailed Student's T-test. ***p<0.0001.

4.3.2 *Click conjugation of liposomes to azide-labeled T cells*

To prove drug-loaded nanoparticles (NPs) can be attached to T cells, we further examined whether the metabolically introduced azide groups will enable the conjugation of NPs to the T cell surface, considering the behavior of larger particles is very different from molecules[16], which may lead to different conjugation efficiency than the previously used DBCO-Cy5. For this purpose, liposomes were chosen as the model nanoparticles because of their versatility for drug delivery and the successful clinical translation of many liposome-based products[17].

Preparation and characterization of DBCO-Liposomes for T cell conjugation.

DBCO modified liposomes (DBCO-LP) were prepared with 1.5 mol% of 1,2-distearoyl-sn-glycero-3-phosphoethanolamine-N-[dibenzocyclooctyl(polyethylene glycol)-2000] (DSPE-PEG_{2000}-DBCP) by a post-insertion to have the functioning DBCO groups oriented towards the outside of liposomes (**Figure 4.2A**). PEGylated liposomes without DBCO (PEG-LP) were prepared as a control. Both liposomes were labeled with DiD for flow cytometry analysis of cell conjugation and had similar liposome characteristics (**Table 4.1**). Successful incorporation of DBCO groups in liposomes was confirmed by the UV-Vis absorption spectrum, characterized by two peaks at 292 nm and 309 nm (**Figure 4.2B**). The DBCO yield in liposomes after purification was quantified by using a standard curve of absorption at 292 nm from serial dilutions of DSPE-PEG-DBCO, and the liposomes ended up with an average mol ratio of 1.3% DBCO in the total formulation. DBCO-LP showed a slightly bigger size (157.2 ± 3.9 nm) than the control PEG-LP (127.4 ± 0.8 nm) and a similar negative surface charge with the zeta potential around -30 mV (**Figure 4.2C,D**) because both liposomes contain a PEGylated lipid with the same length, which is important for the stability of liposomes.

Table 4.1 Composition and characteristics of liposomes. Mean particle size, Polydispersity Index (PDI), and zeta potential were measured in HEPES buffer (10mM), pH 7.4.

Formulation	Mol% of Lipids					Size (nm) ± SD	PDI	ζ-Potential (mV) ± SD
	DSPC	Cholesterol	DSPE-PEG2k	DSPE-PEG2k-DBCO	DiD			
DBCO-LP	59	38	1.5	1.5	0.2	157.2 ± 3.9	0.167	-31.2 ± 1.0
PEG-LP	57	38	3.0	0.0	0.2	127.4 ± 0.8	0.072	-28.3 ± 6.5

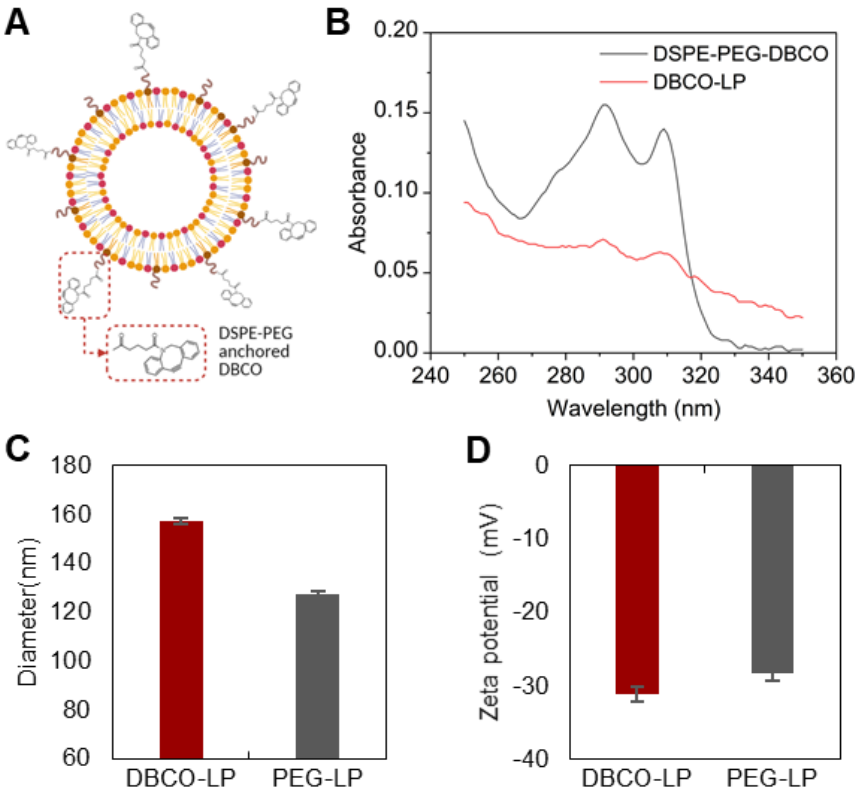

Figure 4.2 Characterization of DBCO liposomes for T cells conjugation. **(A)** Schematic illustration of DBCO-liposomes with DBCO groups modified surface. **(B)** UV-vis spectroscopy of DBCO, the absorption spectrum of DSPE-PEG-DBCO and DBCO-liposomes in ethanol. **(C,D)** Hydrodynamic diameter **(C)** and zeta potential **(D)** of DBCO-LP and control PEG-LP (n=3).

Selective conjugation of DBCO-liposomes through click reaction.

Next, we performed liposome conjugation with the optimized condition described above, murine $CD8^+$ T cells were pretreated with 50 μM of Ac4ManNAz for 24 h followed by incubation with liposomes. After incubation for 1 h, DBCO-LP showed significantly higher cell attachment than PEG-LP and DBCO-LP added on the non-azide labeled untreated cells at all concentrations (**Figure 4.3A**). The results indicate the selective conjugation of DBCO modified liposomes to azide labeled T cells through SPAAC reaction. Even though the DBCO-LP had a similar Zeta-potential than PEG-LP, which is a favorable property for particle stability and *in vivo* circulation and retention, but an unfavorable factor in the context of cell loading as it leads to a repulsive force from the same negatively charged cell membrane, the selective conjugation counteracted the repulsion with a stronger covalent binding. We still saw an increasing trend at the highest lipid concentration (1 mM lipid to 2 million/mL cells), thus the

method could provide a high cell loading capacity of particles. The extent of DBCO-conjugation was further increased by prolonging the incubation time with cells (**Figure 4.3B**), but the signal of unspecific attachment also increased at 4 h. Therefore 2 h was selected to be the applicable incubation time.

The conjugation of liposomes was also confirmed by confocal microscopy. The images showed a much stronger binding of T cells with DBCO-LP than PEG-LP (**Figure 4.3C**), in alignment with the quantitative results from flow cytometry. The distribution of liposomes on T cells was further revealed by a high-resolution three-dimension (3D) volume rendering of the cell. The 3D volume rendering containing cell nuclei and membrane staining showed the localization of liposome fluorescence at the T cells surface in a pattern of spots (**Figure 4.3D**). These images demonstrated that the liposomes were anchored to the cell membrane. Interestingly, 24 hours after conjugation, we found the liposomes were internalized in some cells (**Figure 4.3E**). The liposomes were conjugated to the azide in the sugar end of glycoproteins, glycolipids, or gangliosides on the cell surface, and one assumption is that they were internalized into the cytoplasm via a membrane turnover mechanism[18].

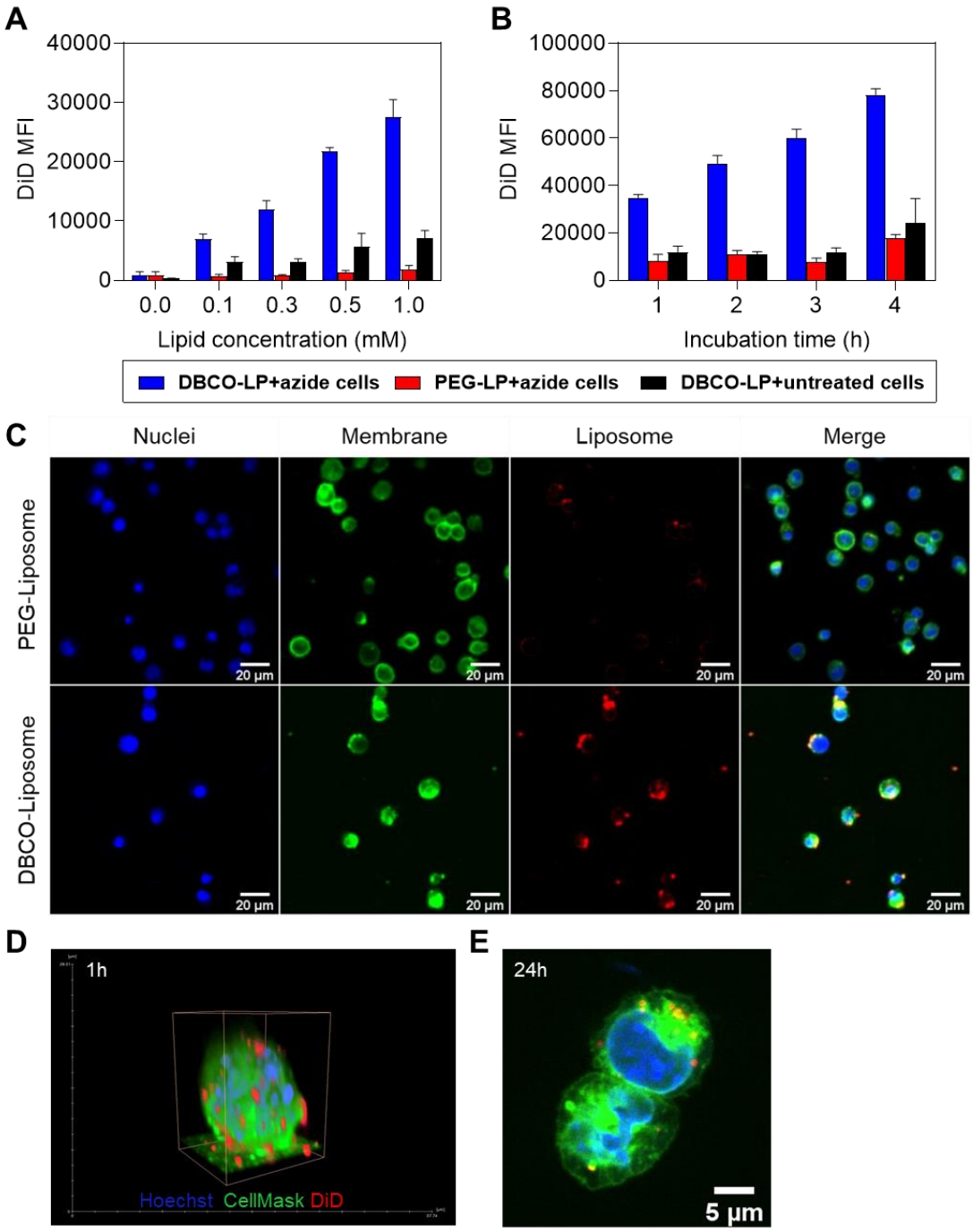

Figure 4.3 Flow cytometry and microscopy analysis of DBCO liposomes conjugation to azide labeled T cells. **(A, B)** Flow cytometry analysis of azide-labeled and unlabeled control T cells for the MFI of liposomes (DiD) after incubation with **(A)** various concentrations of DBCO or PEG liposomes for 1 hour, and **(B)** 1 mM of liposomes for 1-4 hours. T cells were kept at a concentration of 1 x 10^6 /mL. Data are presented as mean ± SD (n=3). **(C)** Confocal microscopy visualization of azide-labeled T cells conjugation with DBCO liposomes after incubation for 1 hour: cells were stained for the nucleus (Hoechst, blue) and the cell membrane (Cellmask, green), and liposomes were labeled with DiD (red). **(D)** 3D-Volume display of the DBCO liposomes conjugation on the surface of T cells. **(E)** Confocal microscopy image of DBCO-LP in T cells 24 hours after initial conjugation. For all the flow cytometry and confocal microscopy, three washing steps were applied after liposome incubation or staining.

Liposomes retention in T cells.

We further assessed the retention of conjugated liposomes in T cells over time. The retention of liposomes mainly depends on three aspects: the first one is the azide presentation on T cells, the second one is the stability of the covalent bond formed through the SPAAC reaction, and the third is related to the dissociation of the anchor lipid or even the break of liposome structure. As the first two have exhibited good stability to enable a long persistence of DBCO-fluorophore in T cells, we focused on the retention of liposome components, including both hydrophobic and hydrophilic molecules which can represent the two drug categories loaded in liposomes. Using the same DBCO liposomes as above, flow analysis of click conjugated T cells showed a slow and gradual decrease in liposome signal (**Figure 4.4A**). The DBCO-liposome MFI decreased by around 60% in the first two days and remained at a high level afterward (**Figure 4.4B).** In contrast, the PEG-liposome showed a low association to T cells and quickly completely lost the signal. To investigate if the integrity of the liposomes remained stable, dual-labeled DBCO liposomes were prepared with the hydrophobic fluorophore DiI in the lipid bilayer and the soluble fluorophore AlexaFlour 647 in the aqueous core. Upon conjugation to T cells, the two signals established a good linear relation and T cells appeared in the upper right quadrant in the plot positive for the two signals (**Figure 4.4C**), indicating the cells carried intact liposomes. Moreover, the two signals resided and fled from T cells simultaneously. This highlights the potential of this strategy to put drugs of various properties in the T cells.

In a summary, the results established that DBCO functionalized NPs can be covalently conjugated to metabolically azide labeled T cells in a highly selective and efficient way. With the need for a small fraction of DBCO (1.5%), a substantially high conjugation yield and stability can be achieved. The observation of long liposome retention is of great importance in the context of using T cell-mediated liposomal drug delivery for cancer therapy. Considering the adoptively transferred T cells require 24-72 hours until they migrate and accumulate in the tumor site, our conjugation strategy combining click chemistry and metabolic T cell engineering prevents premature liposome detachment and drug release before reaching the target tissue.

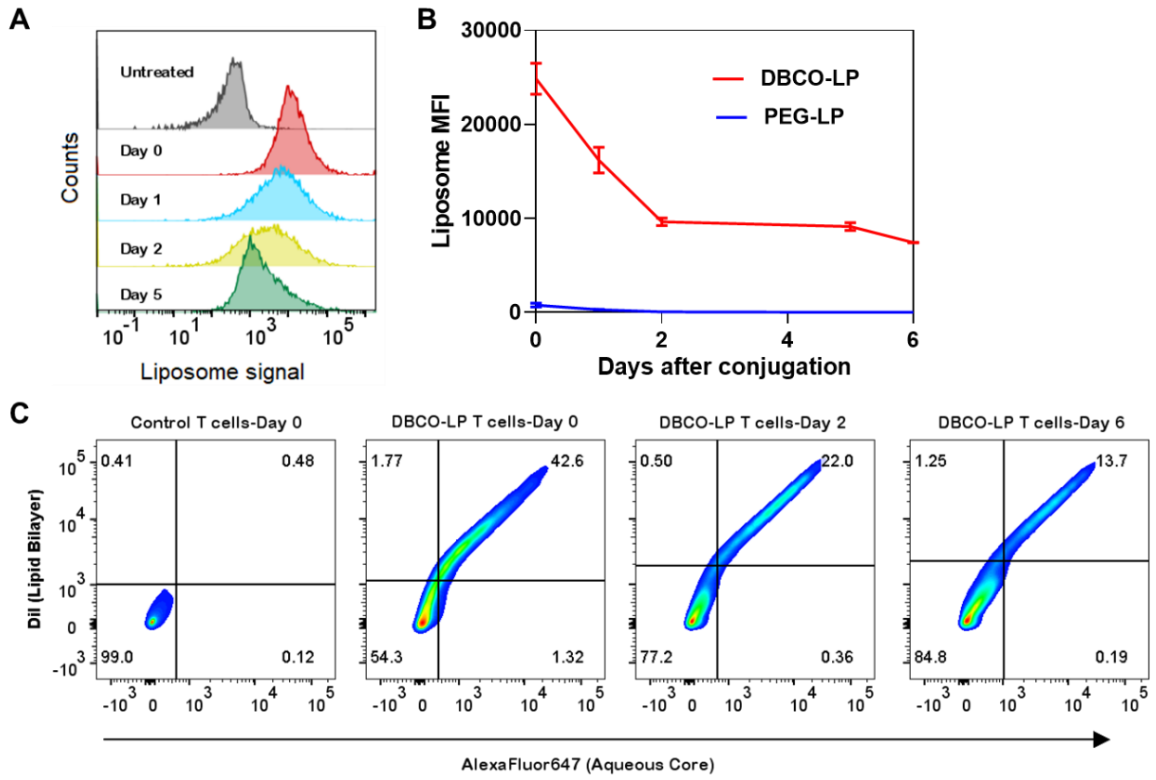

Figure 4.4 Retention of click conjugated liposomes in T cells by flow cytometry. **(A)** Histogram of T cells for liposome signal over days. Azide T cells were conjugated with DiD labeled DBCO liposomes on day 0, washed, and put back in culture with an aliquot taken out for flow analysis at a specific time point. **(B)** Change of liposome MFI from T cells (Mean ± SD, n=3). **(C)** The population of T cells with lipophilic labeling (Y-axis) and hydrophilic labeling (X-axis) of liposomes over time after conjugation.

4.3.3 *Cytotoxic t cells function after liposomes conjugation*

Apart from serving as the vehicle for nanoparticle delivery, cytotoxic $CD8^+$ T cells have the vital function of directly recognizing and killing target tumor cells. Thus, the conjugation of liposomes should not compromise T cell functionalities. To assess the influence of conjugation liposomes on T cells surface on their cytotoxic activity, OT.1 T cells were co-cultured with the target EG.7-OVA cells. The target cells present the OVA-antigen epitope in major histocompatibility class I (MHC-I) that can be recognized by OT.1 cytotoxic T cells, leading to the antigen-specific cell lysis of EG.7-OVA cells. EL4 cells that do not repress the OVA epitope peptide were mixed with EG.7-OVA in equal amounts, followed by co-culturing with OT.1 T cells at the effector: target (E: T) ratios of 1:1, 5:1, and 10:1, respectively. The two cancer cell lines were stained with different concentrations of CFSE, and the cell lysis would lead to a decrease in CFSE fluorescence intensity. As shown in **Figure 4.5**, liposome conjugated T cells and unloaded control T cells showed the same specific cytotoxicity against EG.7-OVA cells. Both T cells were able to lyse around 20% and 30% of EG.7-OVA cells at

the E: T ratio of 1:1 and 10:1. Herein we used low E: T ratios to distinguish the influence of the liposome conjugates on T cells, since the high E: T ratio was supposed to impose strong cytotoxicity and the inhibitory effect of liposomes at high concentration might conceal the impact of the conjugation. Overall, the results indicate that the covalent binding of liposomes to T cell surface through our click conjugation strategy does not impede the TCR-mediated recognition and killing of target tumor cells by cytotoxic T cells. This supports the use of the strategy in the context of adoptive T cells therapy, as the T cells can be used for delivering nanomedicine without affecting their key innate functionalities. What´s more, various drugs targeting T cells to enhance or modify T cells activity can also be applied precisely to T cells through ex vivo loading.

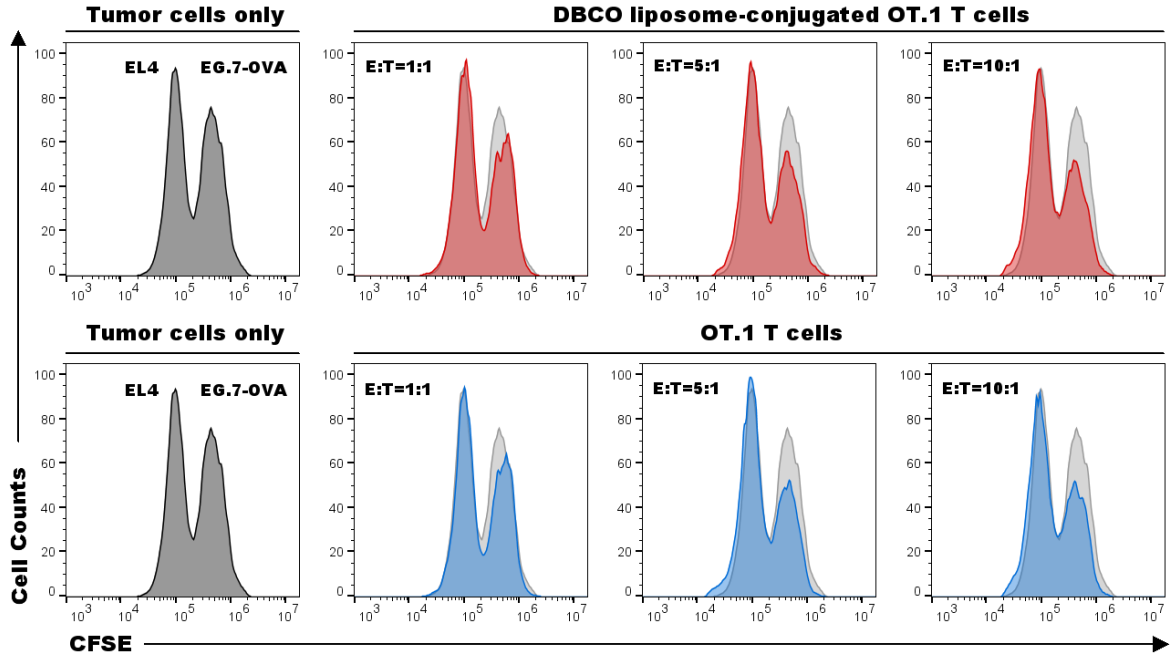

Figure 4.5 Cytolytic assay of DBCO liposome-conjugated OT.1 $CD8^+$ T cells and OT.1 $CD8^+$ T cells after co-culture with EL-4 and EG.7-OVA tumor cells at the different E: T ratios (1:1, 5:1, 10:1). EL-4 and E.G-7 tumor cells were stained with 1μM and 5μM of CFSE, respectively, followed by being co-cultured with DBCO liposome-conjugated OT.1 $CD8^+$ T cells and OT.1 $CD8^+$ T cells for 6 h at 37 ◦C.

4.3.4 *Conjugating mRNA-loaded LNPs to $CD8^+$ T cells*

To test our approach in a therapeutic context, we incorporated DBCO into mRNA-LNPs for conjugating mRNA therapeutics to CD8+ T cells. LNP-mRNA technology paved the way for the recent successes in COVID-19 vaccine development and showed exceptional promise for broad use in cancer, cardiovascular diseases, and other clinical applications[19–21]. mRNA is an

ideal tool for transient gene editing; it takes effect in the cytoplasm where it is transiently transcribed to the target protein, and it has no risk of genomic integration and does not require nuclear localization for expression. The delivery methods are extremely highlighted due to the unique properties of mRNA molecules, which are rapidly degradable, negatively charged, and may lead to off-target hypersensitivity[22]. Additionally, it often requires repeated dosing to achieve therapeutic efficacy and maintain the longevity of transfected cells. Our strategy provides a targeted and sustained delivery method for mRNA.

LNPs containing an ionizable lipid were prepared to package mRNA via microfluidic mixing of one part ethanol phase (containing the lipids) and three parts aqueous phase (containing the mRNA). The mCherry encoding mRNA was used as a model cargo, upon intracellular delivery, the mRNA is translated into mCherry protein that generates a fluorescence allowing detection by flow cytometry. To modify the LNPs with DBCO, DSPE-PEG-DBCO was incorporated by either mixing it with other lipid expedients or post-inserting it to pre-made mRNA-LNPs, which are referred to as DBCO-LNP (pre-mix) and DBCO-LNP (post-insert), respectively. As shown in **Figure 4.6A**, post-insertion of lipid anchored DBCO only led to a slight increase in particle size and showed similar mRNA encapsulation (72.4 ± 3.5%) compared with the PEGylated LNP (74.6 ± 2.2%) as measured by a Ribogreen assay. However, pre-mixing the DSPE-PEG-DBCO interfered with the assembly and complexing process, consequently the particle size became significantly bigger and heterogenous, and more importantly, it has only less than 10% of mRNA encapsulated inside the particles with the majority exposed on the surface, which is vulnerable to nuclease degradation. After incubating with azide labeled T cells for 2 h, both DBCO LNPs showed much higher T cell binding than the PEG LNPs (**Figure 4.6B**). It demonstrated the approach optimized with liposomes is also transferrable to LNPs.

We further checked the expression of mCherry from T cells 24 h and 48 h after conjugation. T cells were incubated with mRNA LNPs for 2 h followed by washing out the unconjugated LNPs, and the mCherry expression was determined by flow cytometry. As shown in **Figure 4.6C**, the DBCO-LNPs prepared by post-inserting DXPE-PEG-DBCO were still bonded to T cells and induced around 11.5% mCherry transgene expression by the T cells after 24 h. In comparison, very few PEG-LNPs were attached to T cells, neither did they transfect T cells with mCherry. Only around 3% of T cells showed the mCherry signal. Moreover, even though the pre-mixing prepared DBCO-LNPs exhibited the same T cell binding ability, they were not

capable of functional mRNA delivery to induce the translation in T cell cytoplasm since the mRNA was not properly packaged.

A

Formulation	Size (nm) ± SD	PDI	mRNA EE (%) ± SD
PEG-LNP	123.1 ± 0.9	0.20	74.6 ± 2.2
DBCO-LNP (pre-mix)	251.3 ± 14.5	0.33	7.7 ± 3.4
DBCO-LNP (post-insert)	119.1 ± 5.1	0.23	72.4 ± 3.5

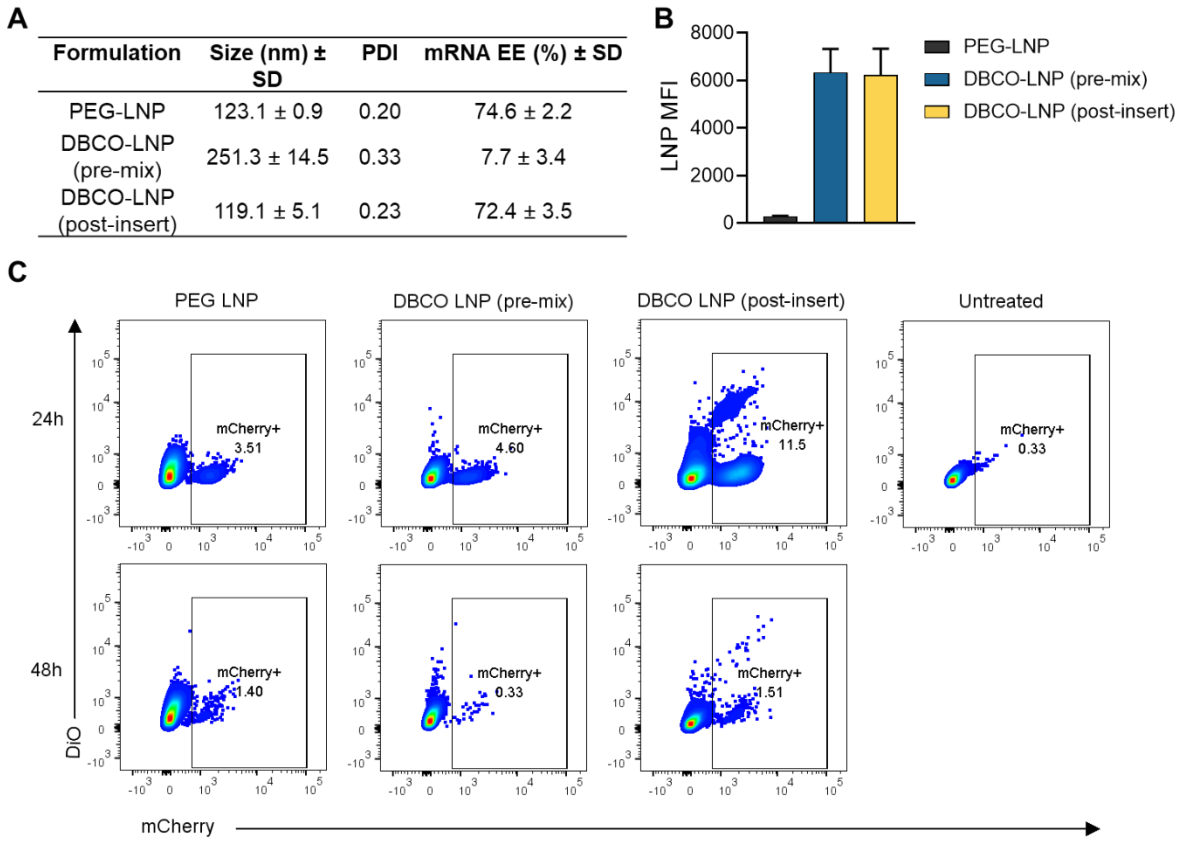

Figure 4.6 The conjugation of mRNA-LNPs to T cells. **(A)** Characterization of mRNA-LNPs. The size and PDI were measured by DLS. mRNA encapsulation efficiency (EE) was defined as the ratio of the mRNA trapped in the core to the total amount of mRNA complexed in LNPs (surface adsorbed and inside trapped), (n=3). **(B)** The signal intensity of LNP fluorophore probe (DiO) from azide labeled T cells after incubation for 2 h. Mean ± SD, n=3. **(C)** Flow cytometry plots representing the T cells incubated with PEG or DBCO modified mRNA-LNPs prepared through pre-mixing or post-insertion technique. The azide labeled T cells were added with mRNA-LNPs for 2 h then washed to remove the unconjugated LNPs (1, 2, and 3) and checked for LNP(DiO) and transgene (mCherry) signals after 24 h or kept in culture with LNPs all the 24 h before checking the signals.

The LNPs are required to direct the mRNA into the cytoplasm, where it can be transiently transcribed before degrading. We hypothesized that our conjugation strategy first allows a high number of LNPs to attach to the surface of T cells and then initiates the cell uptake through endocytosis or membrane turnover to deliver mRNA into the cytoplasm. As displayed in **Figure 4.3E**, we observed the conjugated NPs were internalized in T after 24 h. However, we did not observe significantly prolonged transfection, since the mCherry positive ratio decreased in all LNP groups after 48 h. This might be due to the low mRNA dose we added to T cells,

which were quickly used up by the T cells. Compared with the number of liposomes that were conjugated to azide labeled T cells in the validation experiments, less than one-tenth LNPs were added to T cells for conjugation. Thus, there is still a large capacity of the T cells to conjugate more mRNA LNPs, which we assume would promote the transfection as well as increase longevity. In summary, the results provided preliminary evidence that the metabolic engineering and click conjugation strategy enables an efficient binding of mRNA-LNPs, which can later mediate T cell transfection. Further investigation regarding the formulation, feeding concentration, and subcellular localization of LNPs is required to achieve prolonged and sustained transfection over time.

4.4 Conclusion

In conclusion, we developed a very efficient approach to covalently conjugate lipid-based NPs to the surface of live cells through the combination of metabolic glycoengineering and SPAAC click chemistry. The method was validated using liposomes and LNPs on T cells to show a high and tunable conjugation efficiency, and enabled selective reaction and long persistence of the conjugates, without influencing cell viability and function. We also demonstrated that DBCO modified mRNA-LNPs can mediate mRNA translation in the carrier T cells to express the encoded protein. In the context of adoptive T cell therapy, the strategy allows the formation of an mRNA depot in cells to allow sufficient longevity of mRNA engineered T cells. Based on the promising results, the future investigation will be focused on optimizing the mRNA-LNPs composition carrying therapeutic mRNA for T cell conjugation and sustained expression of self-support cytokines, thereby increasing the therapeutic activity of adoptive T cells. In addition, the anchor lipid for DBCO can be easily altered or functionalized to respond to specific stimuli in the target disease environment, the system can be further modified to change the release and cellular uptake profile according to the target of drug delivery. We believe the approach holds great potential and is applicable to various types of NPs and cells.

4.5 Materials and methods

4.5.1 *Materials*

DSPE, cholesterol, DSPE-PEG_{2000} and DSPE-PEG_{2000} -DBCO for liposome and LNP formulation were purchased from Avanti Polar Lipids. Fluorophores for nanoparticle labeling including DiD, DiI, DIO and Alexa Fluor® 647 Carboxylic Acid were purchased from

ThermoFisher Scientific. DBCO-Cy5 and N-azidoacetylmannosamine-tetraacylated (Ac4ManNAz) were obtained from Sigma-Aldrich.

4.5.2 *Liposome preparation*

Two liposome formulations, PEG-LP: DSPC: Cholesterol: DSPE-PEG (59: 38: 3 mol%) and DBCO-LP: PEG-LP: DSPC: Cholesterol: DSPE-PEG: DSPE-PEG-DBCO (59: 38: 1.5: 1.5 mol%) were prepared. The PEG-LP was prepared by the lyophilization-hydration method as described previous. Briefly, lipids were dissolved in the desired molar ratios in tert-butanol: MQ water (9:1) and lyophilized to obtain the lipid cake, which were then rehydrated in HEPE-saline buffer (10mM HEPES, pH 7.4) to a concentration of 20 mM total lipid for 1 h at 70 °C. The lipid suspension was extruded 21 times through a 100 nm polycarbonate filter (GE Healthcare) using an Avanti mini extruder (Avanti Polar Lipids) at 65 °C for sizing the liposomes. Liposomes were stabilized and stored at 4 °C. For preparing the DBCP-LP, liposomes of the mixed composition without DSPE-PEG-DBCO were made first using the method above. The liposome solution was added to solubilized DSEP-PEG-DBCO to give a theoretical DBCO surface density of 1.5 mol%, and the solution was stirred at 45 °C overnight[23]. Subsequently, the liposomes were run through a size exclusion PD10 column to remove the uninserted DSPE-PEG-DBCO. For fluorescence labeling of liposomes, 0.2mol% of lipid dye were added to the lipid mixture for making the lipid cake, and aqueous phase dye Alexa Fluor® 647 was dissolved in the hydration buffer at 20 µM.

4.5.3 *mRNA-LNP preparation*

LNPs were synthesized by combining an aqueous phase composed of 10 mM nuclease-free sodium acetate buffer (pH 5.2) containing 100 µg/ml mRNA with an ethanol phase containing the lipid and cholesterol components at a molar ratio of KC2: Chol: DSPC: DSPE-PEG = 50:40:10:1.5 via microfluidic mixing on a NanoAssemblr® Ignite device (Precision Nanosystems). The aqueous and ethanol phases were mixed in the microfluidic device at the volume ratio of 1:3. After LNP synthesis the ethanol was removed by washing and concentrating the LNPs multiple times using the Amicon® Ultra-4 Centrifugal Filter Unit. 1.5% DSPE-PEG-DBCO was either mixed in the ethanol phase with other expedients for preparing DBCO-LNP (pre-mix) or post-inserted to LNPs by adding ethanol dissolved DSPE-PEG-DBCO to LNPs and incubating at 45 °C for 4 h for preparing DBCO-LNP (post-insert).

4.5.4 *Nanoparticle characterization*

The total lipid concentration of liposomes was determined by measuring the fluorophore concentration using a spectrofluorometer mounted on a Tecan Spark® multimode microplate reader. For example, the DiD labeled liposomes were dissociated by dissolving in ethanol and the fluorescence intensity was measured at Ex/Em = 644/665 nm with the manually set gain value. Serial dilutions of DiD in ethanol were measured using the same set-up to obtain a standard curve of FI vs. concentration for liposome quantification.

Hydrodynamic diameter, zeta-potential, and polydispersity of the liposomes and LNPs were measured by dynamic light scattering using a ZetaSizer Nano ZS from Malvern Instruments. Nanoparticles were diluted to 50-100 μM total lipids in HEPES buffer and measured as the average from 3 runs of 15 cycles.

mRNA encapsulation efficiency by LNPs was determined using a modified Quant-iT RiboGreen RNA reagent (Life Technologies). mRNA-LNPs were disassembled by adding 0.5% Triton X-100 to fully expose the encapsulated mRNA.

4.5.5 *Isolation, activation, and in vitro metabolic azide labeling of primary murine T cell*

Primary murine $CD8^+$ T cells were isolated from the spleens of OT-1 mice via magnetic negative selection using an EasySep isolation kit (STEMCELL Technologies). T cells were activated using anti-CD3/CD28 antibodies (eBioscience) at a density of 2×10^6 cells/well in a pre-coated 6-well plate. The cells were cultured in RPMI 1640 medium containing 10% (v/v) fetal bovine serum (FBS), 1% penicillin/streptomycin, 1% (v/v) Insulin-Transferrin-Selenium (ITS, Thermo Fisher), recombinant mouse IL-2 (20 ng/ml) and IL-7 (5 ng/ml) at 37 °C. 4 days after activation, cells were collected and suspended at 2×10^6 /mL for azide labeling. To optimize the treatment condition, Ac4ManNAz were added to T cells at various concentrations (0, 5, 10, 20, 50, and 100 μM) and incubated for 24 h to 48 h at 37°C (5% CO_2). Treatment with 50 μM Ac4ManNAz for 24 h was selected as the azide labeling condition in all the following experiments. After treatment, cells were washed with PBS and resuspended at 2×10^6 /mL in serum-free RPMI medium for confirming the azide presentation with DBCO-Cy5 or conjugating with lipid nanoparticles.

4.5.6 *Conjugation of DBCO-Cy5 to azide labeled T cells*

200 µL of azide labeled T cells (2 x 10^6 cells/mL) was added to wells of a U bottom 96 well-plates. In parallel, an equal amount of activated by not azide labeled T cells were seeded in wells as control. Next, cells were added with various concentrations (0 to 100 µM) of DBCO-Cy5 for 1 h at 37℃ (in triplicate). After 1 h, cells were pelleted (380 g, 5 min), washed twice with DPBS, and resuspended in 100 µL DPBS for analysis by flow cytometry and confocal microscopy. For investigating the persistence of azide conjugated DBCO-Cy5, cells were washed twice and resuspended in a complete RPMI1640 medium supplemented with IL-2 and IL-7 at 0.5 x 10^6 /ml incubated at 37℃ (5% CO_2). At predetermined incubation time (1, 2, 3, 5, 7 days post-label), cells were washed and analyzed by flow cytometry for fluorescence change.

4.5.7 *Conjugation of DBCO liposomes and DBCO LNPs to azide labeled T cells*

100 µL of azide labeled T cells and non-labeled T cells (2 x 10^6 cells/mL) was added to wells of a U bottom 96 well-plates. Liposomes were diluted to serial concentrations (0.25 mM, 0.5 mM, 1 mM, 2 mM) in the same serum-free RPMI medium. 100 µL of liposomes of each concentration was added to cells (in triplicate) and incubated at 37℃ for 1-4 h. Cells were washed for analysis or brought back to culture. mRNA-LNPs (mCherry) were diluted to mRNA concentration of 4 µg/mL and the same volume was added to T cells to achieve 2 µg mRNA per million T cells. The conjugation was performed by incubation for 2h followed by washing twice for analysis or brought back to culture. mRNA translation was checked by flow cytometry for the expression of mCherry fluorescence.

4.5.8 *Flow cytometry*

FACS analysis for DBCO-Cy5 and liposomes conjugation was performed using a BD Accuri C6 Plus (BD Biosciences). Cells were washed with DPBS at least twice, resuspended in 150 µL DPBS, and run with the autosampler. The analysis for mRNA-LNPs conjugation and mCherry expression was performed on a BD LSRFortessa. Cells were stained with live-dead fixable far red (Invitrogen). Data were processed by FlowJo software. The gating strategy for all plots was first to select lymphocytes (FSC-A/SSC-A) and single cells using FSC-A/FSC-H.

4.5.9 ***Microscopy***

After liposome conjugation, T cells were stained with Hoechst and CellMask green for 30 minutes on ice according to the manufacturer's protocol, followed by being washed three times with live-cell imaging solution. The cells were then transferred on poly-L-lysine precoated µ-Ibidi chamber slides for imaging using a Spinning disc (SD) confocal microscopy. For 3D images, 100 nm z-stacks were acquired, applying a z-intensity correction for the membrane channel. Acquired images were further processed using Fiji, a distribution of ImageJ (ver.1.52p),17 Nicon NIS-Element AR (ver. 5.11.00) analysis software, and Amira 3D (ver. 2021.1).

4.5.10 ***CFSE based T cell killing assay***

EL4 and E.G7-OVA cells were stained with 1 µM and 5 µM CFSE stain (Invitrogen), respectively, according to the staining protocol. The OT-I CTLs were activated for 4 days with anti-CD3/CD28 antibodies, azide labeled by incubation with 50 µM Ac4ManNAz for 24 h and conjugated with DBCO-liposomes at the concentration of 1 µmol lipid per million T cells for 2 h. After two washing steps to remove unbound liposomes, the OT-I T cells (effector) were co-cultured with an equal mixture of EL4 and E.G7- OVA cells (target) at effector-to-target ratios of 1:1, 5:1, and 10:1. The incubation was performed in a U-bottom 96-well plate in the complete RPMI1640 medium. After 6 h at 37 ℃, the ratio of E.G7-OVA cells compared to EL4 cells was quantified by flow cytometry using an Accuri C6 plus, in which the viable population was selected based on forward scatter/side scatter, and two two cell lines were distinguished by the different CFSE fluorescence intensity signal[24].

4.6 References

1. Tiet, P. & Berlin, J. M. Exploiting homing abilities of cell carriers: Targeted delivery of nanoparticles for cancer therapy. *Biochem. Pharmacol.* **145**, 18–26 (2017).

2. Fesnak, A. D., June, C. H. & Levine, B. L. Engineered T cells: The promise and challenges of cancer immunotherapy. *Nat. Rev. Cancer* **16**, 566–581 (2016).

3. Rajan, T. S., Gugliandolo, A., Bramanti, P. & Mazzon, E. In vitro-transcribed mrna chimeric antigen receptor T cell (IVT mrna car T) therapy in hematologic and solid tumor management: A preclinical update. *Int. J. Mol. Sci.* **21**, 1–13 (2020).

4. Tang, L. *et al.* Enhancing T cell therapy through TCR-signaling-responsive nanoparticle drug delivery. *Nat. Biotechnol.* **36**, (2018).

5. Ayer, M. & Klok, H. A. Cell-mediated delivery of synthetic nano- and microparticles. *J. Control. Release* **259**, 92–104 (2017).

6. Li, P. Y., Fan, Z. & Cheng, H. Cell Membrane Bioconjugation and Membrane-Derived Nanomaterials for Immunotherapy. *Bioconjug. Chem.* **29**, 624–634 (2018).

7. Puppulin, L. *et al.* Bioconjugation strategy for cell surface labelling with gold nanostructures designed for highly localized pH measurement. *Nat. Commun.* **9**, 1–13 (2018).

8. Lamoot, A., Uvyn, A., Kasmi, S. & De Geest, B. G. Covalent Cell Surface Conjugation of Nanoparticles by a Combination of Metabolic Labeling and Click Chemistry. *Angewandte Chemie - International Edition* **60**, 6320–6325 (2021).

9. Agatemor, C. *et al.* Exploiting metabolic glycoengineering to advance healthcare. *Nat. Rev. Chem.* **3**, 605–620 (2019).

10. Prescher, J. A., Dube, D. H. & Bertozzi, C. R. Chemical remodelling of cell surfaces in living animals. *Nature* **430**, 873–877 (2004).

11. Tornøe, C. W., Christensen, C. & Meldal, M. Peptidotriazoles on solid phase: [1,2,3]-Triazoles by regiospecific copper(I)-catalyzed 1,3-dipolar cycloadditions of terminal alkynes to azides. *J. Org. Chem.* **67**, 3057–3064 (2002).

12. Xiao, P. *et al.* Engineering Nanoscale Artificial Antigen-Presenting Cells by Metabolic Dendritic Cell Labeling to Potentiate Cancer Immunotherapy. *Nano Lett.* **21**, 2094–2103 (2021).

13. Moffett, H. F. *et al.* Hit-and-run programming of therapeutic cytoreagents using mRNA nanocarriers. *Nat. Commun.* **8**, (2017).

14. Rurik, J. G. *et al.* CAR T cells produced in vivo to treat cardiac injury. *Science* **375**, 91–96 (2022).

15. Kim, W. *et al.* In vivo tracking of bioorthogonally labeled T-cells for predicting therapeutic efficacy of adoptive T-cell therapy. *J. Control. Release* **329**, 223–236 (2021).

16. Coglitore, D., Edwardson, S. P., Macko, P., Patterson, E. A. & Whelan, M. Transition from fractional to classical Stokes-Einstein behaviour in simple fluids. *R. Soc. Open Sci.* **4**, (2017).

17. Bulbake, U., Doppalapudi, S., Kommineni, N. & Khan, W. Liposomal formulations in clinical use: An updated review. *Pharmaceutics* **9**, (2017).

18. Baumann, H. & Doyle, D. Turnover of Plasma Membrane Glycoproteins and Glycolipids of Hepatoma Tissue Culture Cells*. *J. Biol. Chem* **253**, 4408–4418 (1978).

19. Tombácz, I. *et al.* Highly efficient CD4+ T cell targeting and genetic recombination using engineered CD4+ cell-homing mRNA-LNPs. *Mol. Ther.* **29**, 3293–3304 (2021).

20. Hotz, C. *et al.* Local delivery of mRNA-encoding cytokines promotes antitumor immunity and tumor eradication across multiple preclinical tumor models. *Sci. Transl. Med.* **13**, (2021).

21. Zhang, R. *et al.* DP7-C-modified liposomes enhance immune responses and the antitumor effect of a neoantigen-based mRNA vaccine. *J. Control. Release* **328**, 210–221 (2020).

22. Cullis, P. R. & Hope, M. J. Lipid Nanoparticle Systems for Enabling Gene Therapies. *Mol. Ther.* **25**, 1467–1475 (2017).

23. Eliasen, R., Andresen, T. L. & Larsen, J. B. PEG-Lipid Post Insertion into Drug Delivery Liposomes Quantified at the Single Liposome Level. *Adv. Mater. Interfaces* **6**, (2019).

24. Wayteck, L. *et al.* Hitchhiking nanoparticles: Reversible coupling of lipid-based nanoparticles to cytotoxic T lymphocytes. *Biomaterials* **77**, 243–254 (2016).

Chapter 5

Concluding Remarks

This thesis describes the development and evaluation of a platform to engineer T cells with nanomedicines by loading the T cells with nanoparticles that carry therapeutic reagents. The goal is to enhance T cell therapy to fight cancer, improve the drug delivery efficiency of immunomodulators to T cells for optimized synergy, and explore the novel combination strategies of T cells with other therapies to facilitate the development of cellular cancer immunotherapies.

First, we developed and characterized remote-loading methods for efficiently loading gardiquimod and SHP099 into liposomes (Chapter 2). And to our knowledge, this is the first report of the active-loading of both gardiquimod and SHP099 using transmembrane gradients that allowed the encapsulation of high concentrations of drug nanocrystals and showed sustained drug release and great stability. The formulation of the drug into nanomedicine built the basis for the following application. But it has been reviewed that even for nanoparticles, the drug delivery efficiency remained suboptimal (below 1%) and even lower to target specific immune cell subsets *in vivo*[1].

To address the challenges to anti-cancer drug delivery and precise T cell modification, we designed a lipid formulation functionalized with triArginine motifs to enable the T cell loading of SHP099 before *in vivo* infusion (chapter 3). Immune checkpoint therapies, together with CAR T cell therapy constitute major advances in cancer treatment in the past decade, with reproducible benefit observed in 20–30% of patients with various previously incurable cancers[2]. The combination of these two therapies has also shown great synergy since the checkpoint proteins represent major suppression of T cells[3,4]. However, they may cause serious adverse effects and sizeable costs associated with the long-term repeated administration required. SHP099 is a small molecule checkpoint inhibitor[5], and by loading SHP099 into T cells, we created a depot of supporting drugs to improve their function via blocking PD-1/PD-L1 interaction. We demonstrated the T cell loading technique as a simple and powerful strategy for modulating T cell function, and inhibition of SHP2 in T cells is a promising therapeutic approach to improve their anticancer outcome.

Apart from loading T cells through electrostatic interaction, we further developed a method to covalently conjugate lipid-based NPs to the surface of T cells through the combination of metabolic glycoengineering and SPAAC click chemistry (Chapter 4). The method provided a high, controllable conjugation efficiency, and enabled selective reaction and long persistence of the conjugates, without influencing cell viability and function of T cells. We also

demonstrated that DBCO modified mRNA-LNPs can transfect the carrier T cells to express the encoded protein. In adoptive T cell therapy, it allows sufficient longevity of mRNA engineered T cells, which is a dilemma faced by mRNA technology[6,7]. The approach can potentially be a versatile platform for transfecting T cells for target gene expression.

The development of cancer immunotherapy has brought hope for humans to win the battle against cancer, among all of them, adoptive cell transfer therapy with engineered T cells has unique advantages: they are highly effective for direct cell killing; they are capable of self-renewal and memory formation, thus require only one treatment for durable benefit[8]; CAR T cells have obtained great clinical success such as for acute lymphocytic leukemia that >90% of all patients respond to CAR T[9,10]. However, clinical outcomes in solid tumors remain quite low. A major limitation in the translation of T cell therapies in solid tumors is the heterogeneous immunosuppressive tumor microenvironment (TME) that severely limits the persistence and function of adoptive T cells. The methods to engineer T cells for improving adoptive T cell therapy are often complex and expensive, which limits the clinical translation. Herein this thesis, we present a strategy to load T cells with lipid-based nanoparticles for simple and efficient T cells engineering. We have demonstrated the successful cell loading, modification as well as improved anticancer activity of loaded T cells *in vitro* and *in vivo*. Future studies can focus on looking for more efficient therapeutic combinations, improving the cell loading efficiency, revealing the in vivo behavior of drug-loaded T cells as well as the intracellular fate of loaded nanomedicines.

5.1 References

1. Stefan Willhelm *et al.* Analysis of nanoparticle delivery to tumors. *Nature Reviews Materials* **1**, 16014 (2016).

2. Fesnak, A. D., June, C. H. & Levine, B. L. Engineered T cells: The promise and challenges of cancer immunotherapy. *Nature Reviews Cancer* **16**, 566–581 (2016).

3. Barber, D. L. *et al.* Restoring function in exhausted CD8 T cells during chronic viral infection. *Nature* (2006) doi:10.1038/nature04444.

4. Grosser, R., Cherkassky, L., Chintala, N. & Adusumilli, P. S. Combination Immunotherapy with CAR T Cells and Checkpoint Blockade for the Treatment of Solid Tumors. *Cancer Cell* **36**, 471–482 (2019).

5. Yokosuka, T. *et al.* Programmed cell death 1 forms negative costimulatory microclusters that directly inhibit T cell receptor signaling by recruiting phosphatase SHP2. *Journal of Experimental Medicine* (2012) doi:10.1084/jem.20112741.

6. Hou, X., Zaks, T., Langer, R. & Dong, Y. Lipid nanoparticles for mRNA delivery. *Nature Reviews Materials* **6**, 1078–1094 (2021).

7. Rajan, T. S., Gugliandolo, A., Bramanti, P. & Mazzon, E. In vitro-transcribed mrna chimeric antigen receptor T cell (IVT mrna car T) therapy in hematologic and solid tumor management: A preclinical update. *International Journal of Molecular Sciences* **21**, 1–13 (2020).

8. Louis, C. U. *et al.* Antitumor activity and long-term fate of chimeric antigen receptor-positive T cells in patients with neuroblastoma. (2011) doi:10.1182/blood-2011.

9. Zhang, Q. *et al.* CAR-T Cell Therapy in Cancer: Tribulations and Road Ahead. *Journal of Immunology Research* **2020**, (2020).

10. June, C. H., O'Connor, R. S., Kawalekar, O. U., Ghassemi, S. & Milone, M. C. CAR T cell immunotherapy for human cancer. *Science* **359**, 1361–1365 (2018).